HOKKAIDO UNIVERSITY

Title	Selective Cementaion of Gold Uisng an Iron Oxide and Zero-Valent Aluminum Galvanic System from Gold-Copper Ammoniacal Thiosulfate Solutions
Author(s)	ZOLETA, Joshua Bravo
Citation	. ( ) 15855
Issue Date	2024-03-25
DOI	10.14943/doctoral.k15855
Doc URL	http://hdl.handle.net/2115/92024
Type	theses (doctoral)
File Information	ZOLETA_Joshua_Bravo.pdf

Instructions for use

SELECTIVE CEMENTATION OF GOLD USING AN IRON OXIDE AND ZERO-VALENT ALUMINUM GALVANIC SYSTEM FROM GOLD-COPPER AMMONIACAL THIOSULFATE SOLUTIONS

A DISSERTATION

Presented to the Graduate School of Engineering, Division of Sustainable Resources Engineering, Hokkaido University, Sapporo Japan

In Partial Requirements for the Degree
DOCTOR OF ENGINEERING

By

JOSHUA B. ZOLETA

PROF. NAOKI HIROYOSHI
Supervisor

HOKKAIDO
U N I V E R S I T Y

January 2024

"This work is lovingly dedicated to our ALMIGHTY GOD,

To my parents

Mr. and Mrs. Rafael and Rebecca Zoleta,

To my mentors, Prof. Naoki Hiroyoshi, Prof. Mayumi Ito, Prof. Ilhwan Park Prof.

Yogarajah Elakneswaran and Prof. Sanghee Jeon

To my second Mother, Prof. Gevelyn Itao

To My siblings

Aisha, Joash, Leah Rose, April Joy, John Jay, Catherine, Maricris and Ritchie

and

To my favorite nephew who suffers cerebral palsy, Clarkin"

ABSTRACT

In conventional gold ore processing, two critical problems need to be addressed: one is the use of toxic chemicals during the extraction process, and the other is the depletion of gold ore reserves that can be quickly processed. Thus, the development of eco-friendly alternatives to extract gold from refractory ores is needed. Many studies have been conducted to find alternative solvents, such as thiourea, thiocyanate, halogen-based and thiosulfate. Among the alternatives, ammonium thiosulfate has been highlighted because it has been shown to have higher selectivity and leaching rate to gold, and most importantly, it is less corrosive and non-toxic to humans. While methods to recover gold from the leachate have yet to be established, this causes limitations to commercial operations.

A recent study reported that gold recovery could be achieved by cementing the gold ions via galvanic interactions between activated carbon (electron mediator) and zero-valent aluminum (electron donor) in the gold-copper ammoniacal thiosulfate system. The research also highlighted that metal ions can be recovered via galvanic interactions using Al and other conductive materials.

Considering the semiconductive properties of hematite and magnetite, it may be possible to use them as electron mediators. This dissertation evaluated the technical feasibility of two iron oxides (hematite and magnetite) as electron mediators for the enhanced cementation of gold from ammonia thiosulfate leachate using zero-valent aluminum as an electron donor.

Chapter 1 describes the problem statement and this study's objective. Literature on the recent studies of gold leaching and recovery from leachate using ammonium thiosulfate solutions was reviewed.

In Chapter 2, cementation experiments were conducted using iron-oxides as electron mediators and aluminum as electron donors to investigate metal recovery from a model ammonium thiosulfate leachate containing gold and copper ions. Solution analysis and SEM-EDX observation for cemented material confirmed that copper and gold were cemented from the solution in a reference experiment using activated carbon as an electron mediator. On the other hand, when iron-oxides like magnetite and hematite were used as electron mediators, copper deposition was limited, and gold was selectively deposited. This indicates that selective recovery of gold is possible by using iron-oxides and aluminum.

In Chapter 3, electrochemical experiments were conducted to evaluate the galvanic interaction between the electron donor and electron mediator using Fe_2O_3/Al electrode and Fe_3O_4/Al electrode as the working electrode in ammonium thiosulfate medium containing known concentrations of gold and copper ions. Cyclic voltammetry showed that the current peak due to gold reduction was detected around -1.0 V vs Ag/AgCl, while current peaks due to copper reduction were not detected. Cyclic voltammogram and electrochemical impedance spectrum obtained in the experiments using high-purity iron oxides (magnetite and hematite) specimens as working electrodes also confirmed the selective reduction of gold. The results of SEM-EDX analysis for the cementation products confirmed that only gold was deposited

on the surface of iron oxide electrodes. These results indicate that selective gold deposition is mainly due to the properties of iron oxides.

In Chapter 4, the mechanism for the selective gold deposition from ammonium thiosulfate solutions containing gold and copper ions on the iron oxide surface was discussed based on the results of zeta-potential measurements and investigations for the semiconductive properties of the iron oxides. The results of zeta potential measurements showed that the iron oxide surface was positively charged in ammonium thiosulfate solutions, implying that negatively charged gold thiosulfate complexes are electrostatically attracted to the iron oxide surface, but this is not for positively charged copper ammonium complexes. Investigations of the semiconductive properties of iron oxides showed that they were n-type semiconductors with a band gap energy of 1.0 eV for magnetite and 2.4 eV for hematite. The flat-band potentials were around -0.9 V for magnetite and -1.0 V for hematite. By configuring the energy band diagrams of magnetite and hematite, it was found that the redox potential of gold thiosulfate complexes is near the bottom edge of the conduction band for the iron oxides, which may cause a smooth electron transfer from iron-oxide to gold thiosulfate complexes in solutions. The redox potential of copper ammonium complexes was positioned in the band gap between conduction and valance bands, where the electron density is zero, and this may be caused by the limited electron transfer from the iron oxides to copper ammonium complexes in solutions.

Lastly, Chapter 5 summarizes the essential findings of this dissertation and its implications.

TABLE OF CONTENTS

LIST OF FIGURES

scan.

LIST OF TABLES

CHAPTER I

1.1 BACKGROUND OF THE STUDY

Gold mining is a global business with operations on every continent except Antarctica, and gold is extracted from mines of widely varying types and scales. At a country level, the Philippines is one of the principal producing countries, having produced 25.332 tons of gold as per the data from the Mines and Geosciences Bureau, inferring that the production decreased significantly to 24% in 2021. In addition, based on the amount of gold sold to Bangko Sentral ng Pilipinas (BSP), Small Scale Mines (SSM) plays a vital role in generating the highest amount of gold produced as its contribution to the Gross Production Value of Metallic and Non-metallic Mining reaches to 40% in 2021, implying that most of the production was attributable to small scale operations. With an average of 0.6% of the total mining contribution to total employment, substantial attention towards small-scale operations is critical, primarily when we discuss environmental issues.

In most hydrometallurgical processes for the recovery of gold, elemental gold is solubilized by oxidation to ionic gold and complexation with cyanide. While the use of cyanide for gold recovery systems has been the primary process for the recovery of gold for many decades, the toxicity of cyanide makes introduction to groundwater associated with gold ores highly undesirable (McGrew & Murphy, 1985). In lieu, apart from the toxicity of cyanide to man, its uses impose long-term environmental and waste disposal problems. Furthermore, gold production in the Philippines that treats pyritic ores has an average overall gold recovery of around 54% [55].

Recently, high-grade gold ores have been reported to be gradually depleting, and the refractory gold ores consisting of about one-third of the total gold production from open pit/underground mines and in tailing deposits become the interest of this study. In refractory ores, sulfide-type gold ores, especially gold-pyritic ore, account for a substantial proportion of gold resources (i.e., about 22%), the recovery of gold from gold-pyritic ore has recently come into

the spotlight as a valuable study in resources field [1-4]. Also, it poses environmental hazards upon storing these sulphide-rich minerals, as these minerals potentially form highly acidic water, commonly known as acid mine drainage (AMD) [5].

With the increasing awareness of preserving the environment, the need for other lixiviants in leaching has escalated. The investigation into lixiviants, especially for gold, primarily involves the halogen group and thiosulfate. From halogens, iodine forms the most stable gold complex but is highly corrosive and expensive. For these reasons, the development of alternative technology was focused on thiosulfate, and a recent study reported that gold recovery could be efficiently achieved by cementing the gold ions via galvanic interactions between activated carbon (electron mediator) and zero-valent aluminum (ZVAl) (electron donor) in a gold-copper ammoniacal thiosulfate system [52].

Considering the semiconductive properties of iron oxides such as hematite (Fe_2O_3) and magnetite (Fe_3O_4) [by-products of treating pyritic gold ore], it is possible to use them as an electron mediator in the cementation process proposed by the previous researchers [53-56]. In this case, direct advantages are derived from the lack of immediate pollution of the leach area compared to highly toxic cyanide; also, activated carbon can be eliminated upon processing refractory gold ores, and by treating refractory gold in pyrite (FeS_2), we could mitigate the formation of acid mine drainage (AMD) as we treat the gold from refractory gold deposits in the abandoned tailings dam.

This dissertation study was inspired to make solutions to the current situation in artisanal small-scale gold production units as well as the ongoing and abandoned pyritic gold mines in the Philippines; this manuscript highlights a new technology that shows significant extraction technique as well as its corresponding science that governs the mechanism that can be used for future applications.

1.2 SIGNIFICANCE OF THE STUDY

Despite the enormous research on gold using thiosulfate as lixiviant, a promising technology has been proposed using the galvanic interaction with zero-valent aluminum from the previous research conducted by Jeon et al., 2022. Sustainability is the status quo for future gold resources, and the refractory gold from pyrite in tailings deposits should light a prospect; the challenge for further investigations lies in the feasibility of iron oxides as an electron mediator in a galvanic system with zero-valent aluminum.

In Addition, numerous public and private organizations are concerned with the rules and regulations of environmental protection. This multiplicity is necessary to create an appropriate and practical system of precautions. The significant findings of this study could contribute significantly to the benefit of humanity, considering that it plays an essential role in developing hydrometallurgical-electrometallurgical processes dealing with pyritic refractory gold ores as one of the critical considerations in designing gold-processing plants that could save environmental assets.

1.3 OBJECTIVES OF THE STUDY

The study's general objective is to investigate the potential of iron oxides as electron mediators in galvanic interaction with zero-valent aluminum upon gold cementation in an ammoniacal thiosulfate medium.
Specifically:

1. To investigate the technical feasibility of iron oxides as electron mediators by conducting cementation experiments with zero-valent aluminum under various conditions: aerobic/anaerobic solution condition, electron mediator, electron donor, and electron mediator-electron donor dosage, and time.
2. To investigate the galvanic interaction of iron oxide and zero-valent aluminum.
3. To propose a general cementation mechanism.

1.4 REVIEW OF RELATED LITERATURE

1.4.1The Mechanism of Gold Extraction Using Activated Carbon and Cyanide

The solubility of gold in cyanide solutions was recognized as early as 1783 by Scheele (Sweden) and was studied in the 1840s and 1850s by Elkington and Bagration (Russia), Elsner (Germany), and Faraday (England). Elkington also held a patent for the use of potassium cyanide solutions for electroplating of gold and silver. The dissolution of gold in aerated cyanide solutions and the role of oxygen in the mechanism were investigated by Elsner in 1846 [1] and the reaction reported as follows:

$$2Au + 4KCN + 1/2O_2 + H_2O = 2AuK(CN)_2 + 2KOH \qquad (1.1)$$

Elsner's equation, which is now thought to apply directly to only a minor portion of gold during dissolution, is still quoted in present-day publications on gold leaching. The mechanism is now better understood and is considered in this section.

Simple cyanide salts, such as sodium, potassium, and calcium cyanide, dissolve and ionize in water to form their respective metal cation and free cyanide ions, as follows:

$$NaCN \rightarrow Na^+ + CN^- \qquad (1.2)$$

Table 1.1 Properties of cyanide compounds.

Compound	Available Cyanide (%)	Solubility in Water at 25°C (g/100 cc)
NaCN	53.1	48
KCN	40.0	50
$Ca(CN)_2$	56.5	Decomposes

(*From the Textbook Chemistry of Gold Extraction, J.O Marsden*)

The solubility and relative cyanide content of the different cyanide salts are given in Table 1.1. All three salts have been used effectively on a commercial scale gold extraction as sources of cyanide for leaching. Sodium and potassium cyanide are more readily soluble than calcium cyanide and are generally available in purer form, which has advantages for the handling and

distribution of the reagent in leaching systems. Liquid sodium cyanide (i.e., in aqueous solution), which is widely available in some regions of the world, avoids the need to dissolve the reagent on site, reducing process requirements. Thus, the choice of cyanide type depends on the method of application, cost, and availability.

Cyanide ions hydrolyze in water to form molecular hydrogen cyanide (HCN) and hydroxyl (OH–) ions, with a corresponding increase in pH:

$$CN^- + H_2O \rightarrow HCN + OH^- \qquad (1.3)$$

Hydrogen cyanide is a weak acid, which incompletely dissociates in water as follows [2]:

$$HCN \rightarrow H^+ + CN^- \qquad (1.4)$$

where $Ka(25°C) = 6.2 \times 10^{-10}$ and a relative pKa = 9.31

Figure 1.1 shows the extent of this dissociation reaction at equilibrium as a function of pH. At approximately pH 9.3, half of the total cyanide exists as hydrogen cyanide and half as free cyanide ions. At pH 10.2, >90% of the total cyanide is present as free cyanide (CN^-), while at pH 8.4, >90% exists as hydrogen cyanide. This is important because hydrogen cyanide has a relatively high vapor pressure (100 kPa at 26°C [3]) and consequently volatilizes readily at the liquid surface under ambient conditions, causing a loss of cyanide from the solution. The rate of volatilization depends on the hydrogen cyanide concentration (a function of total cyanide concentration and pH); the surface area and depth of the liquid; temperature; and transport phenomena associated with mixing [3]. As a result, most cyanide leaching systems are operated at a pH that minimizes cyanide loss, typically above pH 10, although adverse effects may be caused by excessively high pH.

Both hydrogen cyanide and free cyanide can be oxidized to cyanate in the presence of oxygen and under suitably oxidizing conditions, as illustrated in the Eh–pH diagram for the CN–H_2O system, given in **Figure 1.2**.

The important reactions are as follows:

$$4HCN + 3O_2 \rightarrow 4CNO^- + 2H_2O \qquad (1.5)$$

$$3CN^- + 2O_2 + H_2O \rightarrow 3CNO- + 2OH \tag{1.6}$$
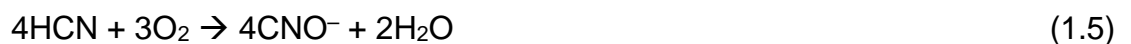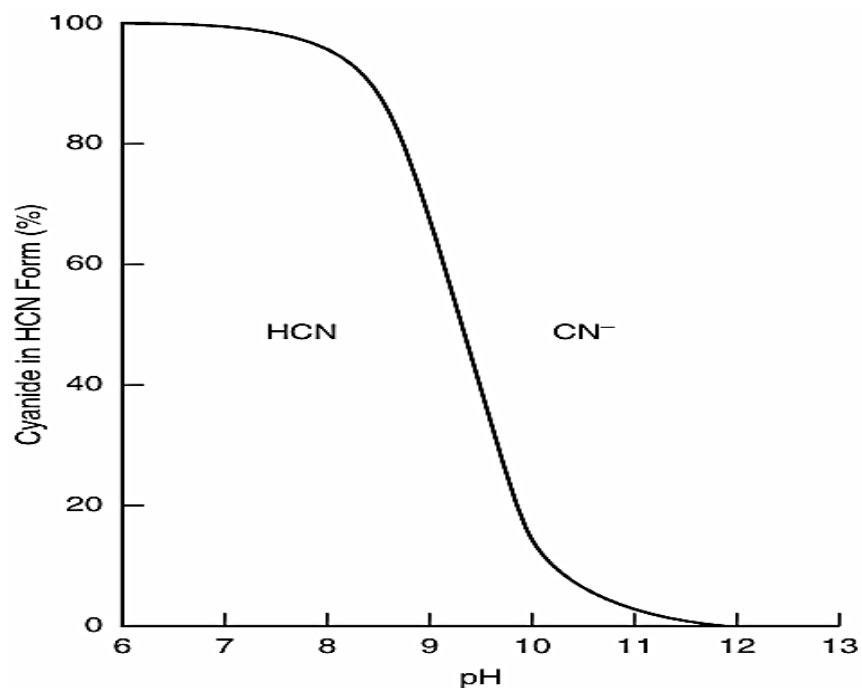
Figure 1.1 Speciation of cyanide and hydrogen in aqueous solution as a function of Ph (*From the Textbook Chemistry of Gold Extraction, J.O Marsden*)
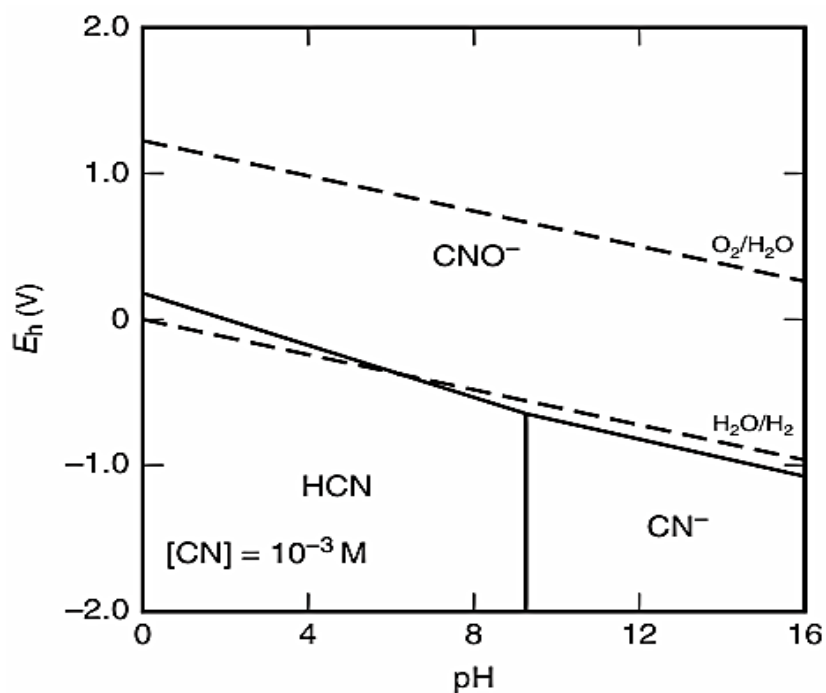
Figure 1.2 Eh-pH diagram of the CN-H_2O system at 25°C. (*From the Textbook Chemistry of Gold Extraction, J.O Marsden*)

These reactions are undesirable during leaching, because they reduce the free cyanide concentration, and the cyanate species formed does not dissolve gold.

Figure 1.2 indicates that oxidation of cyanide to cyanate should occur spontaneously with oxygen, but the reaction is very slow and, in practice, strong oxidizing agents, such as ozone (O_3), hydrogen peroxide (H_2O_2), or hypochlorous acid ($HOCl$), are required for the reaction to proceed at a significant rate. In aerated cyanide solutions, the reaction is extremely slow, but can be accelerated by the action of ultraviolet light, heat, bacteria, and catalysts such as titanium dioxide, zinc oxide, and cadmium sulfide [3]. Some of these oxidation reactions are important for the destruction or degradation of cyanide.

Free cyanide forms complexes with many metal species, principally the transition metals, which vary widely in stability and solubility:

$$M^{x+} + yCN^- \rightarrow M(CN)y^{(y-x)-} \tag{1.7}$$

where $K \leftrightarrow [M^{x+}] \cdot [CN^-]^y / M(CN)_y^{(y-x)-}$.

The complexes may be grouped into three main categories, based on their stability [3]:

1. Free cyanide (HCN, CN^-)
2. Weak acid dissociable (WAD) cyanide complexes (for which log K ≤ approximately 30)
3. Strong cyanide complexes (for which log K > approximately 30)

These categories are used widely in the analysis of process solutions because they help to describe the behavior of the cyanide species present, while avoiding the need to provide detailed analytical information of every cyanide complex present, greatly simplifying analytical procedures. This general grouping is often useful for the evaluation and optimization of metallurgical performance or when working in environmental chemistry. Further information on the speciation of cyanide in aqueous solutions used for leaching is available in the literature [4, 5, 6, 7]. Metal cyanide complexes can

form double salts with a variety of cations, for example, sodium, potassium, calcium, ammonium, and many other metal ions. For example, the iron(II) cyanide complex, $Fe(CN)6$ $4–$, which is common to all gold leaching circuits, forms a large number of salts of varying solubility [8]. The Fe(III) salt, $Fe_4(Fe(CN)_6)_3$, is commonly encountered in process effluents, appearing as "Prussian Blue" precipitate. The formation and solubility of these salts is an important consideration in effluent disposal and treatment.

GOLD DISSOLUTION

Anodic Reactions

In aqueous, alkaline cyanide solution, gold is oxidized and dissolves to form the Au(I) cyanide complex, $Au(CN)^{2-}$, as shown in the Eh–pH diagram, **Figure 1.3**. The Au(III) cyanide complex, $Au(CN)^{4-}$, is also formed, but the Au(I) complex is more stable than the Au(III) species by 0.5 V [16, 6]. For practical purposes, the stoichiometry of the dissolution reaction can be assumed to be:

$$Au(CN)^{2-} + e \rightarrow Au + 2CN \tag{1.8}$$

for which the Nernst equation is:

$$E = -0.60 + 0.118pCN + 0.059 \log a \tag{1.9}$$

Cyclic voltammetry has been used to study the mechanism of gold dissolution [16, 17]. Oxidation proceeds in three stages, as indicated by the three peaks shown in **Figure 1.4.** The peak at approximately –0.4 V probably represents the formation of an adsorbed intermediate species, AuCN, which causes temporary passivation of the gold surface:

$$AuCN_{(ads)} + e \leftrightarrow Au + CN^- \tag{1.10}$$

The second peak at approximately 0.3 V is attributed to the complexation reaction between free cyanide and the adsorbed intermediate $AuCN_{(ads)}$ species [16]:

$$AuCN_{(ads)} + CN^- \leftrightarrow Au(CN)_2^- \tag{1.11}$$
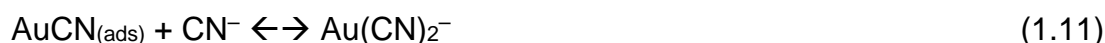
In the treatment of ores and concentrates with alkaline cyanide solutions, passivation of gold rarely occurs, even at low cyanide concentrations, probably due to the presence of low concentrations of heavy metals ions (e.g., lead and mercury), dissolved from the feed material or introduced with reagents, which disrupt the formation of such a passivating layer [17, 18].

The final peak at 0.6 to 0.7 V is thought to be due to the formation of an Au(III) oxide (Au_2O_3) layer which passivates the gold surface. However, such passivation is unlikely to be a problem in practice because of the highly positive potential required for this to occur [6, 16, 17]. The formation of the adsorbed intermediate species (and the associated passivation), the beneficial effect of lead (and other divalent cations), and the passivation due to formation of the oxide layer have been confirmed using surface-enhanced Raman scattering (SERS) spectroscopy to study the gold surface during cyanidation[19].
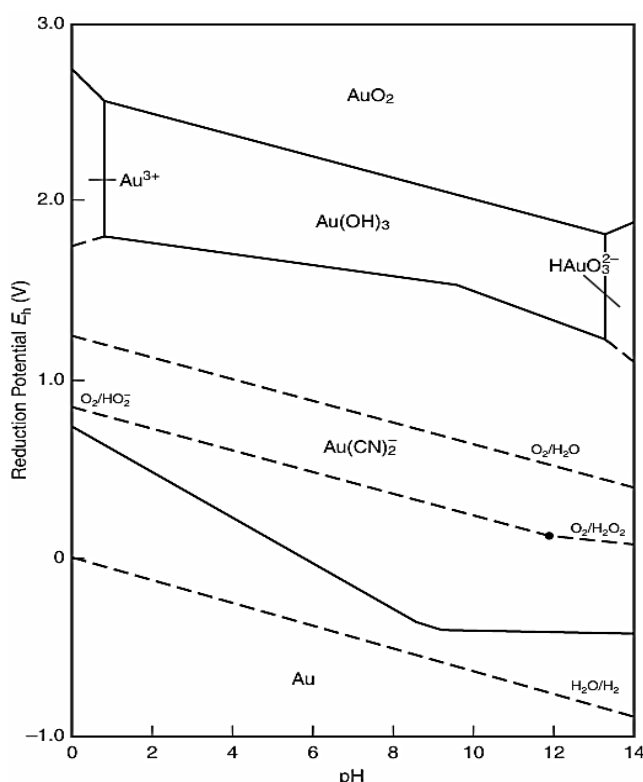
Figure 1.3 Potential-pH equilibrium diagram for the system $Au-H_2O-CN-$ at 25°C. Concentrations of all gold species $=10^{-4}$ M [6]. $[CN^-]_{total} =10^{-3}$ M, $pO_2=pH2=1$ atm, log ($[H_2o_2]- [HO_2^-]/pO_2$). (*From the Textbook Chemistry of Gold Extraction, J.O Marsden*).
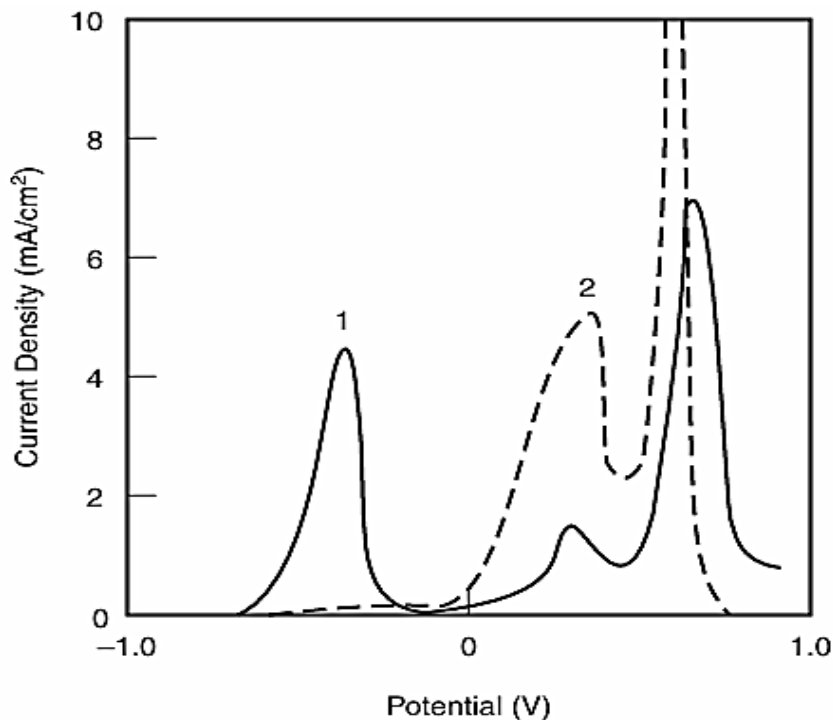
Figure 1.4 Current vs potential for the oxidation of gold in alkaline cyanide solutions; (1) 0.077 M CN⁻, pH 12, (2) 0.1 M CN, 0.1M OH (adapted from [17]).

Cathodic Reactions

In aerated, alkaline cyanide solutions, the anodic dissolution reaction shown in Equation (1.10) is accompanied by the cathodic reduction of oxygen. The mechanism of this reaction has long been controversial and involves several parallel and series cathodic reactions. Experimental investigation of the stoichiometry of gold dissolution has shown the major reaction to be as follows [20]:

$$O_2 + 2H^+ + 2e = H_2O_2; \quad E^0 = +0.682 \tag{1.12}$$

where

$$E = 0.682 - 0.059 \, pH - 0.0295 \, pO_2 \text{ (V)} \tag{1.13}$$

The hydrogen peroxide formed is a strong oxidizing agent, which may take part in further oxidation reactions:

$$H_2O_2 + 2e = 2OH^-; E^0 = +0.88 \text{ (V)} \tag{1.14}$$

The effect of hydrogen peroxide on gold leaching rates in alkaline cyanide solution is a matter of controversy and debate. Early studies indicated that the reduction of hydrogen peroxide on gold surfaces is kinetically hindered, and the dissolution rate of gold in oxygen-free solutions containing hydrogen peroxide is very slow [21, 22].

This work provided evidence of passivation of the gold surface by oxide layer formation, inhibiting gold leaching. On the other hand, hydrogen peroxide decomposes to oxygen and water, thus providing dissolved oxygen in solution as follows:

$$2H_2O_2 \leftrightarrow O_2 + 2H_2O \tag{1.15}$$

It has been demonstrated that as much as 85% of the hydrogen peroxide formed by oxygen reduction (1.12) diffuses away from the reaction site, with only a small proportion reduced directly to hydroxyl ions [21].

Other studies have indicated that hydrogen peroxide can play a direct role [23, 24]. One such investigation has demonstrated that for pure gold the leaching rate could be increased significantly using a concentration of 0.015 M H_2O_2 in a solution containing 0.01 M NaCN at pH 10. However, this study showed that smaller quantities of hydrogen peroxide (i.e., 11) also reduced the gold dissolution rate, due to increased cyanide oxidation and decreased cyanide concentration [24].

Consequently, in general, hydrogen peroxide alone is not considered to be a very effective oxidant for use in gold leaching, except under conditions where dissolved oxy gen is limited (e.g., at high altitude or in the presence of significant oxygen consumers in the ore).

Hydrogen peroxide is very effective for the oxidation of sulfides, although expensive for this purpose. However, it has been used successfully in some cases to accelerate low pressure (atmospheric) oxidation kinetics [25].

Finally, oxygen may be directly reduced to hydroxide ions, rather than to H_2O_2 (1.12) as follows:

$$O_2 + 2H_2O + 4e \leftrightarrow 4OH^-; E^0 = 0.401 \text{ (V)} \qquad (1.16)$$
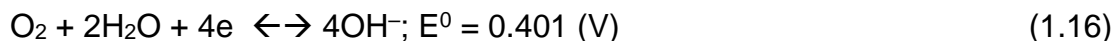
This reaction requires a large overpotential and is very slow but occurs in parallel with (6.11) to a limited extent.

Overall Dissolution Reaction

The overall dissolution of gold in aerated, alkaline cyanide solutions, considering both the anodic and cathodic half-reactions, is most accurately described by the following reaction equations, which proceed in parallel:

$$2Au + 4CN^- + O_2 + 2H_2O \leftrightarrow 2Au(CN)_2^- + H_2O_2 + 2OH^- \qquad (1.17)$$

$$2Au + 4CN^- + H_2O_2 \leftrightarrow 2Au(CN)_2^- + 2OH^- \qquad (1.18)$$
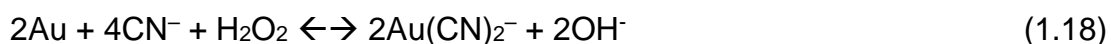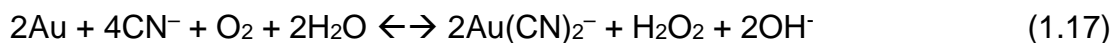
The major reactions are illustrated schematically in **Figure 1.5.** The equation proposed by Elsner:

$$4Au + 8CN^- + O_2 + 2H_2O \leftrightarrow 4Au(CN)_2^- + 4OH^- \qquad (1.19)$$
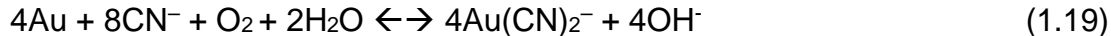
is stoichiometrically correct but does not completely describe the cathodic reactions associated with the dissolution.
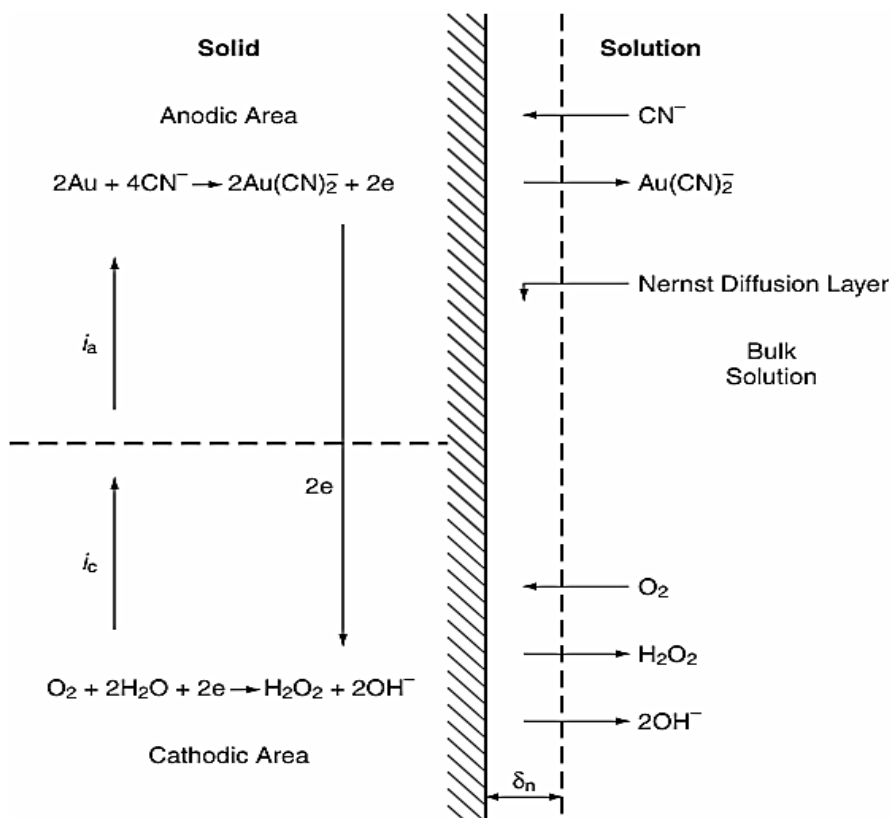
Figure 1.5 Schematic representation of the local corrosion cell at a gold surface in contact with an oxygen-containing cyanide solutions: I_a= the anodic current; I_c= the cathodic current [6].

1.4.2 ALTERNATIVE TECHNOLOGIES FOR THE EXTRACTION OF GOLD

1.4.2.1 CHLORINATION

Chlorination was applied extensively in the 1800s, prior to the introduction of cyanidation, for the treatment of ores containing fine gold and gold occurring with sulfides, which were not amenable to gravity concentration and amalgamation. Chloride media have also been applied in electroplating processes since the early 19th century. Although chlorine–chloride media is no longer used for leaching of primary ores, several processes have been proposed for the treatment of refractory, or semi-refractory, ores as an alternative to cyanide. Chlorination has also been applied for oxidative pretreatment of some carbonaceous refractory ores and significant proportions of the gold in the feed material may be dissolved during this process.

Gold dissolves in aqueous chloride solution to form both the Au(I) and Au(III) chloride complexes, as follows:

$$AuCl_2- + e \longleftrightarrow Au + 2Cl^- ; E^0 = +1.113 \text{ (V)} \tag{1.20}$$
$$AuCl_4- + 3e \longleftrightarrow Au + 4Cl^- ; E^0 = +0.994 \text{ (V)} \tag{1.21}$$
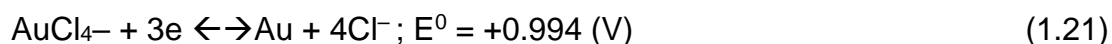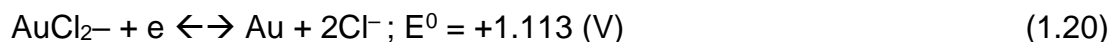
The corresponding solution equilibria are shown on the Eh–pH diagram for the Au–Cl–H_2O system (**Figure 1.6**). The Au(III) complex is more stable than the Au(I) species by approximately 0.12 V. The gold chloride complexes are not as stable as the Au(I) cyanide complex, but one advantage of this is that they are more easily reduced to gold metal.

Oxidation will only occur above approximately 1.2 V, and therefore a strong oxidant, such as chlorine, chlorate ions, or ozone, is required to dissolve gold at a reasonable rate. Chlorine is the most suitable oxidant for this purpose, because it also supplies chloride ions for gold dissolution in addition to the strongly oxidizing hypochlorous species; however, bromine and iodine may also be used to achieve fast dissolution rates. Nitric acid is a sufficiently strong oxidant to dissolve gold in chloride media, and this is applied as aqua

regia (a mixture of 33% HNO_3 and 66% HCl) in a well-established technique for gold analysis.

Several mechanisms have been proposed for gold dissolution in aqueous chloride solutions. The dissolution probably proceeds in two stages with the formation of an intermediate Au(I) chloride on the gold surface during the first stage [26]:

$$2Au + 2Cl^- \longleftrightarrow 2AuCl + 2e^- \tag{1.22}$$

The most likely theory for the second stage suggests that $AuCl_2^-$ is formed as a secondary intermediate, which then is either oxidized further to Au(III), as follows:

$$AuCl_2^- + 2Cl^- \longleftrightarrow AuCl_4^- + 2e^- \tag{1.23}$$

or diffuses into solution as $AuCl_2^-$, depending on the oxidizing potential of the solution [27]. At solution potentials above approximately 1.4 V, the gold surface becomes passivated with an oxide layer.
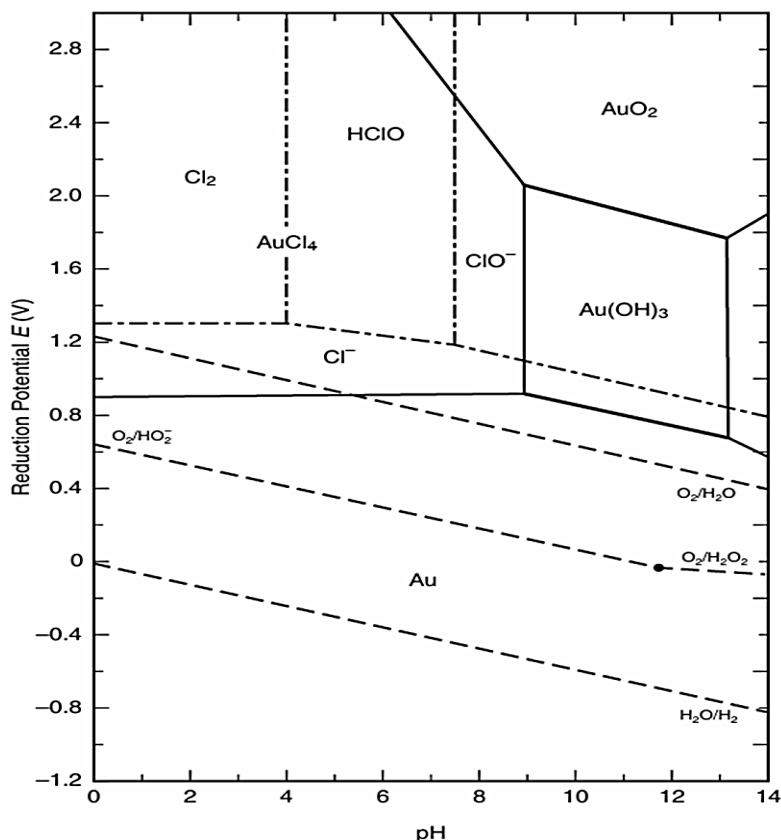
FIGURE 1.6 Potential–pH equilibrium diagram for the system Au–Cl—H_2O at 25°C including some equilibria between chlorine and water: $[Au(III)] = 10^{-2}$ M; $[Cl^-] = 2$ M; $pCl_2 = 0.1$ atm; $[HClO^-] = [Cl^-] = 6 \times 10^{-3}$ M; $pO_2 = pH2 = 1$ atm [6].

1.4.2.2 THIOSULFATE

In locations where environmental regulations and concerns prohibit the use of cyanide, thiosulfate has been proposed as an alternative to cyanide for the recovery of gold from ores and concentrates. The ability of thiosulfate species to form stable complexes with gold has been known for more than 100 years, but serious research into its use as an alternative to cyanide only started in the late 1970s. Extensive, worldwide research into the development of thiosulfate-based leaching processes escalated dramatically in the 1990s as a result of increased concerns over the use of cyanide and other factors.

Until recently, the use of thiosulfate media was proposed only for difficult ores and concentrates, such as those containing large amounts of cyanide-consuming copper, carbonaceous preg-robbing materials, refractory sulfides, and the products of partial oxidative pretreatment (e.g., biological oxidation) of refractory sulfides which contain cyanide consuming sulfur species. One of the drivers for these potential applications is that reactive sulfide minerals and sulfur species react only to a limited extent with thiosulfate and generally do not consume large quantities of the reagent, unlike cyanide.

Much of the research and development work conducted since about 1995 focused on the development of an effective thiosulfate process to replace cyanidation for a broader range of material types. Thiosulfate media have been demonstrated to be capable of effectively dissolving gold, but complex systems are required that include a suitable oxidant (such as Cu(II) or Fe(III) ions) and an effective oxidant stabilizer (such as ammonia, or open chain polyamine ligands for copper, and oxalate for iron) to achieve an acceptable gold dissolution rate, while minimizing the thiosulfate oxidation rate. Despite showing considerable promise, the development of an effective thiosulfate-based process remains elusive because of high reagent consumption and costs (due to thiosulfate oxidation) and difficulties with metal recovery from the leach solution. However, this process continues to be researched aggressively by several of the major gold producers worldwide.

Gold forms a stable complex with thiosulfate species ($S_2O_3{}^{2-}$) in aqueous solution, as follows:

$$Au + 2S_2O_3{}^{2-} \longleftrightarrow Au(S_2O_3)_2{}^{3-} + e^-; \quad E^0 = +0.153 \text{ (V)} \quad (1.24)$$
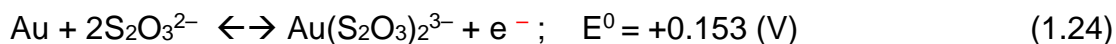
Gold dissolves in alkaline thiosulfate solution, using dissolved oxygen as the oxidant, to form the Au(I) complex, as follows:

$$4Au + 8S_2O_3{}^{2-} + O_2 + 2H_2O \longleftrightarrow 4Au(S_2O_3)_2{}^{3-} + 4OH^- \quad (1.25)$$
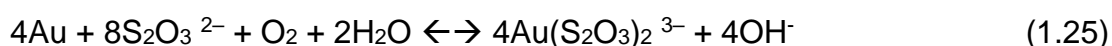
Theoretically, based on Eh–pH data, dissolution should occur over a wide range of pH conditions. However, the reaction proceeds very slowly with oxygen in the absence of a suitable catalyst. Cu(II) is a very effective catalyst for this reaction, provided that it is used in combination with ammonia to stabilize the copper species in solution as Cu(II) tetramine ($Cu(NH_3)_4{}^{2+}$) [27].

$$Cu^{2+} + 4NH_3 \rightarrow Cu(NH_3)_4{}^{2+} \quad (1.26)$$

Gold forms stable complexes in solutions containing ammonia. Therefore, in ammoniacal thiosulfate solution, both the thiosulfate and ammonia species compete to form complexes with gold, according to the following equation:

$$Au(S_2O_3)_2{}^{3-} + 2NH_3 \longleftrightarrow Au(NH_3)_2{}^+ + 2S_2O_3{}^{2-} \quad (1.27)$$
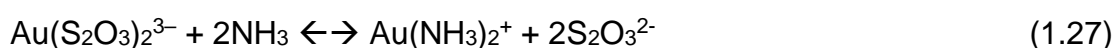
However, the exact values of the stability constants for the preferred thiosulfate and ammonia complexes of gold are in some doubt, and the two values are relatively close, resulting in a lack of clarity and certainty over which species predominates under the conditions applied for gold leaching with thiosulfate. The general consensus is that the thiosulfate complex prevails under the Eh–pH conditions applied for optimal leaching (i.e., a compromise between maximizing gold dissolution rate and minimizing thiosulfate oxidation rate). The Eh–pH diagram that best represents the most likely equilibria for the Au–NH$_3$–S$_2$O$_3{}^{2-}$ - H$_2$O system **(Figure 1.7)** shows that dissolution can occur over a wide range of pH values [28]. Typically, leaching is carried out between pH 9 and 11. Below pH 9, the Cu(I) triamine ($Cu(NH_3)_3{}^+$) complex becomes prevalent, making the copper species less

effective as a catalyst. Commonly, thiosulfate research is conducted using initial solution pH of 10.5 to 11 because the pH decreases during the reaction in batch testing. However, continuously operating thiosulfate systems are likely to be optimized between pH 9.0 and 10.0. Fe(III) species are less suitable as the oxidant in the thiosulfate system because they are unstable above approximately pH 8, depending on the exact solution conditions. The use of Fe(III) with a suitable stabilizer such as oxalate has been proposed [19]. Hydrogen peroxide is also unsuitable because it oxidizes thiosulfate very rapidly and is difficult to stabilize. The chemistry of the ammoniacal copper–thiosulfate system is highly complex, and, despite considerable research and investigation, the exact mechanism of gold dissolution and the catalytic action of Cu(II) species are still not completely understood [28-30]. The major reduction reaction is thought to be as follows:

$$Cu(NH_3)_4{}^{2+} + 5S_2O_3{}^{2-} \longleftrightarrow Cu(S_2O_3)_3{}^{5-} + 4NH_3 + S_4O_6{}^{2-} + e^- \qquad (1.28)$$
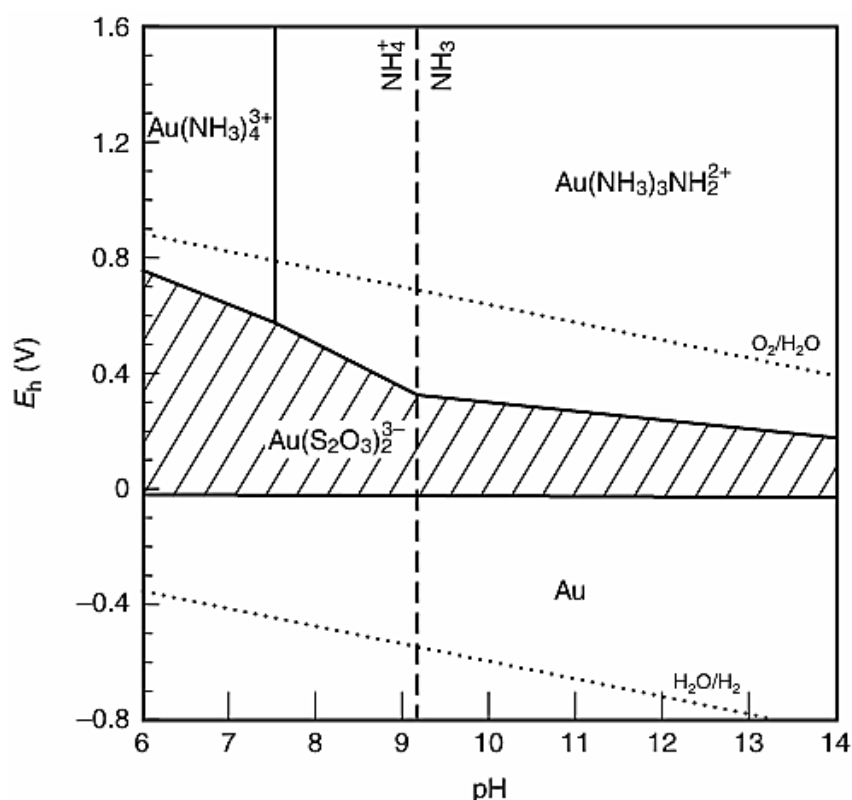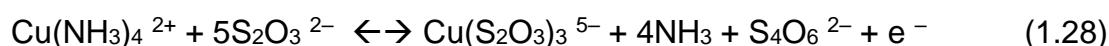
Figure 1.7 Eh–pH diagram for the Au–NH$_3$–S$_2$O$_3{}^{2-}$–H$_2$O system at 25°C: [Au(I)] = 10–5 M, [Na$_2$S$_2$O$_3$] = 0.1 M, [NH$_3$ + NH$_4{}^+$] = 1 M [28]

where the $Cu(S_2O_3)_3{}^{5-}$ species is more stable than the $Cu(NH_3)^{2+}$ complex, under the conditions applied for effective gold dissolution. The reduction of the Cu(II) tetramine species is accompanied by oxidation of thiosulfate to tetrathionate. The oxidant species, Cu(II), is then regenerated by oxygen reduction, according to the following equation:

$$4Cu(S_2O_3)_3{}^{5-} + 16NH_3 + O_2 + 2H_2O \leftrightarrow 4Cu(NH_3)_4{}^{2+} + 8S_2O_3{}^{2-} + 4OH^- \qquad (1.29)$$

Therefore, the overall dissolution reaction for gold in ammoniacal copper–thiosulfate solutions has been proposed as follows [94]:

$$Au + 5S_2O_3{}^{2-} + Cu(NH_3)_4{}^{2+} \leftrightarrow Au(S_2O_3)_2{}^{3-} + 4NH_3 + Cu(S_2O_3)_3{}^{5-} \qquad (1.30)$$

The presence of ammonia is critical to stabilize the Cu(II) species in solution as the Cu(II) tetramine ion, to prevent the formation of $Cu(OH)_2$ and to prevent passivation of the gold surface by preferential adsorption (i.e., avoiding coating with sulfur species). The mechanism of gold leaching in the ammoniacal copper–thiosulfate system is illustrated schematically in **Figure 1.8**. The thiosulfate species is consumed by several possible oxidation and association reactions. These reactions include the formation of various intermediate sulfur species such as trithionate ($S_3O_6{}^{2-}$), tetrathionate ($S_4O_6{}^{2-}$), and other polythionates (e.g., $S_5O_6{}^{2-}$), and finally oxidation to sulfate ($SO_4{}^{2-}$) and, in some cases, elemental sulfur [27-33].

Some examples of the possible oxidation and association reactions are provided as follows:

$$2S_2O_3{}^{2-} + 2Cu^{2+} \leftrightarrow S_4O_6{}^{2-} + 2Cu^+ \qquad (1.31)$$

$$4S_2O_3{}^{2-} + O_2 + 2H_2O \leftrightarrow 2S_4O_6{}^{2-} + 4OH^- \text{ (slow at 25°C)} \qquad (1.32)$$

$$10S_2O_3{}^{2-} + 13O_2 + 4e^- \leftrightarrow 4S_3O_6{}^{2-} + 8SO_4{}^{2-} \qquad (1.33)$$

$$3S_2O_3{}^{2-} + 8Cu^{2+} + 6OH^- \leftrightarrow 2S_3O_6{}^{2-} + 8Cu^+ + 3H_2O \qquad (1.34)$$

$$5S_2O_3{}^{2-} + 3H_2O \leftrightarrow 2S_5O_6{}^{2-} + 6OH^- \qquad (1.35)$$
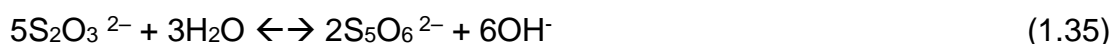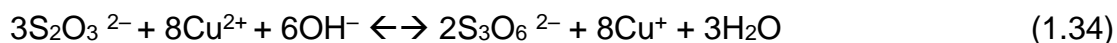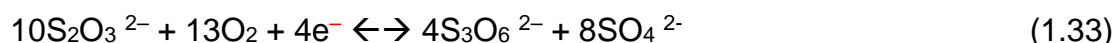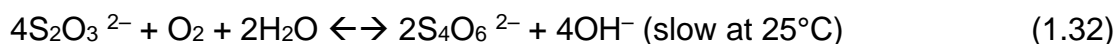
The polythionates, and in particular the trithionate and tetrathionate species, are very detrimental to downstream gold recovery processes because they significantly reduce the loading of gold thiosulfate onto activated carbon and anionic ion exchange resins. Consequently, the formation and effects of these species must be mitigated, or an alternative recovery method must be used. The thiosulfate species can be stabilized to some extent by the addition of small amounts of sulfite ions (SO_3^{2-}), which react with other polythionate and sulfide species in the ore, to regenerate thiosulfate as follows:

$$S_5O_6^{2-} + SO_3^{2-} \longleftrightarrow S_4O_6^{2-} + S_2O_3^{2-} \tag{1.36}$$

$$S_4O_6^{2-} + SO_3^{2-} \longleftrightarrow S_3O_6^{\ 2-} + S_2O_3^{2-} \tag{1.37}$$

$$3SO_3^{2-} + 2S^{2-} + 3H_2O \longleftrightarrow 2S_2O_3^{2-} + 6OH^- + S \tag{1.38}$$
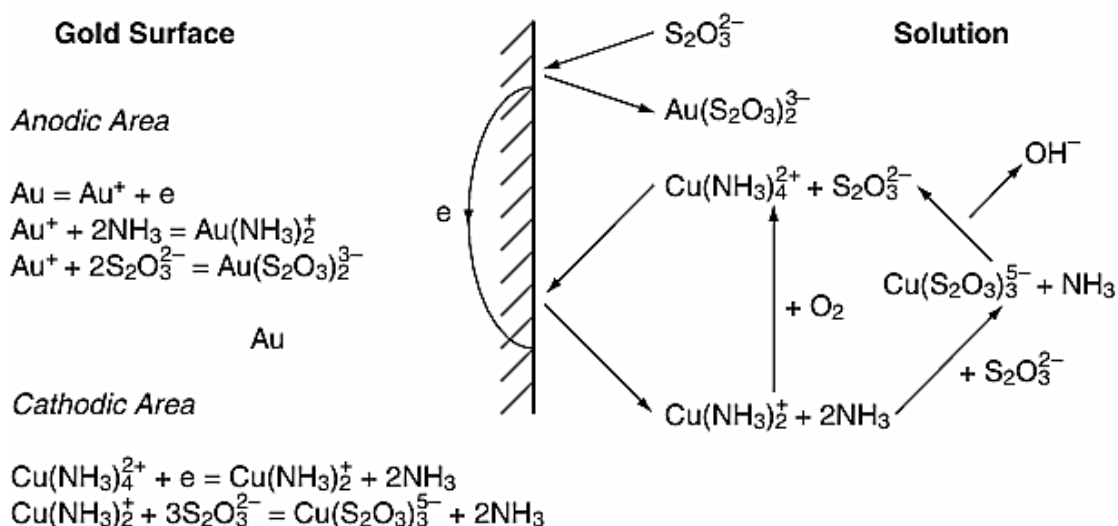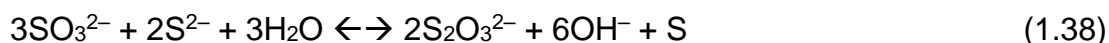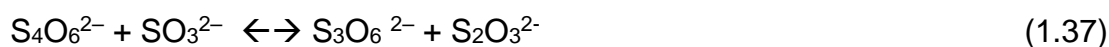
Figure 1.8 Schematic representation of the mechanism of gold leaching with ammoniacal copper–thiosulfate [33].

Other methods of stabilizing thiosulfate have been investigated with varying degrees of success. These methods include the use of multidentate ligands, such as open chain polyamine ligands with 2 to 5 nitrogen donors (e.g., tris[2-aminoethyl]amine) and thiourea to stabilize Cu(II), and oxalate to stabilize Fe(III). The chemistry of these systems is complex and, in the case of

thiourea, is further complicated by the fact that thiourea forms stable complexes with gold [34].

As thiosulfate is oxidized and the thiosulfate concentration in solution decreases, there is a risk that gold will reprecipitate out of solution onto ore constituents. There is evidence to suggest that gold will remain in solution as the thiosulfate complex down to 2 to 3 g/L $S_2O_3^{2-}$, however, this depends on specific solution conditions (e.g., temperature, pH, Eh, [NH_3], etc.) [35].

Silver, silver chloride, and silver sulfide all dissolve readily in thiosulfate media. The addition of sulfite species helps to prevent the precipitation of silver as insoluble sulfide.

The rate of dissolution is dependent on thiosulfate and Cu(II) concentrations, up to a certain point. Thiosulfate concentrations ranging from 0.05 to 2.0 M $S_2O_3^{2-}$ have been used for investigations of gold leaching systems, but most researchers have focused on a thiosulfate concentration range of 0.1 to 0.2 M $S_2O_3^{2-}$ (i.e., about 11 to 22 g/L). Both sodium thiosulfate ($Na_2S_2O_3$) and ammonium thiosulfate((NH_4)$_2S_2O_3$) have been used as the primary reagent.

There is the obvious benefit to using ammonium thiosulfate in cases where the leaching system is ammoniacal copper–thiosulfate in that it provides some of the ammonia required. Sodium thiosulfate may be preferable to use in applications where copper is not used as the catalyst. Copper concentrations applied in these investigations range from 0.0001 to 0.02 M; however, most commonly, Cu(II) concentration of 0.0005 to 0.002 M (i.e., 30 to 120 mg/L Cu^{2+}) is targeted. Unfortunately, the rate of thiosulfate oxidation increases with increasing Cu(II) concentration when all other parameters are held constant, and therefore from a practical standpoint this limits the maximum Cu(II) concentration that can be applied [30]. Ammonia concentration does not have any impact on gold dissolution rates, but it does have a big impact on the overall system effectiveness by stabilizing copper and reducing the thiosulfate oxidation rate. Ammonia concentrations between 0.2 to 0.4 M NH_3 have typically been applied, but up to 2 M NH_3 has been used for investigative work.

Ammonia is lost by volatilization from solution, which is exacerbated by sparging of air or oxygen into the solution phase, and by oxidation reactions. Increased temperature does have a beneficial effect on the rate of gold extraction but also increases the rate of thiosulfate oxidation and the rate of ammonia loss from solution by volatilization. Most investigative work has been done at or slightly above ambient temperatures (i.e., 15°C to 30°C). Elevated temperature operation has been investigated up to 80°C, and a process using thiosulfate at an elevated temperature of 60°C has been proposed, in conjunction with the use of sulfite to stabilize the thiosulfate species at the higher temperature [35]. It has been reported that the presence of carbonates and bicarbonates in the ore can result in excessive oxidation of thiosulfate.

1.4.2.3 THIOUREA

Thiourea has been proposed as an alternative to cyanide for the treatment of sulfidic, cyanide-consuming ores, and for use in locations where environmental concerns make the use of cyanide difficult. Thiourea is a relatively nontoxic reagent, which behaves as a plant fertilizer in the environment, giving the impression that it might be an attractive alternative to cyanide in environmentally sensitive areas. On the other hand, the reagent is suspected to be carcinogenic and is capable of dissolving heavy metals in addition to gold and silver, which presents many similar environmental problems to cyanidation for the handling and disposal of effluents. In addition, thiourea is oxidized and consumed very rapidly under the conditions required for leaching, resulting in prohibitively high reagent costs in most applications, particularly when compared with cyanidation. Thiourea leaching has been used to treat an antimony-rich concentrate in New South Wales (Australia) and has been investigated as a process option for the treatment of several other ores, but no large-scale commercial processes have been developed [36-39].

Thiourea (NH_2CSNH_2) is an organic compound which dissolves readily in acidic solution in a stable molecular form. Gold dissolves in acidic thiourea solution to form a stable complex:

$$Au(CS(NH_2)_2)_2{}^+ + e^- \longleftrightarrow Au + 2CS(NH_2)_2; \; E^0 = -0.38 \; (V) \tag{1.39}$$
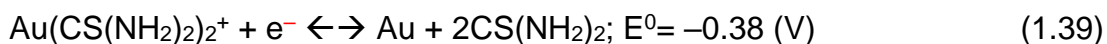
where the pK value for the gold–thiourea complex is 21.75. In this system, no oxide layer is formed as a result of the relatively low solution potentials that can be applied, and no passivation of gold occurs. **Figure 1.9** shows current–potential curves for leaching in thiourea solution. This indicates that gold dissolution will only occur at an acceptable rate if the solution potential is greater than approximately 0.5 V. Consequently, air and oxygen are unsuitable oxidants, and stronger oxidants, such as Fe(III), hydrogen peroxide, or ozone, are required to enable the reaction to proceed at a sufficient rate to achieve adequate gold extraction within practical time scales [40]. The overall equation for the dissolution reaction is:

$$2Au + 4CS(NH_2)_2 + 2Fe^{3+} \longleftrightarrow 2Au(CS(NH_2)_2)_2{}^+ + 2Fe^{2+} \tag{1.40}$$
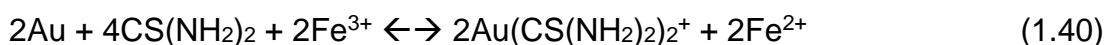
Silver dissolves in aqueous thiourea solutions similarly to gold, as follows:

$$2Ag + 4CS(NH_2)_2 + 2Fe^{3+} \longleftrightarrow 2Ag(CS(NH_2)_2)_2{}^+ + 2Fe^{2+} \tag{1.41}$$
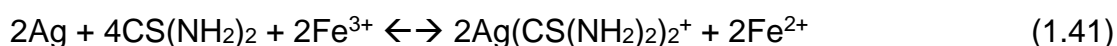
for which pK= 13.1.
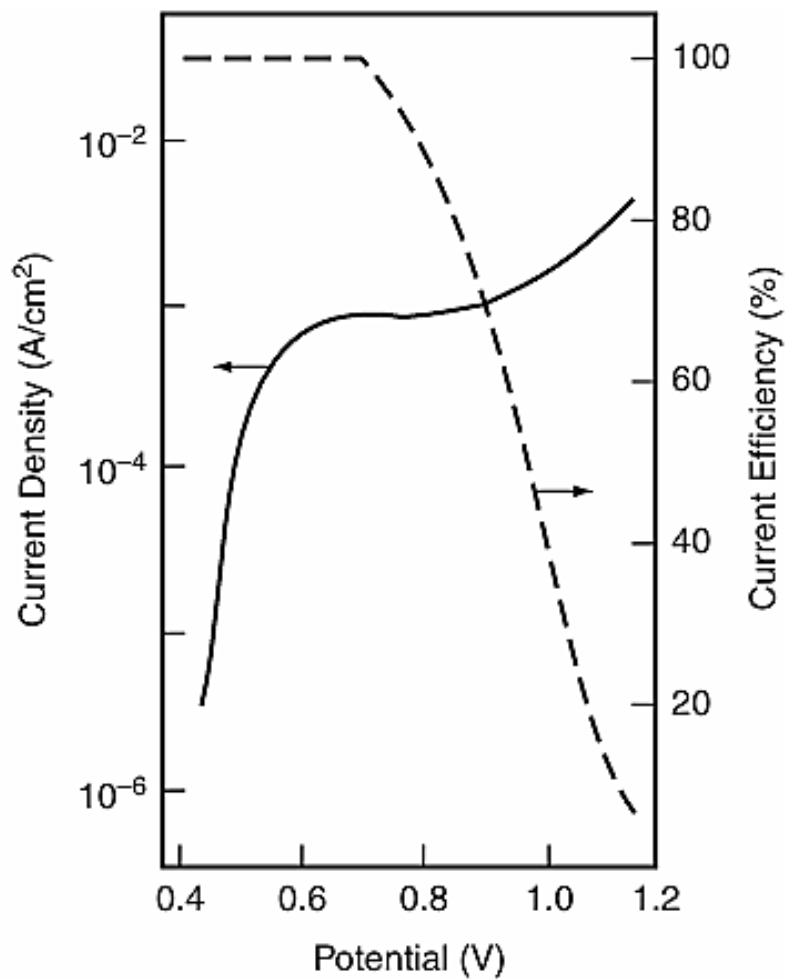
Figure 1.9 Effect of potential on the anodic dissolution of gold and the current efficiency of its dissolution into a solution containing 0.1 M sulfuric acid and 0.1 M thiourea at 30°C [42].

The pH at which thiourea leaching may be carried out is limited at the upper end by two factors:

1. Precipitation of Fe(III) hydroxide above approximately pH 3
2. Sharp increase in the kinetics of thiourea oxidation above pH 3.5–4

Consequently, leaching is generally carried out at a pH of 1.4 to 1.8 [38-39]. Leaching rates in thiourea solutions are very fast—much faster than cyanide dissolution and at least comparable to the other leaching methods available. The rate of gold dissolution in acidic thiourea solutions is usually controlled by the diffusion of reactants to the gold surface and is consequently related to the concentrations of Fe(III), formamidine disulfide, and thiourea species. Formamidine disulfide plays an important role in the kinetics of thiourea leaching, because optimum kinetics are achieved when approximately half the thiourea present in solution is converted to this species [38]. The addition of sodium sulfite (2.5 g/t Na2SO3) to thiourea leach solutions has been shown to be beneficial by reducing thiourea consumption and increasing the gold dissolution rate [41].

1.4.2.4 THIOCYANATE

Gold dissolves in aqueous, acidified thiocyanate (SCN^-) solutions to form both the Au(I) and Au(III) complexes, depending on the solution potential [42]:

$$Au(SCN)^{2-} + e^- \leftrightarrow Au + 2SCN^-; E^0 = +0.662 \text{ (V)} \tag{1.42}$$

$$Au(SCN)_4^- + 3e^- \leftrightarrow Au + 4SCN^-; E^0 = +0.636 \text{ (V)} \tag{1.43}$$
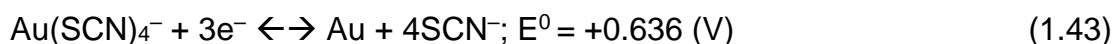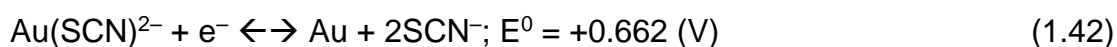
The stability constants for the two complexes, $Au(SCN)_2^-$ and $Au(SCN)_4^-$, are approximately 10^{17} and 10^{42} respectively, and $Au(SCN)_4^-$ is by far the most stable. Fe(III) is the most suitable oxidant for the reaction since the kinetics of dissolution are prohibitively slow if oxygen is used and thiocyanate is oxidized very rapidly by hydrogen peroxide. In addition, the stability of the thiocyanate ion is increased in the presence of Fe(III), presumably due to the many complexes it forms with these ions, as follows:

$$Fe^{3+} + n\ SCN^- \longleftrightarrow Fe(SCN)_n^{(3-n)} \tag{1.44}$$
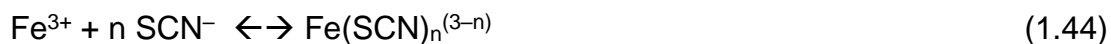
where n =1 to 5.

Figure 1.10 shows the Eh–pH diagram for the Au–SCN–H_2O system under atmospheric conditions. The pH range for the reaction is limited at the low end (below about pH 1) by the reaction:

$$SCN^- + H^+ \longleftrightarrow HSCN;\ pK = 0.85 \tag{1.45}$$

Above about pH 3, Fe(III) is precipitated by hydrolysis. Consequently, the optimum pH for gold leaching is in the range of 1.5 to 2.5.

The stability of thiocyanate species is strongly potential dependent, with stability achieved below approximately 0.64 V (vs. SHE). On the other hand, a potential >0.64 V is required to achieve satisfactory gold leaching rates at practical thiocyanate concentrations. In practice, a compromise between these two requirements is required to achieve acceptable gold leaching rates and to avoid excessive oxidation of thiocyanate, according to the following reactions:

$$SCN^- + 4H_2O \longleftrightarrow SO_4^{2-} + CN^- + 8H^+ + 6e^- \tag{1.46}$$

$$SCN^- + 5H_2O \longleftrightarrow SO_4^{2-} + CNO^- + 10H^+ + 8e^- \tag{1.47}$$

$$SCN^- + 7H_2O \longleftrightarrow NH_3 + CO_3^{2-} + SO_4^{2-} + 11H^+ + 8e^- \tag{1.48}$$
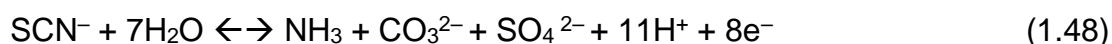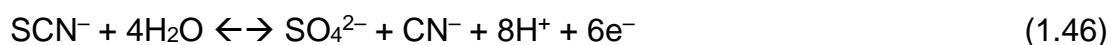
A number of other intermediate species also may be formed, including trithiocyanate $(SCN)_3^-$ and thiocyanogen $(SCN)_2$.

The rate of gold dissolution increases with increasing thiocyanate concentration and, to a lesser extent, Fe(III) concentration. Thiocyanide concentrations of 0.5 to 5 g/L (0.01 to 0.10 M) and Fe(III) concentrations of 6 to 12 g/L (0.1 to 0.2 M) have been used in laboratory column leach testing and small-scale pilot work. Because the thiocyanate consumption rises with increasing thiocyanate concentration, it is important to maintain sufficient thiocyanate concentration for effective gold dissolution but no excess. The oxidant, Fe(III), must be regenerated, and this can be accomplished using either air and/or oxygen or by some other means [31].

 Increasing temperature increases gold dissolution rate but also significantly increases the rate of thiocyanate consumption, and, in view of the high reagent consumptions even at ambient temperatures, elevating leaching temperature is not likely to be a viable option.
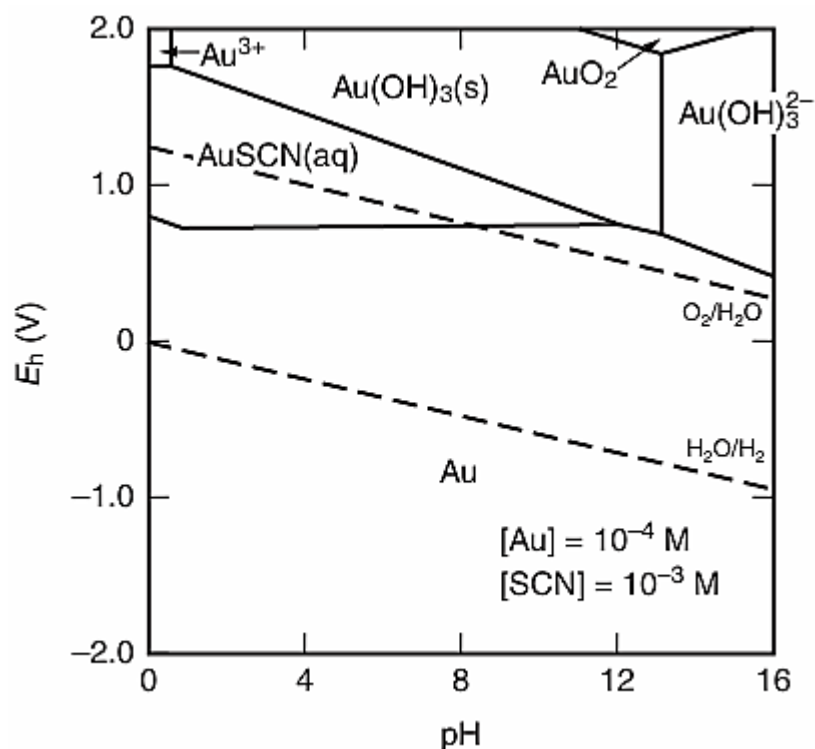
Figure 1.10 Eh–pH diagram for the Au–SCN–H$_2$O system at 25°C [43]

1.4.2.5 OTHER LIXIVIANTS

Other halide systems, such as bromine–bromide, iodine–iodide, and bromine–chloride, are capable of dissolving gold at very fast rates, as predicted by the electrode potentials of the relevant reduction reactions, for example:

$$Au + 2Br^- + Br_2 \leftrightarrow AuBr_4^- + e^- ; E^0 = +0.95 \text{ (V)} \quad (1.49)$$

$$Au + 2I^- + I_2 \leftrightarrow AuI_4^- + e^- ; E^0 = +0.69 \text{ (V)} \quad (1.50)$$
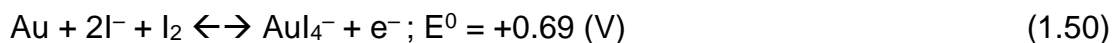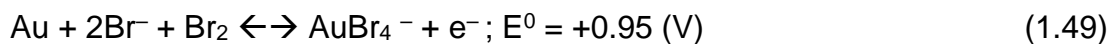
These systems are strongly oxidizing, and dissolution rates are typically several orders of magnitude faster than those achieved with cyanide and oxygen under ambient conditions [31]. In addition, they are capable of dissolving many sulfide minerals, and bromine chloride solution has been used commercially on a small scale for leaching of refractory gold-bearing materials. The dissolutions rate of gold in halide media is strongly dependent on the concentration of complexant and oxidant and can be increased significantly at elevated temperatures (e.g., 150°C to 180°C) [44]. Unfortunately, the commercial application of bromine and iodine solutions for gold leaching is restricted by the high cost of the reagents, the high cost of materials of construction to withstand the severe process conditions, and industrial hygiene and health issues associated with their use.

Any process developed must be able to effectively regenerate the reagent to make it economic. One possible means of achieving this is by electrolytically regenerating the bromine or iodine from solution, with the potential for simultaneous recovery of gold and other metals [45-46]. Other leaching systems using cyanamide, cyanoform, organic nitrile, and malononitrile related compounds for gold dissolution have been proposed; however, despite some potential advantages, there is little prospect for commercial development, and they are currently of academic interest only [31, 47].

1.4.3 REFRACTORY GOLD IN PYRITE

The sulfide mineral most commonly associated with gold, pyrite is very common throughout the world and is ubiquitous in sulfide orebodies. Although not usually an accessory mineral in primary igneous rocks, it is common in ore veins and metamorphic ores.

Pyrite has a commonly displayed cubic cleavage, a brassy yellow color, and a metallic luster, which is sufficiently close to that of gold to warrant the phrase "fool's gold." The density of pyrite is 4,800 to 5,000 kg/m^3, and it is relatively hard, with a value of 6 to 6.5 on the Mohs scale. Pyrite is a semiconductor

with either n-type or p-type properties (**Table 1.2**). It can occur in cubic or framboidal habits, each of which has different reactivity in aqueous solution.

Pyrite is a very stable mineral in aqueous solutions, and its high standard reduction potential results in unreactivity under the mildly oxidizing conditions typical of cyanide leaching. Consequently, fine gold inclusions in pyrite require more extreme grinding and/or strongly oxidizing conditions to liberate the gold. Gold can occur in solid solution (i.e., invisible) within pyrite grains at concentrations from <0.2 to 132 ppm [48].

In contrast, when gold is relatively coarse and accessible to cyanide leach solutions, this unreactivity is an advantage as reagent consumptions are not increased by a side reaction with pyrite. Consequently, pyrite is usually only a problem in processing if it affects gold liberation; it is rarely a significant cyanide (cyanide consumer). Leaching of fine gold grains contained within pyrite is a major difficulty in gold ore treatment and this is an important source of refractory gold.

Gold can occur in many textural associations with pyrite (and arsenopyrite), as shown schematically in **Figure 1.11**. For gold–sulfide association types 1 to 3 in the figure, gold may be readily liberated. However, for types 5, 6, and possibly 4, gold may remain unliberated even at fine sizes.

Table 1.2 Electronic and Structural properties of selected sulfide and oxide minerals [49].

Formula	Name	Resistivity (Ωm)	Usual Conductor Type	Structure	Ionic Structure
Cu_5FeS_4	Bornite	10^{-3} to 10^{-6}	p	Tetragonal	$(Cu^+)_5Fe^{3+}(S^{2-})_4$
Cu_2S	Chalcocite	4×10^{-2} to 8×10^{-5}	p	Orthorhombic	$(Cu^+)_2S^{2-}$
$CuFeS_2$	Chalcopyrite	2×10^{-4} to 9×10^{-3}	n	Tetragonal	$Cu^+Fe^{3+}(S^{2-})_2$
CuS	Covellite	8×10^{-5} to 7×10^{-7}	Metallic	Hexagonal	$(Cu^+)_2(S^{2-})_2$
PbS	Galena	1×10^{-5} to 7×10^{-6}	n & p	Cubic	$Pb^{2+}S^{2-}$
MoS_2	Molybdenite	7.5 to 8×10^{-3}	n & p	Hexagonal	$Mo^{4+}(S^{2-})$
FeS_2	Pyrite	3×10^{-2} to 1×10^{-3}	n & p	Cubic	$Fe^{2+}(S^{2-})_2$
ZnS	Sphalerite	3×10^{-3} to 1×10^{-4}	—	Cubic	$Zn^{2+}S^{2-}$
SnO_2	Cassiterite	10^2 to 10^{-2}	n	Tetragonal	$Sn^{4+}(O^{2-})_2$
Cu_2O	Cuprite	10^{11} to 10	p	Cubic	$(Cu^+)_2O^{2-}$
Fe_2O_3	Hematite	2.5×10^{-1} to 4×10^{-2}	n & p	Trigonal	$(Fe^{3+})_2(O^{2-})_3$
Fe_3O_4	Magnetite	2×10^{-4} to 4×10^{-5}	n & p	Cubic	$Fe^{3+}[Fe^{3+}Fe^{2+}](O^{2-})_4$
MnO_2	Pyrolusite	10^{-1} to 10^{-3}	n	Tetragonal	$Mn^{4+}(O^{2-})_2$
TiO_2	Rutile	10^4 to 10	n & p	Tetragonal	$Ti^{4+}(O^{2-})_2$
UO_2	Uraninite	20 to 4×10^{-1}	—	Cubic	$(U^{4+})_{1-x}(O^{2-})_{2+x}$

NOTE: Dashes indicate information is not applicable.

For example, Plate 7 shows a gold grain within a coarser pyrite grain (type 3). Increasingly, ores containing type 6 mineralization are being treated (e.g., Carlin-type ores) in which both coarse cubic pyrite (10 to 100 μm) and more abundant fine spheroidal pyrite (1 to 10 μm) occur.

Gold grains are typically <1 μm in diameter and occur within pyrite grains, as coatings on pyrite, and dispersed in grains of amorphous carbon. These ores may exhibit preg-robbing characteristics due to the presence of both carbon and ultrafine spheroidal pyrite. An oxidative pretreatment step is usually required to increase gold extraction for these ores. Pyrite can also be recovered by flotation as a by-product to gold , and the concentrate is sometimes roasted to produce sulfuric acid (H_2SO_4) and to liberate contained gold. In the past, elemental sulfur has also been produced commercially from pyrite.
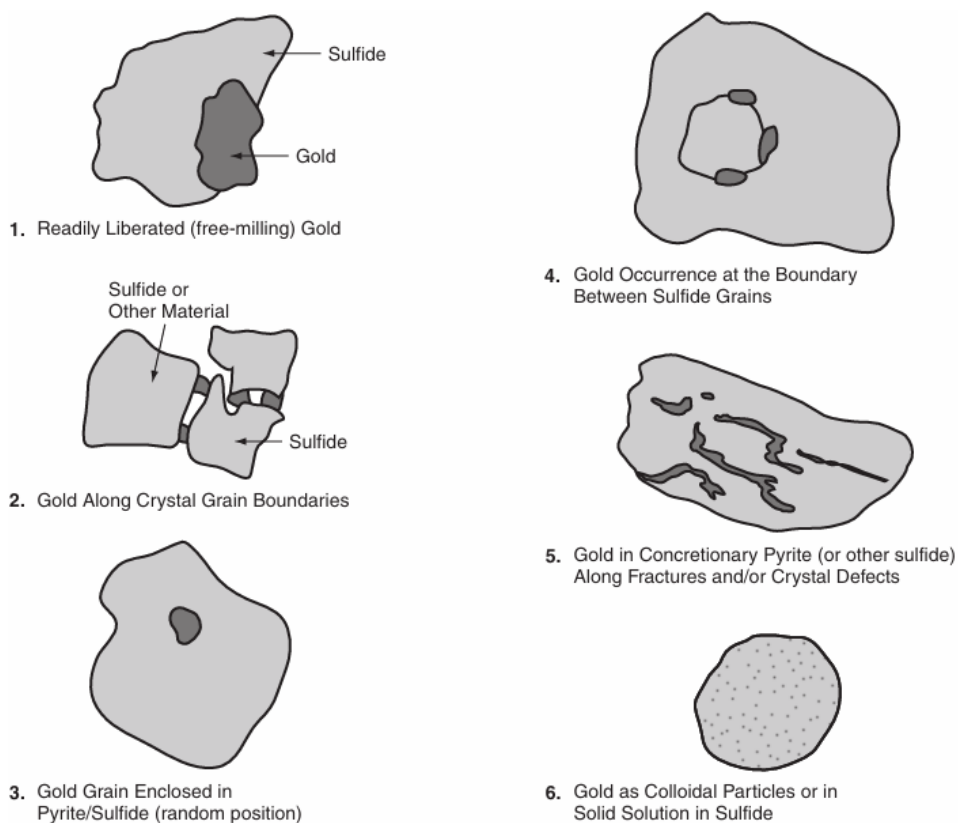
Figure 1.11 Schematic representation of types of gold associations with sulfide minerals. (*From the Textbook Chemistry of Gold Extraction, J.O Marsden)*

In the gold ores of the Barberton Mountain land (Transvaal, South Africa), gold is present as free gold, and gold associated with pyrite and arsenopyrite (e.g., at Fairview 50% with pyrite, 20% with arsenopyrite, and 30% free). Although some coarse gold is present, the majority of gold occurs as fine (5 to 30 μm) inclusions in the sulfides, leading to poor cyanidation performance. The remainder occurs interstitially between sulfide grains or in the no sulfide gangue. The gold usually contains about 10% silver, although some pink-colored gold grains containing nickel and antimony have been detected.

The refractory sulfide components of these ores must be oxidized prior to cyanide leaching to achieve acceptable gold recovery. This can be achieved with or without prior concentration by flotation. The flowsheet options are summarized in **Figure 1.12.**
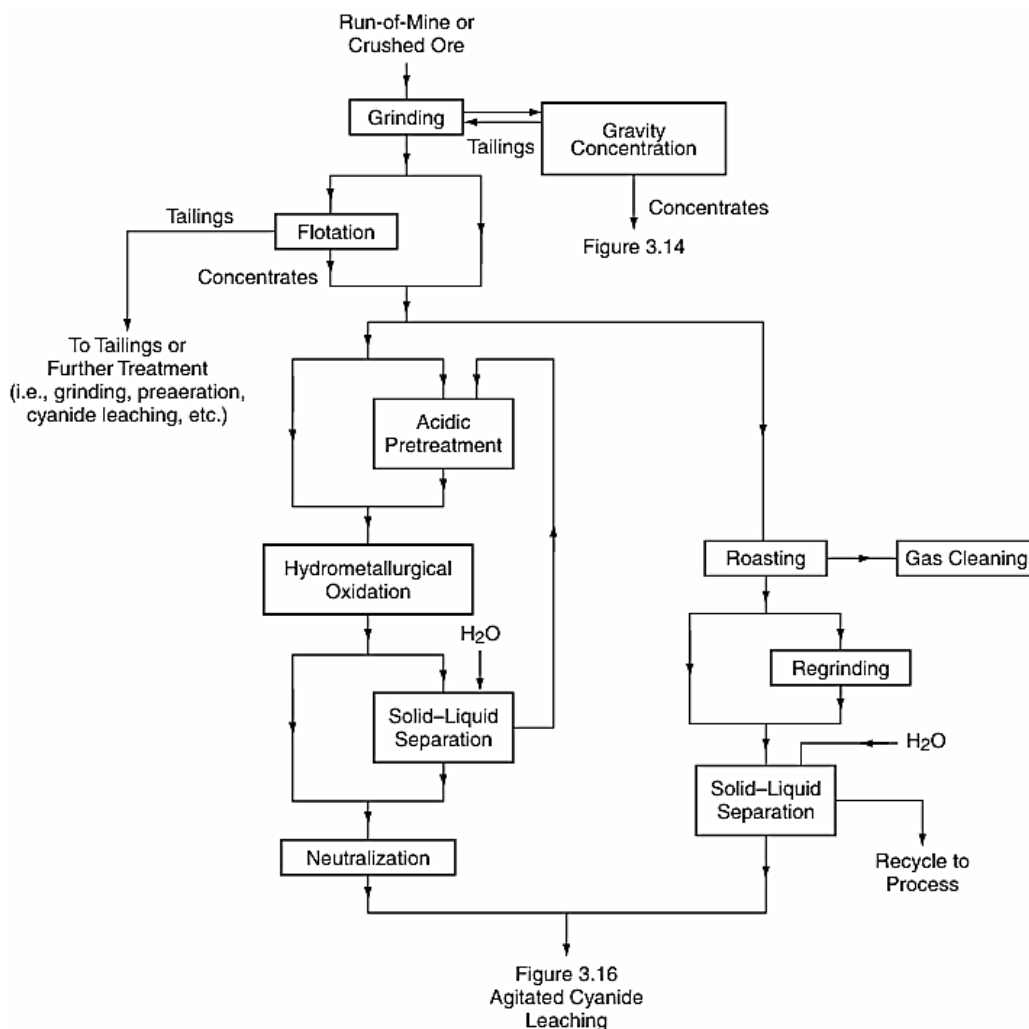
Figure 1.12 Flowsheet options for refractory sulfidic ores

This is suitable for refractory sulfide ores that are not amenable to concentration processes because of one of the following:

1. Gold recovery to the concentrate is unacceptably low and the gold in the tailings is refractory.
2. The concentrate produced is less suitable for oxidation than the whole ore, for example, the sulfide sulfur content is too high.

Pretreatment with acid may be required prior to oxidation to neutralize acid consumers. Options available for sulfide oxidation include pressure oxidation, roasting, and biological oxidation. The oxidation products are then neutralized (with or without prior solid–liquid separation) and cyanide leached.

Flotation can be included in this flowsheet as a method of smoothing and optimizing the sulfide content of the feed to the oxidation circuit. Concentrates may be stored and reclaimed as needed to control the feed to the oxidation circuit.

1.4.4 ALUMINUM PRECIPITATION

The use of aluminum for precipitation of gold from alkaline cyanide solutions was originally proposed and patented by Moldenhauer in 1893 [50]. Despite some advantages over zinc, the process has not been applied widely because of the more favorable eco nomics of zinc precipitation. Aluminum was used commercially at Nipissing and at the Deloro smelter (both in Canada) and has recently been tested for the recovery of gold and silver from various leaching systems other than cyanide. The oxidation of aluminum in aqueous solution is given by:

$$Al^{3+} + 3e \leftrightarrow Al \tag{1.51}$$

where

$$E = -1.66 + 0.0197 \log [Al^{3+}] \ (V)$$

The aluminate ion (AlO_2^-) can hydrolyze further to form a relatively insoluble hydroxide:

$$AlO_2^- + 2H_2O \longleftrightarrow Al(OH)_3 + OH^- \tag{1.52}$$

The equilibrium of this reaction can be kept to the left, favoring the aluminate species, by keeping the pH >12 to avoid passivation of the aluminum surface by hydroxide layer formation. The overall stoichiometry of the gold precipitation reaction is:

$$3Au(CN)_2^- + Al + 4OH^- \longleftrightarrow 3Au + 6CN^- + AlO_2^- + 2H_2O \tag{1.53}$$

Several other stoichiometries have been proposed based on plant observations, which take into account some of the many side reactions that may occur, but these are usually dependent on specific solution conditions [51].

The stoichiometric requirement of aluminum is less than zinc, because the metal reduction is a three-electron reaction compared with the two-electron reaction for zinc. Also, it can be seen from Equation (1.53) that the gold cyanide reduction yields 2 moles of cyanide for every mole of gold, unlike the zinc precipitation reaction that actually consumes 2 additional moles of cyanide for every mole of gold precipitated. Consequently, the cyanide is effectively regenerated by aluminum precipitation.

An important disadvantage of aluminum is that lime cannot be used for pH control because highly insoluble calcium aluminate is formed, which tends to foul filters and contaminates the final gold precipitate, as follows:

$$2AlO_2^- + Ca(OH)_2 \longleftrightarrow CaAl_2O_4 + 2OH^- \tag{1.54}$$
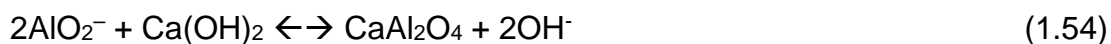
Therefore, solutions containing even moderate calcium content would have to be treated for calcium removal prior to aluminum precipitation. This could be achieved by the addition of sodium carbonate to precipitate calcium carbonate, with the added benefit of a net increase in pH. Aluminum precipitates gold much more slowly than zinc, despite a larger electro chemical driving force, due to the faster dissolution rate of zinc in complexing cyanide solution. It is far less effective than zinc for recovery from solutions

containing little or no silver but works quite well for the precipitation of silver, or both gold and silver, from solutions containing >50 g/t silver. Deaeration of solutions is required prior to precipitation because of the rapid oxidation of aluminum in the presence of oxygen; however, the metal is less affected by "poisoning" ions, such as sulfide, arsenic, and antimony, than is zinc.

1.4.5 PREVIOUS RESEARCH

A previous study conducted by Jeon et. al, 2022 T describes a simple and highly efficient technique for Au(I) ion recovery from thiosulfate medium based on galvanic interactions between aluminum (Al) and activated carbon (AC) under various industrially relevant conditions. The results showed that when only AC or Al are used, Au recoveries were negligible under the following conditions: 0.15 g of AC or Al with 10 ml thiosulfate solution containing 100 mg/l of Au ions at 25 °C for 24 h with 120 rpm. With Al (0.15 g)-AC (0.15 g) mixture, however, Au recovery significantly increased reaching over 99% as shown in **Figure 1.13.**

	Al	Fe	Cu	AC	Al+Fe	Al+Cu	Al+AC	Fe+AC	Cu+AC
Au_R :1	0	0	0	0	0.15	0.5	0.99	0.02	0
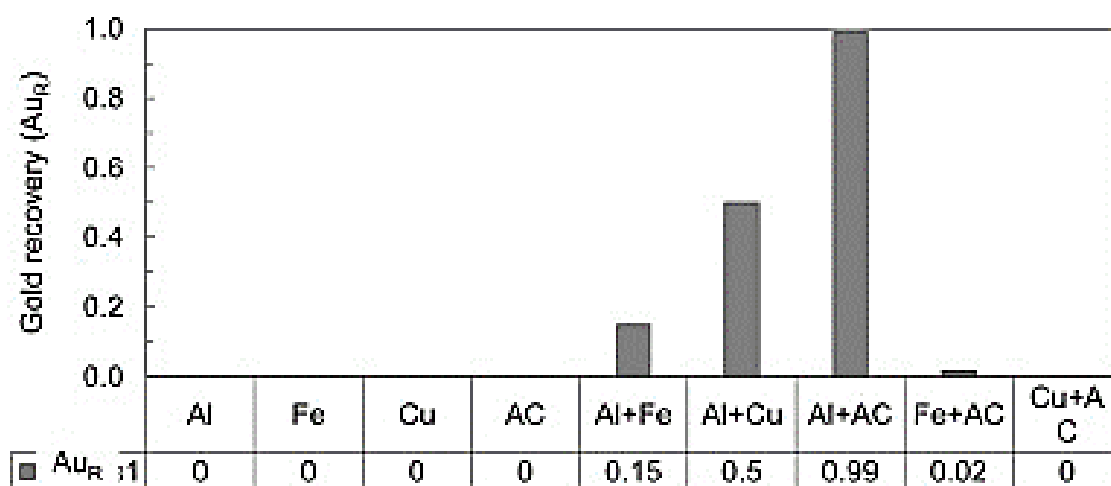
Figure 1.13 Recovery of Au ions from ammonium thiosulfate solution by various materials and their mixtures (Al, Fe, Cu, AC, Al–Fe, Al–Cu, Al-AC, Fe-AC, and Cu-AC) (Note that AC denotes activated carbon) Jeon et. al, 2022.

The effects on Au recovery of various parameters, including recovery time, dissolved oxygen, mixing ratio of Al and AC, solid-to-liquid ratio, and temperature, were also evaluated and the highest Au recovery was obtained

under the following conditions: 1 h recovery time without oxygen, 1:1 of Al and AC, and 0.3 g/10 ml at 25 °C. Using scanning electron microscopy with energy dispersive spectroscopy coupled with electrochemical experiments, the critical role of AC on Au recovery was identified as a reduction mediator between Al and Au(I)-thiosulfate complex in the solution as shown in **Figure 1.14**.
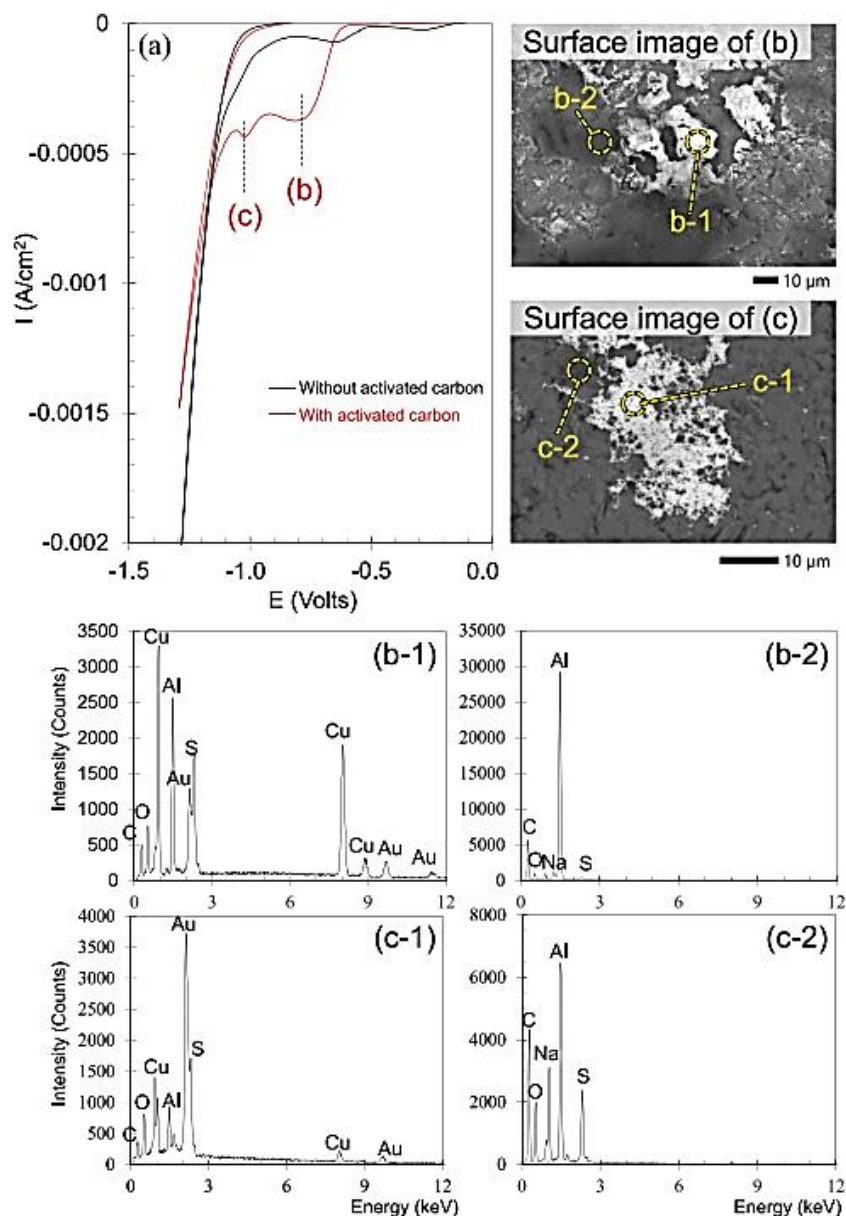
Figure 1.14   The linear voltammetry sweep using oxidized Al working electrode with and without AC, and point analysis of the surface of the working electrode after chronoamperometry at (b) -0.8 V, and (c) -1.0 V.

Finally, this previous research proposed a sequence of processes to explain Au recovery by Al-AC in thiosulfate medium: (i) AC is lodged into Al oxide micro-cracks or "attached" on Al oxide film, (ii) electrons moved from Al to AC, (iii) Au(I) ions receive electrons from AC, and (iv) metallic Au is cemented on AC.

1.4.6 SUMMARY

In refractory ores, sulfide-type gold ores, especially gold-pyritic ore, account for a substantial proportion of gold resources (i.e., about 22%). The recovery of gold from gold-pyritic ore has recently become a valuable study in the resources field. Also, it poses environmental hazards upon storing these sulphide-rich minerals, as these minerals potentially form highly acidic water, commonly known as acid mine drainage (AMD). Currently, upon processing refractory gold ore, conventional processing is done through roasting followed by the cyanidation process. In the later leaching process, where cyanide is conventionally employed, the solvent poses health and environmental hazards due to its potential toxicity if not appropriately managed.

For these reasons, many studies have been conducted to find alternative solvents to mitigate the risk of using cyanide, such as thiourea, thiocyanate, halogen-based and thiosulfate. Among the alternatives, ammonium thiosulfate has been highlighted because it has been shown to have higher selectivity and leaching rate to gold, and most importantly, it is less corrosive and non-toxic to humans.

Amongst all pretreatment processes, roasting has been conventionally employed to convert pyrite into various porous iron oxides such as hematite (Fe_2O_3) and magnetite (Fe_3O_4), so that gold grains can be exposed to leach solutions, making it susceptible to extraction.

To further explore the potential of the research conducted by Jeon et al., 2022, this research is focused on investigating the behavior of iron oxides as electron mediators with zero-valent aluminum in gold-copper ammoniacal thiosulfate systems.

1.4.7 REFERENCES:

[1] Weast, R.C. 1981. *Handbook of Chemistry and Physics.* 62nd edition. Boca Raton,FL: CRC Press.

[2] Smith, R.M., and A.E. Martell. 1976. *Critical Stability Constants.* Volume 4. NeYork: Plenum Press.

[3] Huiatt, J.L., J.E. Kerrigan, F.A. Olson, and G.L. Potter. 1983. Cyanide from mineral processing. *Proceedings of Workshop Sponsored by National Science Foundation, USBM* & *Industry.* Salt Lake City, UT: Utah Mining and Mineral Resources Research Institute.

[4] Bellomo, A. 1970. Formation of copper(II), zinc(II), silver(II) and lead(II) ferrocyanide.*Talanta* 7:1109–1114.

[5] Adams, M.D. 2001. A methodology for determining the deportment of cyanide losses in gold plants. *Minerals Engineering* 14(4):383–390.

[6] Finkelstein, N.P. 1972. The chemistry of the extraction of gold from its ores.
Pages 284–351 in *Gold Metallurgy on the Witwatersrand.* Edited by R.J. Adamson.Cape Town, South Africa: Cape & Transvaal Printers Ltd.

[7] Adams, M.D. 1990. The chemical behaviour of cyanide in the extraction of gold.1. Kinetics of cyanide loss in the presence and absence of activated carbon. *Journal of South African Institute of Mining and Metallurgy* 90(2):37–44.

[8] Wang, X., and K.S.E. Forssberg. 1990. The chemistry of cyanide–metal complexesin relation to hydrometallurgical processes of precious metals. *Mineral Processing*& *Extractive Metallurgy Reviews* 6:81–125.

[9] Dean, J.A., editor. 1985. *Lange's Handbook of Chemistry.* 13th edition. New York:
McGraw-Hill.

[10] Sillen, L.G., and A.E. Martell. 1964. *Stability Constants of Metal–Ion Complexes.* Publication No. 17. London: The Chemical Society.

[11] Sillen, L.G., and A.E. Martell. 1970. *Stability Constants of Metal–Ion Complexes.*Supplement No. 1. Publication No. 25. London. The Chemical Society.

[12] Sharpe, A.G. 1976. *The Chemistry of Cyano-Complexes of the Transition Metals.*London: Academic Press.

[13] Perrin, D.D. 1964. Pages 56–66 in *Organic Complexing Reagents: Structures, Behaviour and Application to Inorganic Analysis.* New York: Wiley Interscience.

[14] Capone, S., A. Robertis, and S. Sammartano. 1986. Studies on hexacyano-ferrate(II) complexes: Formation constants for alkali metals. *Thermochemica Acta* 112(3):1–14.

[15] Hogfeldt, E. 1982. *Stability Constants of Metal–Ion Complexes. Part A: Inorganic Ligands.* No. 21. New York: Pergamon Press.

[16] Nicol, M.J. 1980. The anodic behaviour of gold. Part II. Oxidation in alkaline solutions.*Gold Bulletin* 13:105–111.

[17] Nicol, M.J., C.A. Fleming, and R.L. Paul. 1987. The chemistry of the extraction of gold. Pages 831–905 in *The Extractive Metallurgy of Gold.* Monograph M7. Edited by G.G. Stanley. Johannesburg: South African Institute of Mining and Metallurgy.

[18] Jeffrey, M., and I. Ritchie. 2000. Electrochemical aspects of gold cyanidation.
Pages 176–186 in *Proceedings of Electrochemistry in Mineral & Metal Processing V*. Edited by R. Woods and F.M. Doyle. Pennington, NJ: The Electrochemical Society.

[19] Jeffrey, M.I., I. Chandra, I.M. Ritchie, G.A. Hope, K. Waling, and R. Woods. 2005. Innovations in gold leaching research and development. Pages 207–221 in *Innovations in Natural Resource Processing: Proceedings of Jan D. Miller Symposium*. Edited by C.A. Young, J.J. Kellar, M.L. Free, J. Drelich, and R.P. King. Littleton, CO: SME.

[20] Habashi, F. 1966. The theory of cyanidation. *Transactions of the Mineralogical Society of AIME* 235:236–239.

[21] Zurilla, R.W., R.K. Sen, and E.Yeager. 1978. The kinetics of oxygen reduction reaction on gold in alkaline solution. *Journal of Electrochemical Society* 125:1103–1109.

[22] Kirk, D.W., F.R. Foulkes, and W.F. Graydon. 1978. A study of anodic dissolution of gold in aqueous alkaline cyanide. *Journal of Electrochemical Society* 125:1436–1443.

[23] Ball, S.P., A.J. Monhemius, and P.J. Wyborn. 1989. The use of inorganic peroxides as accelerators for gold heap leaching. Pages 149–164 in *Precious Metals '89.* Edited by M.C. Jha and S.D. Hill. Warrendale, PA: TMS.

[24] Guzman, L., M. Segarra, J.M. Chimenos, M.A. Fernandez, and F. Espiell. 1999. Gold cyanidation using hydrogen peroxide. *Hydrometallurgy* 52:21–35.

[25] Lee, V., P. Robinson, and F. Merz. 1989. Peroxide addition improves gold recovery and saves reagents at Pine Creek Gold Mine. Pages 170–182 in *Proceedings Randol Gold Conference.* Golden, CO: Randol International Ltd.

[26] Putnam, G.L. 1944. Chlorine as a solvent in gold hydrometallurgy. *Engineering and Mining Journal* 145(3):70–75.

[27] Aylmore, M.G., and D.M. Muir. 2001. Thermodynamic analysis of gold leaching by ammoniacal thiosulfate using Eh/pH and speciation diagrams*. Mineral & Metallurgical Processing Journal* 18(4):221–227.

[28] Breuer, P.L., and M.I. Jeffrey. 2003. A review of the chemistry, electrochemistry and kinetics of the gold thiosulfate leaching process. Pages 139–154 in *Hydrometallurgy 2003: Proceedings 5th International Symposium Honoring Prof. I.M. Ritchie.* Edited by C.A. Young, A. Alfantazi, C. Anderson, A. James, D. Dreisinger, and B. Harris. Warrendale, PA: TMS.

[29] Senayake, G., W.N. Perera, and M.J. Nicol. 2003. Thermodynamic studies of the gold(III)/(I)/(0) redox system in ammonia-thiosulfate solutions at 25°C. Pages 155–168 in *Hydrometallurgy 2003: Proceedings 5th International Symposium Honoring Prof. I.M. Ritchie.* Edited by C.A. Young, A. Alfantazi, C. Anderson, A. James, D. Dreisinger, and B. Harris. Warrendale, PA: TMS.

[30] Peri, K., G. Yuan, and K.N. Han. 1999. Dissolution behavior of gold in ammoniacal solutions with iodine as an oxidant. SME Preprint No. 99–117. Littleton, CO: SME.

[31] Lam, A.E., and D.B. Dreisinger. 2003. The importance of the Cu(II) catalyst in the thiosulfate leaching of gold. Pages 195–211 in *Hydrometallurgy 2003: Proceedings of 5th International Symposium Honoring Prof. I.M. Ritchie.* Edited by C.A. Young, A. Alfantazi, C. Anderson, A. James, D. Dreisinger, and B. Harris. Warrendale, PA: TMS.

[32] Hiskey, J.B., and V.P. Atluri. 1988. Dissolution chemistry of gold and silver in different lixiviants. *Mineral Processing & Extractive Metallurgy Review* 4:95–134.

[33] Nicol, M.J. 1980. The anodic dissolution of gold. Part I. Oxidation in acidic solutions. *Gold Bulletin* 13:46–55.

[34] Zipperian, D., S. Raghavan, and J.P. Wilson. 1986. Thiosulphate technology for precious metal recovery. Paper presented at 115th American Institute of Mining, Metallurgical, and Petroleum Engineers Convention, New Orleans, LA, March 2–6.

[35] Brown, T., A. Fischmann, L. Spiccia, and D.C. McPhail. 2003. Alternative copper(II) catalysts for gold leaching: Use of multidentate ligands to control thiosulfate oxidation. Pages 213–226 in *Hydrometallurgy 2003: Proceedings of 5th International Symposium Honoring Prof. I.M. Ritchie.* Edited by C.A. Young, A. Alfantazi, C. Anderson, A. James, D. Dreisinger, and B. Harris. Warrendale, PA: TMS.

[36] Ji, J., C.A. Fleming, P.G. West-Sells, and R.P. Hackl. 2003. A novel thiosulfate system for leaching gold without the use of copper and ammonia. Pages 227–244 in *Hydrometallurgy 2003: Proceedings 5th International Symposium Honoring Prof. I.M. Ritchie.* Edited by C.A. Young, A. Alfantazi, C. Anderson, A. James, D. Dreisinger, and B. Harris. Warrendale, PA: TMS.

[37] Wan, R.Y., and M. LeVier. 2003. Solution chemistry factors for gold thiosulfate heap leaching. *International Journal of Mineral Processing* 72(1–4):312–322.

[38] Hisshion, R.J., and C.G. Waller. 1984. Recovering gold with thiourea. *Mining Magazine* (September):237–243.

[39] Raudsepp, R., and R. Allgood. 1987. Thiourea leaching of gold in a continuous pilot plant. Pages 87–96 in *Proceedings of International Symposium on Gold Metallurgy.* Edited by R.S. Salter, D.M. Wyslouzil, and G.W. McDonald. New York: Pergamon Press.

[40] Marchant, P.B., L.M. Broughton, and M.J. Lake. 1988. Comparative analysis of cyanidation and acidothioureation. Pages 171–178 in *Proceedings Randol Gold Forum.* Golden, CO: Randol International Ltd.

[41] Groenewald, T. 1977. Potential applications of thiourea in the processing of gold. *Journal of South African Institute of Mining and Metallurgy* 77:217–223.

[42] Deng, T., and M. Liao. 2002. Gold recovery enhancement from a refractory flotation concentrate by sequential bioleaching and thiourea leach. *Hydrometallurgy* 63:249–255.

[43] Osseo-Asare, K., T. Xue, and V.S.T. Ciminelli. 1984. Solution chemistry of cyanide leaching systems. Pages 173–197 in *Precious Metals: Mining, Extraction and Processing.* Edited by V. Kudryk, D.A. Corrigan, and W.W. Liang. Warrendale, PA: TMS.

[44] Muir, D., S. Vukcevic, and J. Shuttleworth. 1995. Optimizing the ammonia–cyanide leaching process for copper–gold ores. Pages. 225–229 in *Proceedings Randol Gold Forum Perth '95.* Golden, CO: Randol International Ltd.

[45] Dadgar, A., Sanders, B.M., J.A. McKeown, R.H. Sergent, and R.H. Jacobson. 1990. Leaching and recovery of gold from black sand concentrate and electrochemical regeneration of bromine. Pages 75–90 in *Advances in Gold and Silver Processing. Proceedings of GOLDTech 4 Symposium.* Edited by M.C. Fuerstenau. New York: American Institute of Mining, Metallurgical, and Petroleum Engineers.

[46] Hiskey, J.B., and P.H. Qi. 1990. Leaching and electrochemical behavior of gold in iodine solutions. Part I: Dissolution kinetics. SME Preprint No. 90–112. Littleton, CO: SME.

[47] Woodcock, J.T. 1988. Innovations and options in gold metallurgy. Pages 115–131 in *Proceedings of XVI International Mineral Processing Congress, Stockholm, Sweden.* Edited by E.K.S. Forssberg. Amsterdam: Elsevier.

[48] Chryssoulis, S.L., and L.J. Cabri. 1990. Significance of gold mineralogical balances in mineral processing. *Transactions of the Institution of Mining and Metallurgy* 99:C1–C10.

[49] Hiskey, J.B., and M.E. Wadsworth. 1981. Electrochemical processes in the leaching of metal sulfides and oxides. Pages 304–325 in *Proceedings and Fundamental Considerations of Selected Hydrometallurgical Systems*. Edited by M.C. Kuhn. New York: SME-AIME.

[50] Bard, A.J., and L.R. Faulkner. 1980. *Electrochemical Methods: Fundamentals and Applications.* New York: John Wiley & Sons.

[51] Pourbaix, M. 1974. *Atlas of Electrochemical Equilibria in Aqueous Solution.* 2nd edition. Houston, TX: National Association of Corrosion Engineers.

[52] S. Jeon et. al, 2021. "The effects of Coexisting Copper, Iron, Cobalt, nickel and zinc ions on Gold recovery by enhanced cementation via Galvanic Interactions between zero-valent aluminum and activated carbon in ammonium thiosulfate system." Metals 2021, 11, 1352. https://doi.org/10.3390/met11091352

[53] S. Jeon et. al., 2020. "Enhanced Cementation of gold via galvanic interaction using activated carbon and zero-valent aluminum: A novel Approach to recover gold ions from ammonium thiosulfate medium. http://dx.doi.org/10.1016/j.hydromet.2019.105165

[54] S. Jeon et.al, 2021. "A simple and efficient recovery technique for gold ions from ammonium thiosulfate medium by galvanic interactions of zero-

valent aluminum and activated carbon: A parametric and mechanistic study of cementation. https://doi.org/10.1016/j.hydromet.2021.105815

[55] S. Jeon et. al, 2022. "A kinetic study on enhanced cementation of gold ions by galvanic interactions between aluminum as an electron donor and activated carbon as an electron mediator in ammonium thiosulfate system." https://doi.org/10.3390/min12010091

[56] Mines and Geosciences Bureau of the Philippines: http://databaseportal.mgb.gov.ph/mgbpublic/api/attachments/download?key=Jld1rclzSpO9F5qkSV7crlfEJ1qcuVsYpKDN3wtU3qpbl8YwwYU9rkHH2WiTgAVS

CHAPTER II

CEMENTATION INVESTIGATION USING IRON- OXIDES AND ZERO-VALENT ALUMINUM IN GOLD-COPPER AMMONIACAL THIOSULFATE MEDIUM

ABSTRACT

Ammonium thiosulfate leaching is a promising alternative to the conventional cyanide method to extract gold from ores. However, strategies for recovering gold from the leachate were less commercially used due to its low affinity to gold. The present study investigated the recovery of gold from the leachate using iron oxides (hematite, Fe_2O_3 or magnetite, Fe_3O_4). Cementation experiments were conducted by mixing 0.10 mg of aluminum powder as an electron donor and 0.10 mg of electron mediator (activated carbon, hematite, or magnetite) in 10 ml of ammonium thiosulfate leachate containing 100 mg/L gold ions and 10 mM cupric ions for 24 hours at 25°C. The results of solution analysis showed that when activated carbon, AC was used, gold was recovered together with copper (recoveries were 99.99% for gold and copper). However, selective gold recovery was observed when iron oxides were used: gold and copper recoveries were 89.7 % and 21 % for hematite, and 85.9 % and 15.4% for magnetite, respectively. The electrochemical experiment was also conducted to evaluate the galvanic interaction between the electron donor and electron mediator in a conventional electrochemical set-up (Fe_2O_3/ Fe_3O_4 -Al as the working electrode, Pt as the counter electrode, Ag/AgCl as the reference electrode) in gold thiosulfate medium. Cyclic voltammetry showed a gold reduction "shoulder-like" peak at -1.0 V using Fe_2O_3/Al and Fe_3O_4/Al electrodes. Chronoamperometry was conducted and operated at a constant voltage (-1.0V) determined during cyclic voltammetry and further analyzed using SEM-EDX. The results of SEM-EDX analysis for the cementation products and electrochemical experiments confirmed that gold was selectively deposited on iron oxide's surface as an electron mediator.

2.1 INTRODUCTION

Recently, high-grade gold ores have been reported to be gradually depleting, and the refractory gold ores consisting of about one-third of the total gold production from open pit/underground mines and in tailing deposits become the interest of this study. In refractory ores, sulfide-type gold ores, especially gold-pyritic ore, account for a substantial proportion of gold resources (i.e., about 22%), the recovery of gold from gold-pyritic ore has recently come into the spotlight as a valuable study in resources field [1-4]. Also, it posters environmental hazards upon storing these sulphide-rich minerals, as these minerals are potentially forming highly acidic water, commonly known as acid mine drainage (AMD) [5]. Currently, upon processing refractory gold ore, conventional processing is done through roasting followed by the cyanidation process. This current technology is being practiced in industrial mining plants, like the roasting-cyanidation leaching plant of Zhongyuan Gold Smelter Co Ltd in Henan Province, China [6]. In the later leaching process, where cyanide is conventionally employed, the solvent posters health and environmental hazards due to its potential toxicity if not appropriately managed [1-2, 7, 32]. For these reasons, many studies have been conducted to find alternative solvents to mitigate the risk accompanied by using cyanide, such as thiourea [8-10], thiocyanate [11], halogen-based [12-15] and thiosulfate [16-22]. Among the alternatives, ammonium thiosulfate has been highlighted because it has been shown to have higher selectivity and leaching rate to gold, and most importantly, it is less corrosive and non-toxic to humans [16-22]. While methods to recover gold from the leachate have not been extensively practiced due to its low affinity to carbon during the gold-adsorption recovery process [17-19, 23-26], this causes limitations to commercial operation.

For these reasons, the development of an alternative recovery method for gold ions in the ammonium thiosulfate system is needed. A recent study reported that gold recovery could be efficiently achieved by cementing the gold ions via galvanic interactions between activated carbon (electron mediator) and zero-valent aluminum (ZVAl) (electron donor) in a gold-copper ammoniacal thiosulfate system [17]. The recovery results using ZVAl or AC in a single system were negligible. However, when mixed (binary system), over

99% of Au ions could be recovered through the following suggested mechanisms: ZVAl acts as an electron donor (i.e., anode), and activated carbon (AC) acts as an electron mediator (i.e., cathode), making the galvanic cell, and finally leading to reductive deposition of the gold-thiosulfate complex onto activated carbon attached to ZVAl [17-19]. To further explore the potential of this technique, further researched was conducted to understand the behavior of gold ions in an ammonium thiosulfate system in the presence of various metallic combinations of electron donors, zero-valent aluminum, and electron mediators such as Fe and Cu, and the results showed that about 20% and 40% of gold ions were recovered, respectively [16]. Although it was not discussed on the recovery of gold ions, Choi with co-authors also further conducted a study to remove cadmium (Cd2+) and zinc (Zn^{2+}) ions from the sulfate-based solvents using aluminum and iron oxide materials (e.g., Fe_3O_4). The results showed that about 83% of Cd^{2+} and 92% of Zn^{2+} were removed from the acid solutions. In contrast, recovery efficiency was negligible employing the ZVAl sole system (i.e., 0% recovery of Cd^{2+} and Zn^{2+}) due to the thin insulating oxyhydroxide film on the surface of ZVAl. Although the recovery efficiencies were lower than the Al/AC system, the research highlighted that metal ions could be recovered via galvanic interactions using ZVAl and other conductive materials [27].

As previously mentioned, when dealing with pyritic refractory ores, the leaching agent cannot contact gold in the ore because gold grains are encapsulated in sulfide minerals like pyrite, FeS_2 [28]. Amongst all pretreatment processes, roasting has been conventionally employed to convert pyrite into various porous iron oxides such as hematite (Fe_2O_3) and magnetite (Fe_3O_4), so that gold grains can be exposed to leach solutions, making it susceptible to extraction [3,5,29-31].

Considering the semiconductive properties of hematite (Fe_2O_3) and magnetite (Fe_3O_4), it is possible to use them as an electron mediator in the cementation process proposed by the previous researchers [16-19]. In this case, activated carbon can be eliminated upon processing refractory gold ores, and by treating refractory gold in pyrite (FeS_2), we could mitigate the formation of acid mine drainage (AMD). In the present study, the technical feasibility of two iron oxides (hematite (Fe_2O_3) and magnetite (Fe_3O_4)) (conventional products

of pyrite roasting) as electron mediators for the enhanced cementation of gold from ammonia thiosulfate leachate was evaluated using zero-valent aluminum as an electron donor.

2.2 MATERIALS AND METHODS

2.2.1 Materials

All chemicals used were purchased from Wako Pure Chemical Industries, Ltd., Japan. In cementation experiments, ZVAl (99.99%, CAS No.: 012-19172) was used as an electron donor. For electron mediators, activated carbon (99.99%, CAS No.: 031-02135) having about 800–1500 m^2g^{-1} of specific surface area, hematite (Fe_2O_3, 99.99%, CAS No: 096-02821) and magnetite (Fe_3O_4, 99.99%, CAS No: 093-01035) were used.

2.2.2 Solution Preparation

The Au-ammonium thiosulfate solution was prepared by dissolving 50 mg of Au powder (99.999%, CAS No.: 937902 Wako Pure Chemical Industries, Ltd., Japan) in 500 ml of ammonium thiosulfate solution containing 1 M $Na_2S_2O_3$.$5H_2O$ (CAS No.: 197-03585), 0.5 M NH_3 (CAS No.: 016-03146), 0.25 M $(NH_4)_2SO_4$ (CAS No.: 016-03445), and 10 mM $CuSO_4$ (CAS No.: 034-04445) in a beaker; the solution was agitated using a magnetic stirrer with a built-in heater, a part of a thermocouple was submerged in the solution to maintain the temperature at 30°C for 24 h with a constant shaking frequency of 600 min^{-1}. Electrolyte solutions were prepared by dissolving $Na_2S_2O_3$.$5H_2O$ and metal ions (Cu^{2+} and Au^+) in 0.1 M NH_3 / 0.05 M $(NH_4)_2SO_4$ buffer solutions.

2.2.3 Cementation Experiments

2.2.3.1 The Effect of Atmosphere

The latter investigated the effects of atmosphere, using air (aerobic) and by purging oxygen in the flask and solution with ultra-pure nitrogen (N_2) gas (anaerobic). Cementation experiments were derived from the previous research performed by Jeon et. al, 2019 where the researchers conducted the cementation process by mixing 0.10 mg of electron donor (ZVAl) and 0.10

mg of electron mediator (AC, Fe_2O_3, or Fe_3O_4) with 10 ml of Au-ammonium thiosulfate solution in 50-ml Erlenmeyer flasks using thermo-stated water bath shaker (shaking amplitude, 40 mm; frequency, 120 min^{-1}) maintained at 25°C.

2.2.3.2 The Effects of Galvanic Constituents Dosage

The latter investigated the effects of different galvanic constituents (magnetite, hematite, activated carbon, and aluminum) dosage in single system (10 mg, 50 mg, 100 mg, 150 mg, 200 mg, 300 mg and 500 mg) upon cementation process in anaerobic atmosphere. The solid-liquid separation is the same as previously mentioned in **section 2.3.1.**

2.2.3.3 The Effects of Time

The latter investigated the effects of time (1, 2, 3, 4, 5,10,15, 20, 30, 60, 120, 240, 360,1440 in minutes) using different galvanic constituents (magnetite, hematite, activated carbon, and aluminum) in single and binary system upon cementation process in anaerobic atmosphere. The solid-liquid separation is the same as previously mentioned in **section 2.3.1.**

2.2.3.4 The Effects of Electron Donor Dosage (ZVAL)

The latter investigated the ZVAl dosage (5 mg, 10 mg, 20 mg, 40 mg, 80 mg, 150 mg, 300 mg) using 10 mg different electron mediators (magnetite and hematite) in binary system upon cementation process in anaerobic atmosphere. The solid-liquid separation is the same as previously mentioned in **section 2.3.1.**

2.2.3.5 The Effects of Using Different Electron Donor (Scrap Aluminum)

The latter investigated the effects of using aluminum scrap with different iron oxides (magnetite and hematite) upon cementation process in anaerobic atmosphere. The solid-liquid separation is the same as previously mentioned in **section 2.2.3.1.**

2.2.4 Characterization Experiments

The cementation residues were thoroughly washed with deionized water (DI), followed by drying the residues in a vacuum oven at 40°C and then further analyzed by Scanning Electron Microscopy with Energy Dispersive X-ray (SEM-EDS, JSM-IT200TM, JEOL Co., Ltd., Japan), operated at an accelerating voltage of 15 kV, 1000x to 1500x magnification and a working distance (WD) of 10 mm. The elemental maps were taken at 2,000 cps with 60 min time constant and high pixel resolutions of 256x256 (~10-minute scans).

2.2.5 Solution Analysis

The concentrations of gold ions that remained in the sterile solution were determined using inductively coupled plasma atomic emission spectroscopy (ICP-AES) (ICPE-9820, Shimadzu Corporation, Japan, with a margin of error= ±2%) and Au recovery (*AuR*) was then calculated according to the following equation:

$$Au_R = \frac{[Au_i]-[Au_f]}{[Au_i]} \times 100 \qquad (1)$$

where [*Aui*] and [*Auf*] are denoted as dissolved Au's initial and final concentrations, respectively. Note that dissolved initial and final gold concentrations were measured, and the recovery experiments were done in three replicate samples.

2.3 RESULTS AND DISCUSSIONS

2.3.1   Effects of solution condition

Figure 2.1 shows the percent (%) recovery of gold and copper ions from gold-copper ammoniacal thiosulfate solution using different galvanic constituents; **a)** ZVAl/ and or activated carbon (AC), **b)** ZVAl/ and or hematite (Hem), and **c)** ZVAl/ and or magnetite (Mag) in aerobic conditions, respectively.
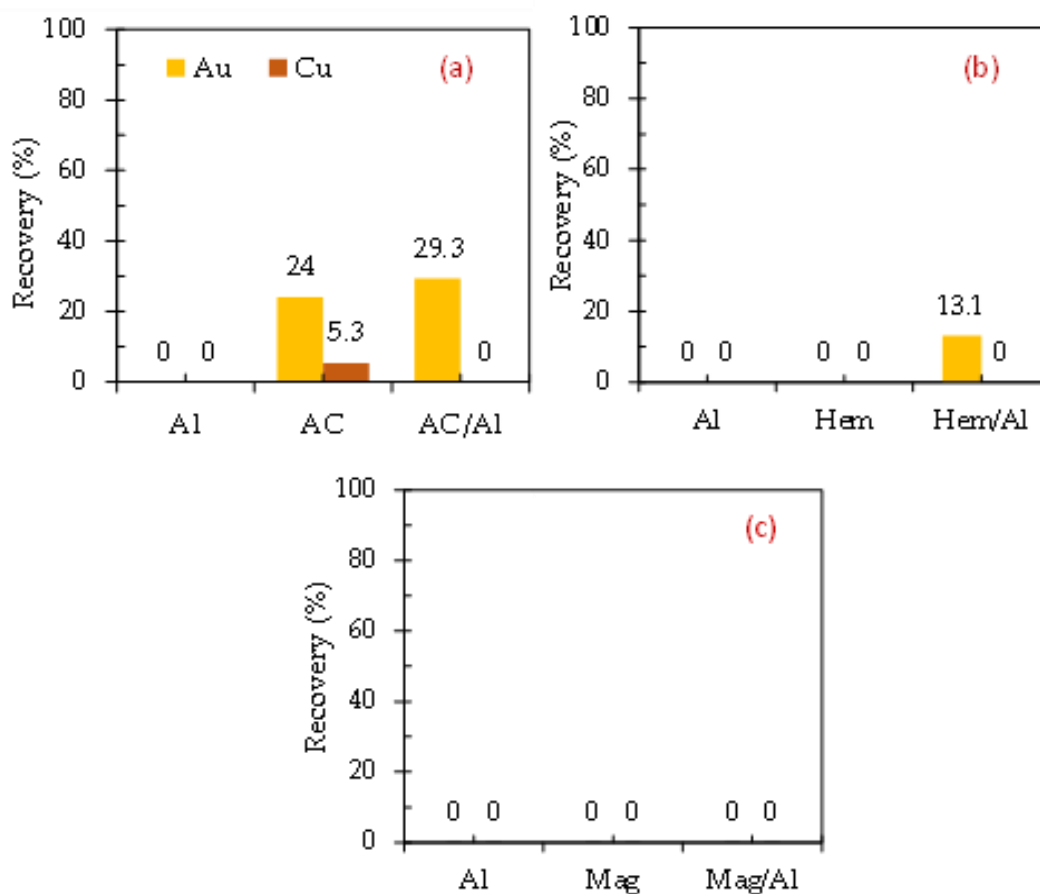
Figure 2.1 Percent (%) recovery of gold, Au and copper, Cu from different galvanic constituents in air atmosphere after 24hrs **a)** activated carbon (AC) and or /ZVAl **b)** hematite (Hem) and or/ ZVAl and **c.)** magnetite (Mag) and or /ZVAl.

Figure 2.1 (a) showed that gold recovery was negligible when ZVAl was used without electron mediators like AC because of the passivation of the ZVAl surface with insulator aluminum oxide; This passivation layer (aluminum oxide layer) will hinder the transfer of electrons from ZVAl to gold ions in the solution phase, suppressing the electrochemical deposition of gold and copper [16-19]. Activated carbon has a high specific surface area. It may function as an adsorbent for metal ions even without electron donors like ZVAl, while gold and copper recoveries with activated carbon were around 24% and 5%, respectively. The low recoveries indicate limited adsorption of gold and copper complexes from the aqueous phase to activated carbon [17-19]. Copper and gold recoveries were also deficient even when activated carbon and ZVAl were used together. From **Figure 2.1(b)** for hematite and **Figure 2.1(c)** for magnetite, it was also found that gold and copper recoveries were limited when using iron oxides alone or iron oxide and ZVAl.
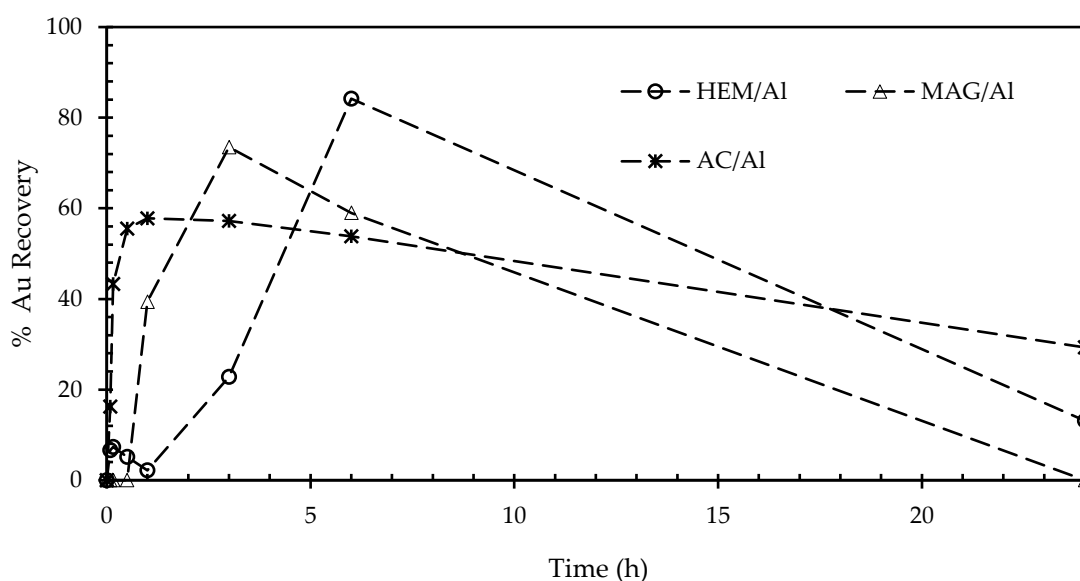
Figure 2.2 Percent (%) recovery of gold ions, Au with respect to time using ZVAl and different electron mediators in aerobic condition after 24 hrs.

The low recoveries of gold after 24 hr in the air may be due to the dissolution of cemented gold by oxidation with O_2 [17-19]. **Figure 2.2** shows the recoveries of gold with ZVAl and electron mediators as a function of time. It was observed that gold recoveries increased with time to reach the maximum of 58 % at the first 1 hr for AC/Al, 75 % at 3 hr for Fe_2O_3/Al, and 84 % at 6 hr for Fe_3O_4/Al, then gold recoveries decreased with time. The increase in gold

recoveries in the initial period suggested that gold was deposited in the presence of both ZVAl and electron mediators in the short term due to the following:

$$2Au(S_2O_3)_2^{3-} + 6Al^0 + 6H^+ = 2Au^0 + 8S^0 + 3Al_2O_3 + 3H_2O \qquad (2)$$
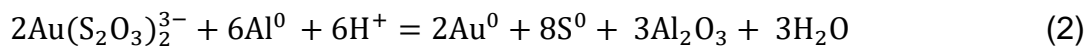
However, the decrease of gold recoveries after the maxima observed in **Figure2.2** may be due to the oxidation of deposited gold with dissolved oxygen,

$$4Au^0 + 8(S_2O_3)^{2-} + O_2 + 2H_2O = 4\ Au(S_2O_3)_2^{3-} + 4\ OH^- \qquad (3)$$
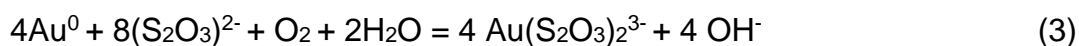
Since the dissolution of gold was significantly affected in the presence of oxygen, O_2, the subsequent cementation experiments were conducted without O_2 (anaerobic) by purging the gold thiosulfate solution with N_2 gas for 45 mins, as presented in **Figure 2.3a-c,** using ZVAl as an electron donor and various electron mediators**.**
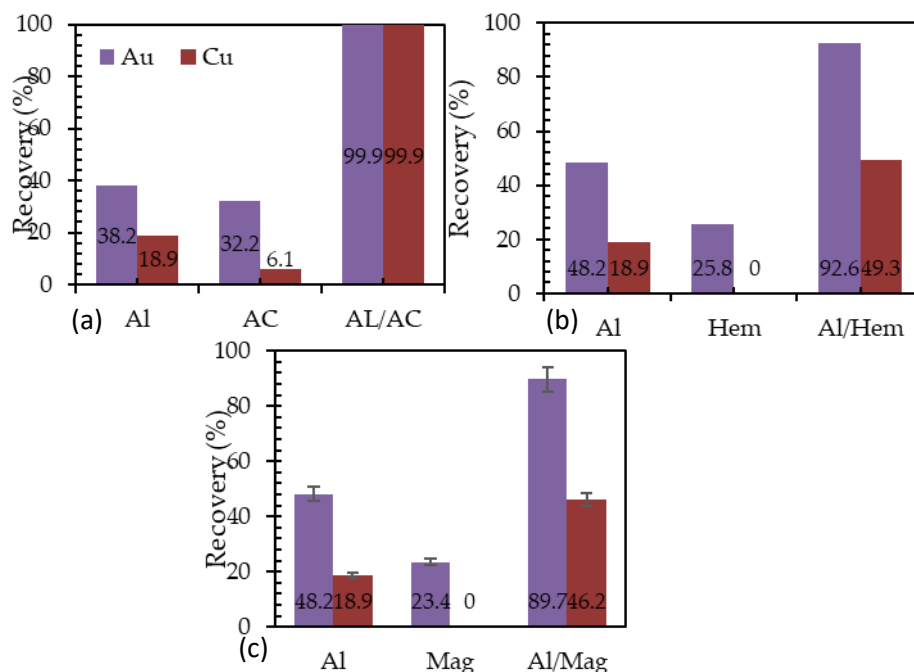
Figure 2.3 Percent (%) recovery of gold, Au and copper, Cu ions from different galvanic constituents in nitrogen atmosphere (anerobic) **a)** activated carbon (AC) and or /ZVAl **b)** hematite (Hem) and or/ ZVAl and **c.)** magnetite (Mag) and or /ZVAl.

When ZVAl was used without electron mediators, gold and copper recoveries were slightly improved; the recoveries were 35 % for Au and 29 % for Cu. These results may be due to the limited passivation of the Al_2O_3 layer on the ZVAl surface, allowing limited electron transfer from the electron donor (ZVAl) to the metal ions. The insignificant gold and copper recoveries were observed when only electron mediators were used (without ZVAl); the recoveries for Au and Cu were less than 40 %, regardless of the electron mediator. This result may indicate that the ability of AC, Fe_2O_3, and Fe_3O_4 as adsorbent to the metal ions is limited.

However, when both ZVAl as an electron donor and the electron mediators were used together (binary system), high gold recoveries were observed; the recoveries were 99% with AC/Al, 92.6% with Fe_2O_3/Al, and 89.7% for Fe_3O_4/Al, respectively. This result may suggest that galvanic couples composed of ZVAl as electron donors and the electron mediators (AC, Fe_2O_3, and Fe_3O_4) are remarkably effective in recovering Au from ammonia thiosulfate solutions. The results' selective recovery of Cu can be observed noticeably; Cu recoveries were 99.9 % with AC/Al while it was 49.3% with Fe_2O_3/Al and 46.2% for Fe_3O_4/Al. These results indicate that Fe_2O_3/Al and Fe_3O_4/Al can be used for the selective recovery of gold from copper-ammoniacal thiosulfate solutions.

2.3.2 Effects of Electron Mediator Dosage

In lieu of the results presented in **Figures 2.1-3,** the proceeding experiments were conducted in anaerobic conditions, where electron mediator was investigated with respect to varying dosage (10, 50, 100, 150, 200, 300, 500 mg) with 0.10 mg of electron donor (ZVAl), for 24 hr cementation time as presented in **Figure 2.4.**
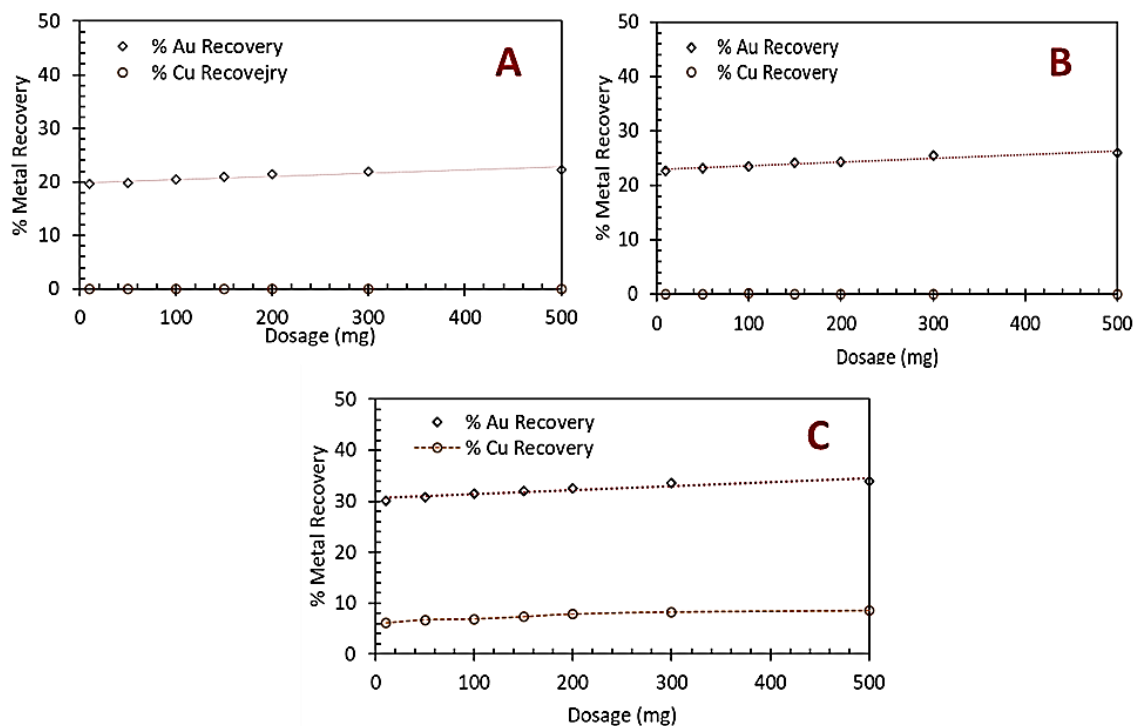
Figure 2.4. Effects of electron mediator dosage [(10, 50, 100, 150, 200, 300, 500) mg] upon cementation experiments after 24 hr a) Magnetite b) Hematite, and c) Activated carbon.

The results of solution analysis obtained a metal recovery of 19 % Au-0 % Cu, 22.6 % Au- 0 % Cu, 30.1 % Au- 6.1 % Cu for magnetite, hematite, and activated carbon, respectively, using 10 mg dosage of electron mediators. Compared to the highest dosage of 500 mg which is fifty-fold higher than the initial dosage, it doesn't have to show a significant increase of metal recoveries, where Au-Cu % recovery obtained 22.3 % Au- 0 % Cu for magnetite, 26.0 % Au – 0 % Cu for hematite, and 34.0 % Au- 8.49 % for activated   carbon.

2.3.3 The Effects of Cementation Time

The latter experiments investigated the effect of cementation time (5, 10, 20, 30, 45, 60, 120, 240, 360, and 1400 min) with 10 mg electron mediator dosage, as presented in **Figure 2.5**
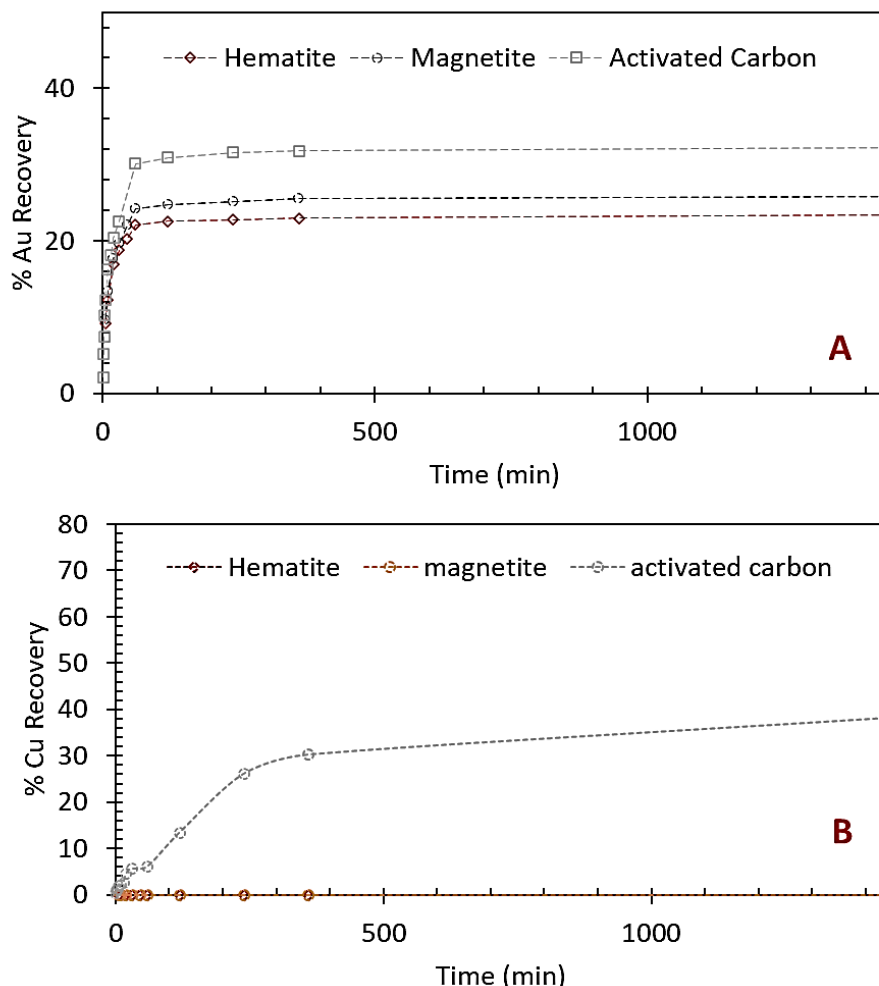
Figure 2.5 Effects of cementation time [(5, 10, 20, 30, 45, 60, 120, 240, 360, and 1400) min] with 10 mg of electron mediator dosage (single system) on a) % Au recovery and b) %Cu recovery.

The results of solution analysis obtained that all electron mediators obtained a significant increase of gold recovery after 60 minutes cementation time; 22.1 %, 24.2 %, and 30.1 % Au recovery was obtained for magnetite, hematite and activated carbon, respectively. Comparing the recovery after 1440 minutes cementation; 23.4%, 25.8% and 32.2% Au recovery was obtained for magnetite, hematite and activated carbon, respectively. Suggesting that 60 minutes was the optimum cementation time for single system as shown in

Figure 2.5a. Furthermore, the results of solution analysis for copper recoveries was presented in **Figure 2.5b**; magnetite and hematite recovered 0% Cu in all cementation time, while the used of activated carbon, a significant increase was observed after 240 minutes (26.1 % Cu) and further increase insignificant after 1400 minutes obtaining 38.1% Cu recovery.
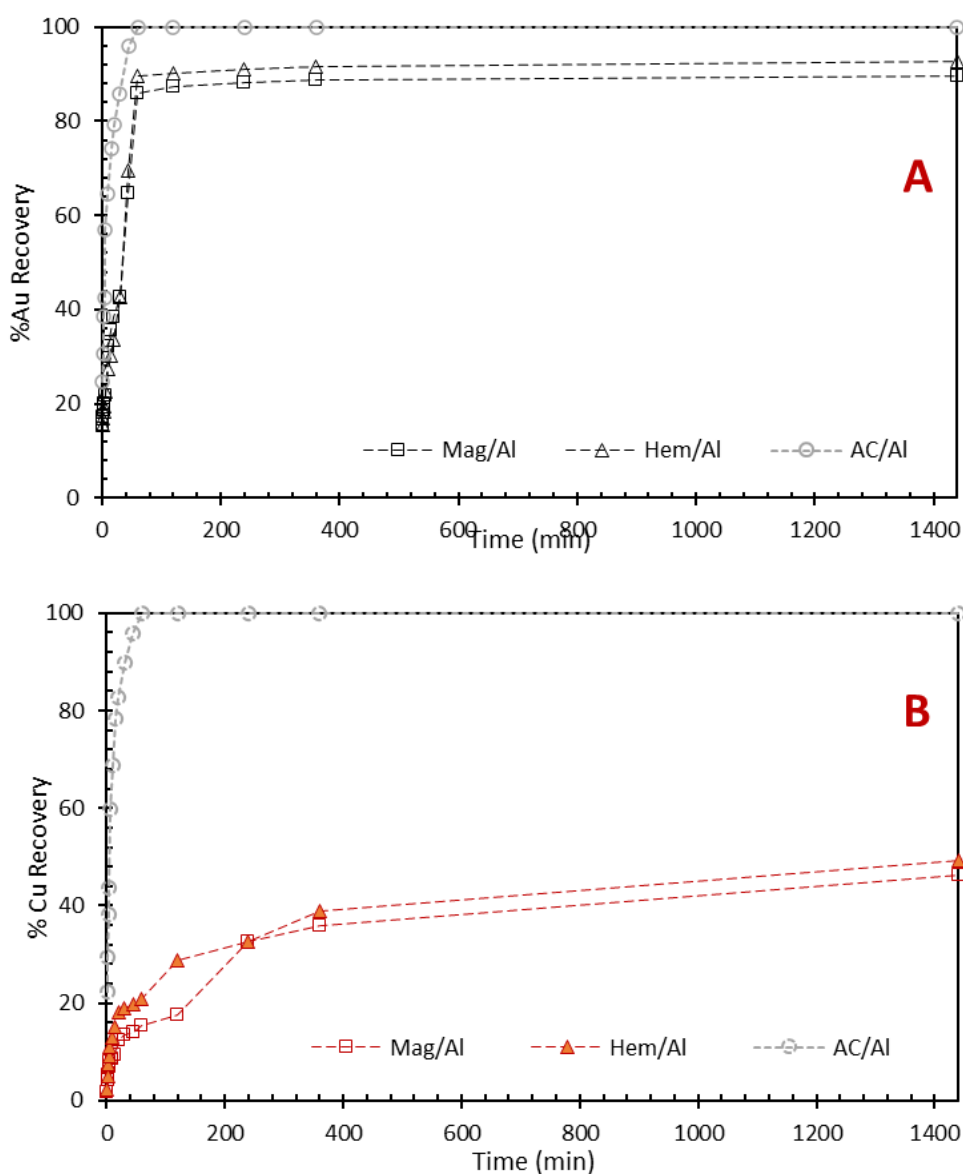
Figure 2.6 Effects of cementation time [5, 10, 20, 30, 45, 60, 120, 240, 360, and 1400 min] with 10 mg of electron mediator dosage and 10 mg of electron donor (1:1) (binary system) on a) % Au recovery and b) %Cu recovery.

Similar to the single system, the results of solution analysis in binary system (**Figure 2.6**) obtained a significant increase of gold recovery after 60 minutes cementation time; 85.9 %, 89.7 %, and 99.9 % Au recovery was obtained for

Mag/Al, Hem/Al and AC/Al, respectively. Comparing the recovery after 1440 minutes cementation; 89.7 %, 92.6 % and 99.9% Au recovery was obtained for Mag/Al, Hem/Al and AC/Al, respectively as shown in **Figure 2.6a.** At 1440 minutes, copper recoveries were 46.2 %, 49.3 %, and 99.9 % for Mag/Al, Hem/Al and AC/Al, respectively. We can observe in **Figure 2.6b** that the increase of copper recovery is limited to only after 60 minutes, along with the significant increase of gold recovery, suggesting that the optimum recovery considering the selective cementation of gold is only 60 minutes for 10 mg of electron mediator-electron donor dosage.

2.3.4 **The Effect of Aluminum Dosage**

In **Figure 2.7,** the effects of aluminum dosage [(5, 10, 20, 30, 40, 150, 300) mg] with 10 mg of electron mediator donor (1:1) (binary system) on % metal recovery were shown. Interestingly, as we increase the amount dosage of electron donor, a significant increase of gold and copper recoveries can be observed. The highest amount of gold and copper reveries was obtained when adding 300 mg of electron donor with 10 mg of electron mediator: having 99.7 % Au- 84.2 % Cu and 99.9% Au- 86.9% Cu, for magnetite and hematite respectively. Although great amounts of gold and copper was recovered when adding 300 mg of ZVAl, selective recovery of gold is more advantageous than that of having both gold and copper, using 5 mg of electron donor obtained the lowest % metal recovery, but compared to 10 mg of ZVAl, a competitive amount of gold was recovered and selective cementation was achieve having 85.9 % Au- 15.4 % Cu and 89.7 % Au- 21.0 % Cu when using magnetite and hematite, respectively.

Selective deposition of gold in an ammonia thiosulfate leaching system is significant and industrially attractive since this system requires cupric ions as a leaching catalyst, and extremely high concentrations of copper ions coexist with low concentrations of gold leached from ores. If selective deposition of gold is possible, separating gold and copper is not required after the deposition step, and the process becomes more straightforward compared to previous research conducted by Jeon et. al, 2022.
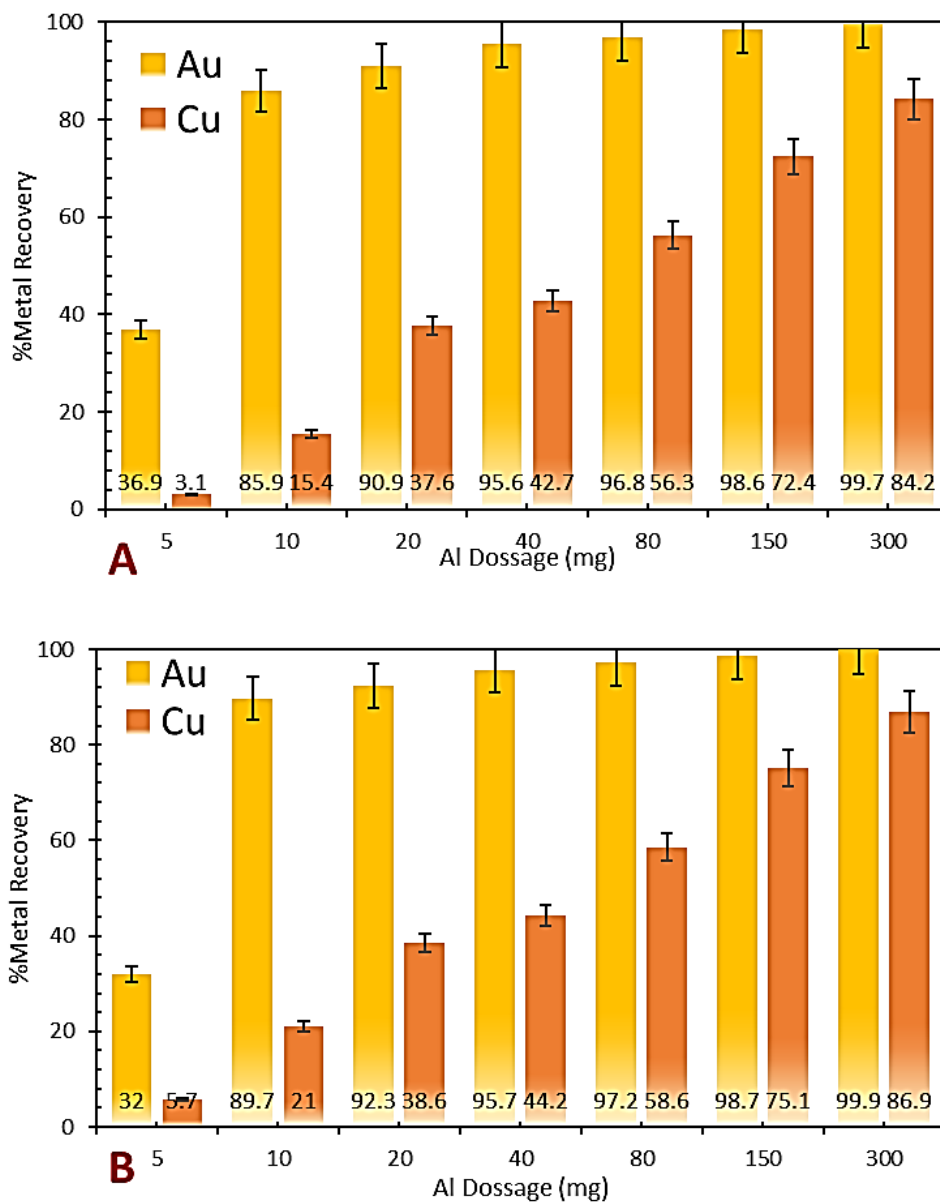
Figure 2.7 Effects of aluminum dosage (5, 10, 20, 30, 40, 80, 150, 300 mg) on Au and Cu recoveries with 10 mg of electron mediator (binary system) in % metal recovery using A) Magnetite B) Hematite as electron mediator.

For the selective recovery of Au, this research suggests that the optimum parameters were determined to be 10 mg of electron donor and 10 mg electron mediator for 60 mins cementation time in anaerobic (N_2 purged) solution condition maintained in pH 9-10 at 25°C. These optimum conditions obtained gold and copper recoveries of 89.7 % and 21 % for hematite and 85.9 % and 15.4% for magnetite, respectively. The results of cementation experiments using iron oxide as electron mediator is selective to gold compared to iron oxides as summarized in **Figure 2.8.**
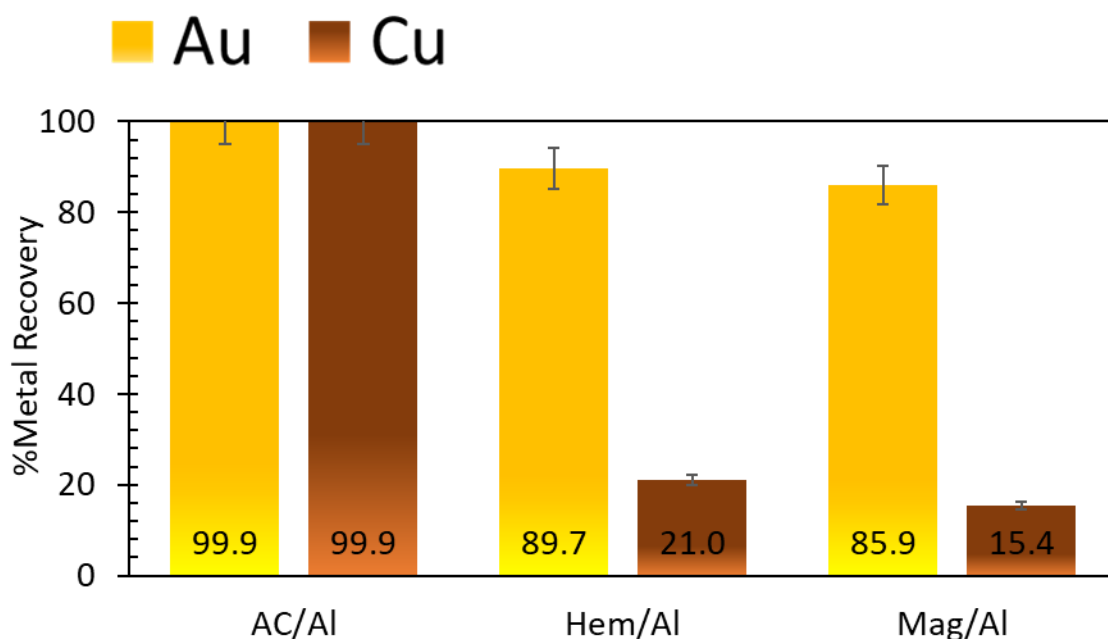
Figure 2.8 % Metal recovery of the optimized cementation parameters. (60 mins cementation time in anaerobic (N_2 purged) solution condition maintained in pH 9-10 at 25°C using 10mg electron mediator and 10 mg electron donor.

2.3.5 Surface Characterization of Cementation Residue
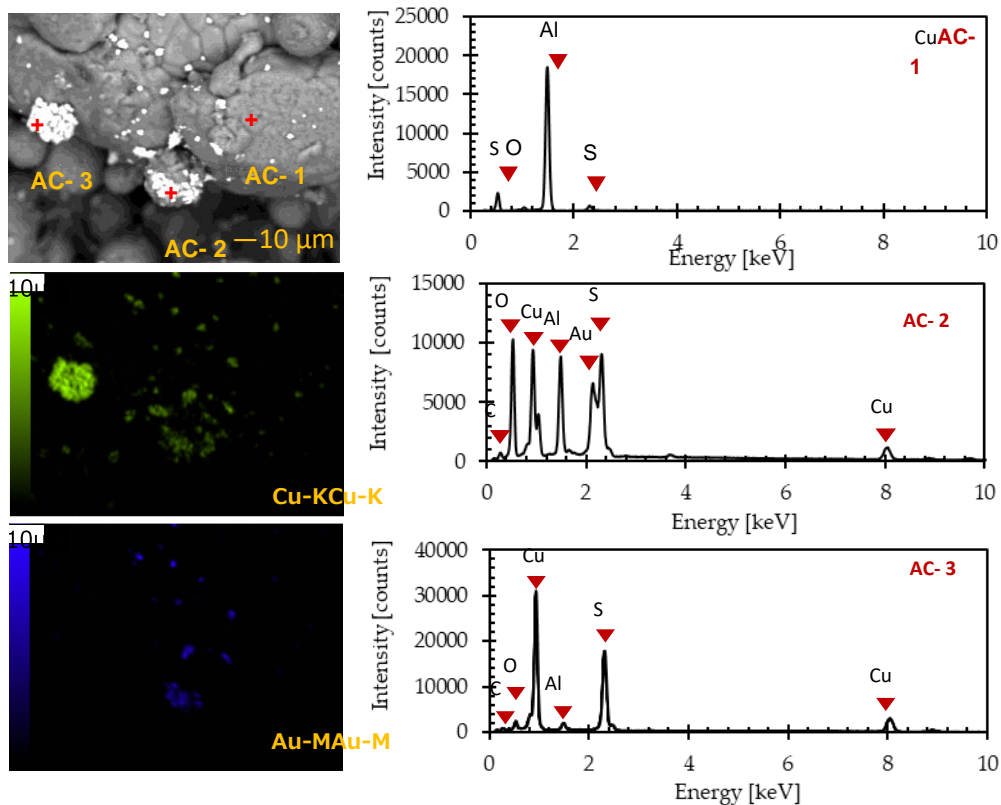
Figure 2.9. Back scattered electron photomicrograph with energy dispersive point analysis with elemental mapping of the leach residue using Al and AC galvanic system.

To investigate the associations of cemented Au and Cu, morphological analysis of the representative particles on the residues from the cementation experiments was examined in detail by SEM-EDX analysis, as shown in **Figures 2.9 to 2.11**. The results shown in **Figure 2.9** for the residue with AC/Al are consistent with the previously reported results [17-19]; In the SEM-BSE image, bright (white) domains (points **AC-2** and **AC-3)** were observed on the surface of the grey particle (point **AC-1**). The point spectrum data showed that at the grey particles (point AC-1), firm Al and O peaks were detected with a minor S peak, suggesting that the grey particle is ZVAl with an oxidized surface. In the spectrum at the bright domains (**AC-2** and **AC-3),** Au and Cu

peaks were observed together with the C peak, suggesting that the bright domains correspond to Au and Cu deposited on AC.
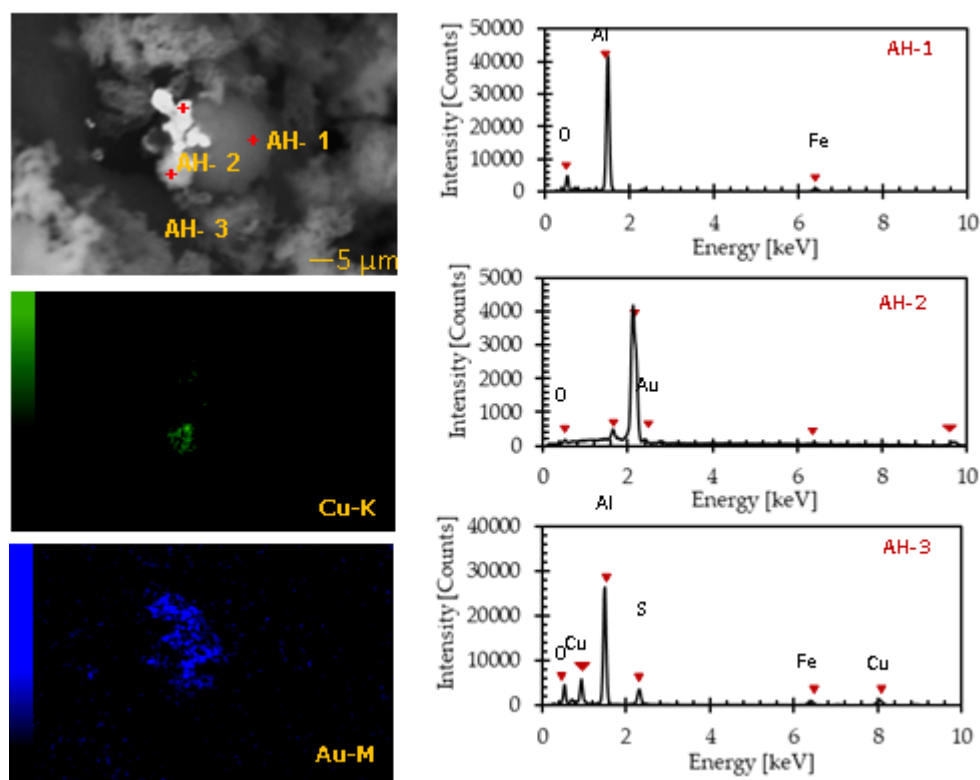
Figure 2.10. Back scattered electron photomicrograph with energy dispersive point analysis with elemental mapping of the leach residue using Al and Hematite galvanic system.

The SEM-EDX mapping image confirmed that Au and Cu were always deposited on AC attached to ZVAl. **Figures 2.10 and 2.11** show the results of SEM-EDX analysis for the solid residues obtained in the cementation experiments with Fe_2O_3/Al and Fe_3O_4/Al, respectively. The point spectrum and mapping results in **Figure 2.10** and **Figure 2.11** suggest that Au was deposited on the iron oxide particles attached to the ZVAl surface. Noticeably, copper signal intensity ranged from 200 to 6000 cps, as illustrated in **Figure 2.10 AH-3** and **Figure 2.11 AM-3,** while the values are higher (1000-31,000 cps), as illustrated in **Figure 2.9 AC-2** and **AC-3**, implying that copper deposition is limited for iron oxide/Al system. Analysis of the spectra from 40 different points on illuminated bright particles was conducted. The results showed that the ratio of gold signal to copper signal was higher for the residues with iron oxide/Al than with AC/Al. This result agrees with the result

illustrated in **Figure 2.9** and confirms that Au was preferably cemented than Cu when iron oxides were used as the electron mediators.
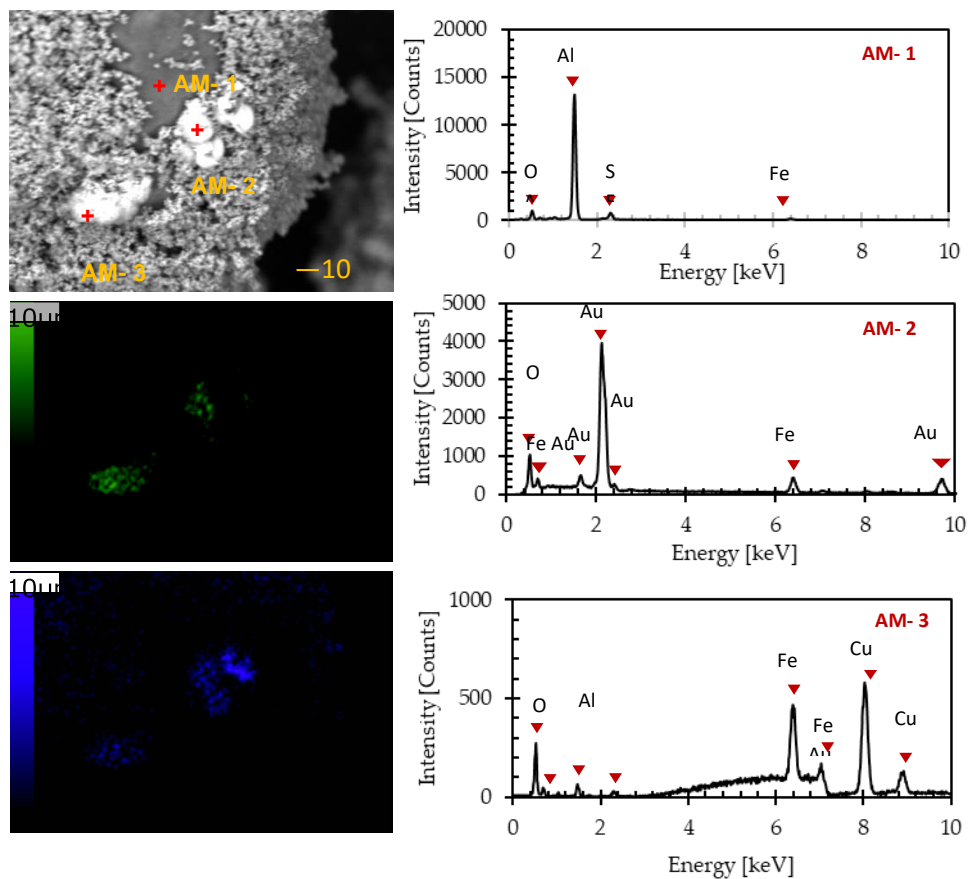
Figure 2.11. Back scattered electron photomicrograph with energy dispersive point analysis with elemental mapping of the leach residue using Al and Magnetite galvanic system.

2.4 CONCLUSIONS

The present study investigated the technical feasibility of recovering gold from leachate using synthetic iron oxides (hematite, Fe_2O_3 or magnetite, Fe_3O_4) as intermediate by-products of roasting pyritic refractory gold ores. Parametric cementation experiments were conducted by firstly mixing a predetermined dosage of aluminum powder as an electron donor and electron mediator (activated carbon, hematite, or magnetite) in 10 ml of ammonium thiosulfate leachate containing 100 mg/L gold ions and 10 mM cupric ions for 24 hours at 25°C in aerobic and anaerobic solution conditions. The results of solution analysis showed that anaerobic conditions obtained the most significant metal recovery where activated carbon, AC was used, and gold was recovered together with copper (recoveries were 99.99% for gold and copper). However, selective gold recovery was observed when iron oxides were used.

Further cementation parameters were investigated concerning electron mediator dosage, cementation time in single and binary systems, and electron donor dosage in binary systems. All experiments obtained consistency concerning the selective cementation of gold using iron oxides with zero-valent aluminum, and the optimum parameters were determined to be 10 mg of electron donor and 10 mg electron mediator for 60 mins cementation time in anaerobic (N_2 purged) solution condition maintained in pH 9-10 at 25°C. These optimum conditions obtained gold and copper recoveries of 89.7 % and 21 % for hematite and 85.9 % and 15.4% for magnetite, respectively.

References:

1. Hong Qin et. al, 2020. "Pyrite enhanced chlorination roasting and its efficacy in gold and silver recovery from gold tailing." https://doi.org/10.1016/j.seppur.2020.117168

2. Hong Qin et. al, 2021. "Recovery of Gold from sulfide refractory gold ore: Oxidation roasting pretreatment and gold extraction." Minerals Engineering 164 (2021) 106822. https://doi.org/10.1016/j.mineng.2021.106822

3. K.T. Konadu et. al, 2019. "Sequential pretreatment of double refractory gold ore (DRGO) with a thermophilic iron oxidizing archaeon and fungal crude enzymes." https://doi.org/10.1016/j.mineng.2019.04.043

4. Dong, Z., Jiang, T., Xu, B., Yang, Y., Li, Q., 2017. Recovery of gold from pregnant thiosulfate solution by the resin adsorption technique. Metals 7 (12), 555. http://dx.doi.org/10.3390/met7120555

5. K.T. Konadu, R.J. Huddy, S.T.L. Harrison, K. Osseo-Asare, and K. Sasaki, Sequential pretreatment of double refractory gold ore (DRGO) with a thermophilic iron oxidizing archeaon and fungal crude enzymes, *Miner. Eng.*, 138(2019), p. 86. https://doi.org/10.1016/j.mineng.2019.04.043

6. Xin-yuan Nan, Xin Cai, Jun Kong, Pretreatment Process on Refractory Gold Ores with As, ISIJ International, 2014, Volume 54, Issue 3, Pages 543-547, Released on J-STAGE April 08, 2014, Online ISSN 1347-5460, Print ISSN 0915-1559. DOI: https://doi.org/10.2355/isijinternational.54.543

7. Feng XIE, Jun-nan CHEN, Jian WANG, Wei WANG, Review of gold leaching in thiosulfate-based solutions, Transactions of Nonferrous Metals Society of China, Volume 31, Issue 11, 2021, Pages 3506-3529, ISSN 1003-6326, https://doi.org/10.1016/S1003-6326(21)65745-X.

8. Qin, H., Guo, Xy., Tian, Qh. *et al.* Recovery of gold from refractory gold ores: Effect of pyrite on the stability of the thiourea leaching system. *Int J Miner Metal Mater* 28, 956–964 (2021). https://doi.org/10.1007/s12613-020-2142-9

9. Sun, Cb., Zhang, Xl., Kou, J. *et al.* A review of gold extraction using noncyanide lixiviants: Fundamentals, advancements, and challenges toward alkaline sulfur-containing leaching agents. *Int J Miner Metal*

Mater **27,** 417–431 (2020). https://doi.org/10.1007/s12613-019-1955-x

10. L. Tremblay, G. Deschênes, E. Ghali, J. McMullen, and M. Lanouette, Gold recovery from a sulphide bearing gold ore by percolation leaching with thiourea, *Int. J. Miner. Process.* 48(1996), No. 3–4, p. 225. https://doi.org/10.1016/S0301-7516(96)00029-4

11. C.J. Ma, J.Y. Li, and R.J. Liu, A review of thiocyanate hydrometallurgy for the recovery of gold, *Appl. Mech. Mater.*, 768(2015), p. 53. https://doi.org/10.4028/www.scientific.net/AMM.768.53

12. R. Ahtiainen and M. Lundström, Cyanide-free gold leaching in exceptionally mild chloride solutions, *J. Cleaner Prod.*, 234(2019), p. 9. https://doi.org/10.1016/j.jclepro.2019.06.197

13. R. Ahtiainen, M. Lundström, and J. Liipo, Preg-robbing verification and prevention in gold chloride-bromide leaching, *Miner. Eng.*, 128(2018), p. 153. https://doi.org/10.1016/j.mineng.2018.08.037

14. Wang, Hx., Sun, Cb., Li, Sy. *et al.* Study on gold concentrate leaching by iodine-iodide. *Int J Miner Metal Mater* **20,** 323–328 (2013). https://doi.org/10.1007/s12613-013-0730-7

15. S.S. Konyratbekova, A. Baikonurova, G.A. Ussoltseva, C. Erust, and A. Akcil, Thermodynamic and kinetic of iodine-iodide leaching in gold hydrometallurgy, *Trans. Nonferrous Met. Soc. China*, 25(2015), No. 11, p. 3774. https://doi.org/10.1016/S1003-6326(15)63980-2

16. S. Jeon et. al, 2021. "The effects of Coexisting Copper, Iron, Cobalt, nickel and zinc ions on Gold recovery by enhanced cementation via Galvanic Interactions between zero-valent aluminum and activated carbon in ammonium thiosulfate system." Metals 2021, 11, 1352. https://doi.org/10.3390/met11091352

17. S. Jeon et. al., 2020. "Enhanced Cementation of gold via galvanic interaction using activated carbon and zero-valent aluminum: A novel Approach to recover gold ions from ammonium thiosulfate medium. http://dx.doi.org/10.1016/j.hydromet.2019.105165

18. S. Jeon et.al, 2021. "A simple and efficient recovery technique for gold ions from ammonium thiosulfate medium by galvanic interactions of zero-valent aluminum and activated carbon: A parametric and mechanistic

study of cementation. https://doi.org/10.1016/j.hydromet.2021.105815

19. S. Jeon et. al, 2022. "A kinetic study on enhanced cementation of gold ions by galvanic interactions between aluminum as an electron donor and activated carbon as an electron mediator in ammonium thiosulfate system." https://doi.org/10.3390/min12010091

20. M.G. Alymore and D.M. Muir, Thiosulfate leaching of gold—A review, *Miner. Eng.*, 14(2001), No. 2, p. 135. https://doi.org/10.1016/S0892-6875(00)00172-2

21. Arima, H., Fujita, T., Yen, W., 2002. Gold cementation from ammonium thiosulfate solution by zinc, copper, and aluminum powders. Mater. Trans. 43 (3), 485–493. http://dx.doi.org/10.2320/matertrans.43.485

22. Bin Xu et. al, 2017. A review of thiosulfate leaching of gold: Focus on thiosulfate consumption and gold recovery from pregnant solution. Metal-open access metallurgy journal 7(6):222. DOI:10.3390/met7060222

23. D. Feng, J.S.J. van Deventer, AMMONIACAL Thiosulfate leaching of gold in the presence of pyrite, Hydrometallurgy 82 (2006) 126-132. https://doi.org/10.1016/j.hydromet.2006.03.006

24. D. Feng, J.S.J. van Deventer, Effect of hematite on thiosulphate leaching of gold, International Journal of Mineral Processing, Volume 82, Issue 3, 2007, Pages 138-147, ISSN 0301-7516, https://doi.org/10.1016/j.minpro.2006.09.003.

25. Karavasteva, M., 2010. Kinetics and deposit morphology of gold cemented on magnesium, aluminum, zinc, iron, and copper from ammonium thiosulfate-ammonia solutions. Hydrometallurgy 104 (1), 119–122. https://doi.org/10.1016/j.hydromet.2010.04.007

26. Gallagher, N.P., Hendrix, J.L., Milosavljevic, E.G., Nelson, J.H., Solujic, L., 1990. Affinity of activated carbon towards some gold (I) complexes. Hydrometallurgy 25, 305–316. https://doi.org/10.1016/0304-386X(90)90046-5

27. Sanghyeon Choi et. al, 2021. "Addition of Fe3O4 as electron mediator for enhanced cementation of cd2+ and Zn2+ on aluminum powder from sulfate solutions and magnetic separation to concentrate cemented metals from cementation products". Journal of Environmental Chemical Engineering 9(2021) 106699. https://doi.org/10.1016/j.jece.2021.106699

28. Guilin Hu et. al, 2006. "Decomposition and Oxidation of Pyrite." doi: 10.1016/j.pecs.2005.11.004

29. I. Alp, O. Celep, D. Paktunç, and Y. Thibault, Influence of potassium hydroxide pretreatment on the extraction of gold and silver from a refractory ore, *Hydrometallurgy*, 146(2014), p. 64. https://doi.org/10.1016/j.hydromet.2014.03.007

30. J. C. Balarini, Ludmila de Oliveira Polli, Tânia Lúcia Santos Miranda, Roberto Machado Zica de Castro, Adriane Salum, Importance of roasted sulphide concentrates characterization in the hydrometallurgical extraction of zinc, Minerals Engineering, Volume 21, Issue 1, 2008, Pages 100-110, ISSN 0892-6875, https://doi.org/10.1016/j.mineng.2007.10.002

CHAPTER III

ELECTROCHEMICAL INVESTIGATION OF METAL DEPOSITION MODEL OF IRON OXIDE-ALUMINUM GALVANIC INTERACTION IN GOLD-COPPER AMMONIACAL THIOSULFATE MEDIUM

ABSTRACT

The electrochemical experiment was conducted to evaluate the galvanic interaction between the electron donor and electron mediator in a conventional electrochemical set-up (Fe_2O_3/ Fe_3O_4 -Al as the working electrode, Pt as the counter electrode, Ag/AgCl as the reference electrode) in gold thiosulfate medium. Cyclic voltammetry showed a gold reduction "shoulder-like" peak at -1.0 V using Fe_2O_3/Al and Fe_3O_4/Al electrodes. High-purity iron oxides (magnetite and hematite) specimen was also used as the working electrode to confirm if the reduction peaks were made possible using the electron mediator itself, and results obtained the same reduction peaks using iron oxides. Chronoamperometry was conducted and operated at a constant bias potential (-1.0 V) determined during cyclic voltammetry, and the surface of the working electrodes was further analyzed using SEM-EDX. SEM-EDX analysis and electrochemical experiments confirmed that gold was selectively deposited on iron oxide's surface as an electron mediator.

3.1 INTRODUCTION

In Chapter 2, cementation experiments were conducted, and it was found that the use of iron oxides (magnetite and hematite) as electron mediators with zero-valent aluminum (ZVAI) as an electron donor selectively deposited gold ions from gold-copper ammoniacal thiosulfate medium: significant amounts of gold was reductively deposited on iron-oxides from the solution while copper deposition was limited. In this chapter, for the better understanding of the phenomena, the selective deposition of gold with iron oxides were investigated using electrochemical techniques like cyclic voltammetry and chronoamperometry.

Cyclic Voltammetry (CV) is the most widely used technique to acquire quantitative information about electrochemical reactions. CV provides information on redox processes, heterogeneous electron transfer reactions and adsorption processes. It offers a rapid location of redox potentials of the electroactive species. During the potential sweep, the potentiostat measures the current resulting from electrochemical reactions occurring at the electrode interface and consecutive to the applied potential. The cyclic voltammogram is a current response plotted as a function of the applied potential. Furthermore, the chronoamperometry technique was also employed; this technique can be achieved by applying a constant potential (Ei) for a duration of time, and the current is measured. This technique can also be applied to the study of electrode surface mechanisms.

The present work investigates the electrochemical profile of the different working electrodes (Fe_2O_3/ Fe_3O_4 -AI) in ammoniacal thiosulfate solutions containing gold and copper ion complexes.

3.2 MATERIALS AND METHODS

3.2.1 Materials

All chemicals used were purchased from Wako Pure Chemical Industries, Ltd., Japan. Aluminum electrode was prepared using a high purity aluminum sheet purchased from WAKO chemical (99.99%, CAS No.:7429-90-5) . For electron mediators, activated carbon (99.99%, CAS No.: 031-02135) having about 800–1500 $m^2 g^{-1}$ of specific surface area, hematite (Fe_2O_3, 99.99%, CAS No: 096-02821) and magnetite (Fe_3O_4, 99.99%, CAS No: 093-01035) were used.

3.2.2 Solution Preparation

The Au-ammonium thiosulfate solution was prepared by dissolving 50 mg of Au powder (99.999%, CAS No.: 937902 Wako Pure Chemical Industries, Ltd., Japan) in 500 ml of ammonium thiosulfate solution containing 1 M $Na_2S_2O_3$.$5H_2O$ (CAS No.: 197-03585), 0.5 M NH3 (CAS No.: 016-03146), 0.25 M $(NH_4)_2SO_4$ (CAS No.: 016-03445), and 10 mM $CuSO_4$ (CAS No.: 034-04445) in a beaker; the solution was agitated using a magnetic stirrer with a built-in heater, a part of a thermocouple was submerged in the solution to maintain the temperature at 30°C for 24 h with a constant shaking frequency of 600 min^{-1}. Electrolyte solutions were prepared by dissolving $Na_2S_2O_3$.$5H_2O$ and metal ions (Cu^{2+} and Au^+) in 0.1 M NH_3 / 0.05 M $(NH_4)_2SO_4$ buffer solutions.

3.2.3 Electrochemical Set-up

Electrochemical experiments were done using a conventional three electrode system connected to computerized driven potentiostat (SP-300, Biologic, France). The setup of the electrochemical measurements system is shown in
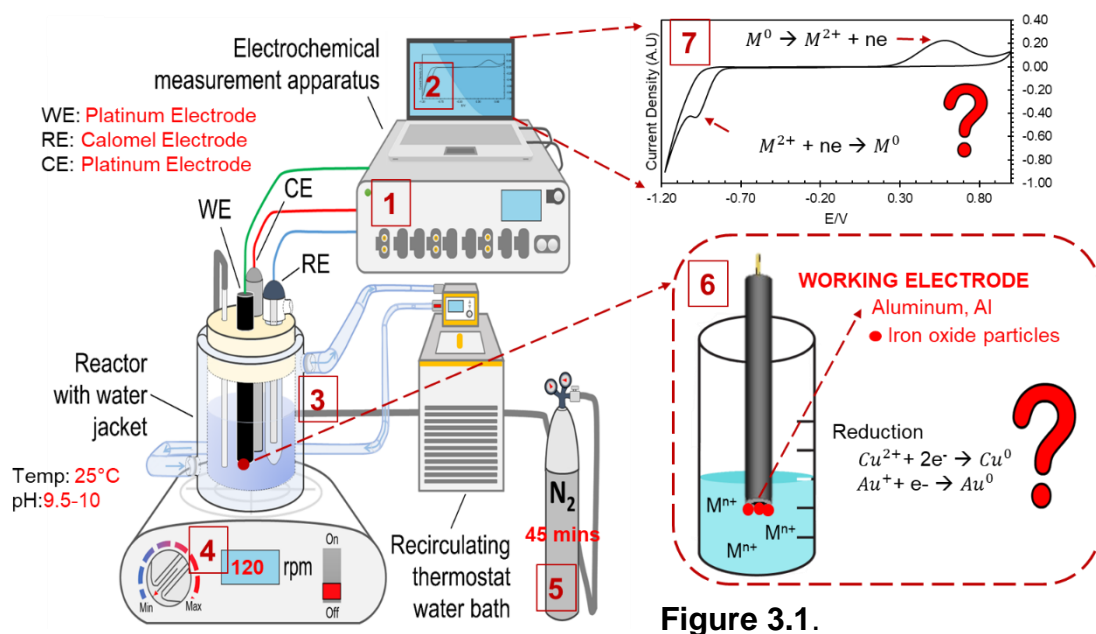
Figure 3.1.

Figure 3.1 Illustrates the electrochemical set-up numbered in different parts as follows:

1. SP-300 ECLab Biologic, Farnce; Potentiometer apparatus.
2. Computer with installed software (ECLab) used various electrochemical operations.
3. Electrode set-up, with built -in recirculating thermostat water bath glass-type container.
4. Magnetic stirrer with manual agitation speed operation.
5. Nitrogen-gas system for solution purging to achieve anaerobic solution condition.
6. Working electrode illustration, ZVAl attached with electron mediator particles.
7. Illustration of ECLab-generated voltammogram spectra after electrochemical operation

Electrode Preparation

Improvised Al electrode was prepared by cutting a cuboid (10 × 10 × 2 mm) out of a large aluminum metal sheet using a diamond cutter, connecting it to copper wires with silver conducting paste, and fixing it inside a plastic mold (25 mm diameter and 10 mm height) with Technovit® non-conductive resin. Next, the surface of the Al electrode was exposed by polishing it using silicon carbide (SiC) papers of decreasing grain size (#200, #600, #1000, #1500), followed by polishing with 5 and 1 μm Al_2O_3 pastes on a smooth glass plate. Finally, the polished electrode was ultrasonically cleaned for 5 min to remove residually attached Al_2O_3 particles and washed several times with DI water. After which, the exposed surface of the polished Al working electrode was oxidized under atmospheric conditions for 2 days to mimic the oxide layer on Al upon the cementation process; the oxidized Al working electrode was subjected to SEM-EDX analysis using SEM-EDS, JSM-IT200TM, JEOL Co., Ltd., Japan to elucidate the magnitude of oxide being formed. Iron oxide powder attached to Al electrodes was then prepared by mixing 0.05g of iron oxide powder (Fe_3O_4 or Fe_2O_3) with 5 mL acetone, and the resulting mixture was then carefully attached to the surface of Al electrode. After evaporating acetone, iron oxide/Al electrodes were used as the working electrode. This procedure was chosen to prevent "scratching" of the Al oxide layer formed on the electrode and has been successfully used in previous electrochemical studies [32].

Before conducting electrochemical measurements of the improvised Fe_xO_x/Al working electrodes, **Figure 3.2** illustrates the backscatter electron photomicrograph with elemental mapping and point EDX analysis of the aluminum electrode. The result shows that traces of O were detected after exposing the surface of the aluminum electrode for two (2) days, which were dispersedly formed at the surface of the electrode. The presence of this layer mimics the surface oxide layer of ZVAl during the gold recovery process. Thus, the addition of iron oxides on the Al electrode surface was conducted to understand the electrochemical property of hematite and magnetite upon Au recovery.
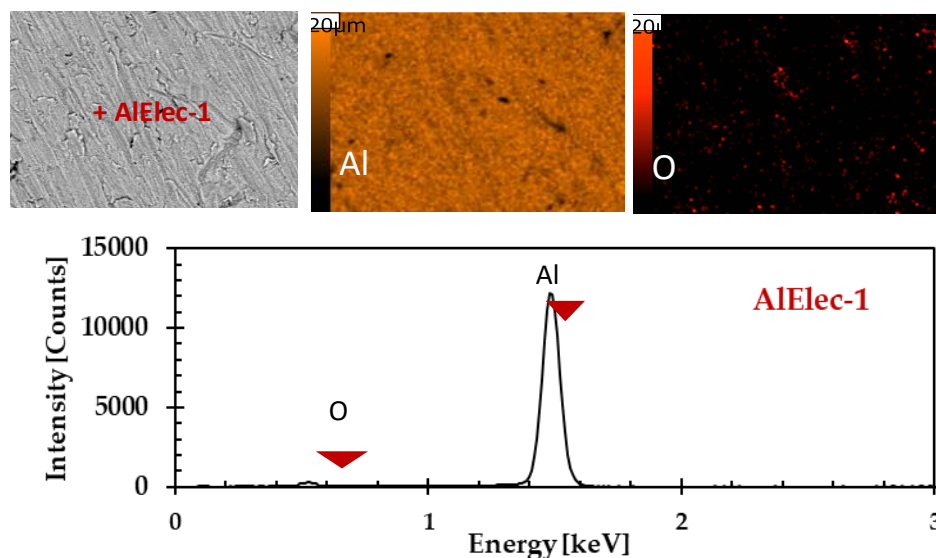
Figure 3.2. Back scattered electron photomicrograph with elemental mapping and point EDS analysis of improvised aluminum electrode.

3.2 Electrochemical Experiments

3.3.1 Cyclic Voltammetry (CV) Measurements

To elucidate the electrochemical properties of iron oxide/Al electrodes, cyclic voltammetry (CV) was conducted using a computerized driven potentiostat (SP-300, Biologic, France) with a conventional three-electrode system, composed of iron oxide/Al electrode as working electrode, Ag/AgCl electrode filled with saturated KCl as reference electrode, and platinum (Pt) electrode as the counter electrode. The measurements were conducted in an anoxic condition (without dissolved oxygen, O_2) by purging the prepared 150 ml electrolyte solution with ultrapure N_2 gas (99.99%) for 45 min before electrochemical measurements. Three electrodes were immersed in a glass cell with a water jacket before N_2 purging and equilibrated at 25°C for 30 min. In all cases, measurements were always done after the equilibration of the working electrode to its open circuit potential (OCP). Equilibrium here means that the measured electrode potential of the working electrode did not change by more than 2 mV for 60 s. After that, the scan started from the OCP and

moved towards more negative potentials at a rate of 20 mV/s up to -1.5 V, after which the sweep direction was reversed and moved towards increasingly positive potentials. The scan direction was again reversed after reaching +1.0 V and then moved back to the starting position (i.e., OCP). This entire process constituted one cycle; each measurement lasted 3 cycles under unstirred conditions. After each experiment, the electrode was then re-polished using fine-grained SiC papers (#1200 and #1500), and Al_2O_3 pastes (5 μm and 1μm) to expose a new and unreacted surface for the next run and attached new 5 mg of iron oxide particles at the surface. Triplicate measurements were done using this technique.

3.3.2 Chronoamperometry (CA) and Electrode Surface Characterization

Electrodes for surface characterization were prepared by applying the chronoamperometry technique using a computer-driven potentiostat electrochemical measurement (SP-300, Biologic, France) with a conventional three-electrode system at 25°C. After equilibration of the working electrode to the OCP, it was polarized at a fixed electrode potential of -1.0 V (this potential was selected since the reduction peak of gold was observed upon cyclic voltammetry) for 10 min using Au and Cu electrolytes, and the process was agitated in a constant speed of 120 rpm using a magnetic stirrer. After the process, the working electrode was removed from the cell, immersed in DI water, and cured in a vacuum oven at 40°C for 24 h. The surface of the working electrode was then investigated using scanning electron microscopy with energy-dispersive X-ray, SEM-EDX.

3.4 RESULTS AND DISCUSSIONS

Cementation of Au and Cu from ammonium thiosulfate solutions is an electrochemical process. When ZVAI is used as an electron donor, anode reaction is as follow,

$$Al = Al^{3+} + 3\ e^- \hspace{3cm} (1)$$

For cathodic reactions (deposition of Cu and Au) are assumed as

$$Cu\ (NH_3)_4{}^{2+} + 2\ e^- = Cu + 4\ NH_3 \qquad\qquad (2)$$

$$Au\ (S_2O_3)_2{}^{3-} + e^- = Au + 2\ S_2O_3{}^{2-} \qquad\qquad (3)$$

Note that the anodic reaction is common for Cu and Au deposition, while cathodic reactions differ for Cu and Au. This suggests that the selective deposition of Au observed in the previous chapter is because Au cathodic reaction is preferred to that of Cu when iron-oxide is used as an electron mediator. A series of electrochemical experiments were conducted to confirm the results.

To identify the reduction potential of $Cu\ (NH_3)_4{}^{2+}$ and $Au(S_2O_3)_2{}^{3-}$, cyclic voltammetry was conducted using a Pt working electrode in NH_4/NH_3 buffer solutions containing different electrolytes. **Figure 3.3(a)** presents the effects of $S_2O_3{}^{2-}$ and gold ions on cyclic-voltammogram. In the voltammogram spectra for a control experiment using NH_4/NH_3 buffer solution without metal ions, the current density was almost zero between - 0.7 V and +1.0 V, indicating no electrochemical reaction occurred in the range. However, below - 0.7 V, the current decreased with decreasing electrode potential, and this may be due to the reduction of H_2O to form H_2 gas.

In the case of the experiment with $S_2O_3{}^{2-}$, a new cathodic current peak appeared at - 0.9 V, which can be assigned to the reduction of $S_2O_3{}^{2-}$. In the anodic region in the cyclic voltammogram with $S_2O_3{}^{2-}$, a significant anodic peak was observed around + 0.6 V. This peak was observed even when the initial potential scan direction was positive, indicating that the anodic current peak is due to the oxidation of $S_2O_3{}^{2-}$.

When gold ions were added with $S_2O_3{}^{2-}$, $Au(S_2O_3)_2{}^{3-}$ is formed. In the experimental results with $Au(S_2O_3)_2{}^{3-}$, a cathodic current peak was observed at - 0.9 V. When comparing cyclic voltammograms, peak current density at - 0.9 V was more substantial with $Au(S_2O_3)_2{}^{3-}$ than with $S_2O_3{}^{2-}$, implying that not only $S_2O_3{}^{2-}$ but also Au^+ in $Au(S_2O_3)_2{}^{3-}$ is reduced at almost similar redox potentials.
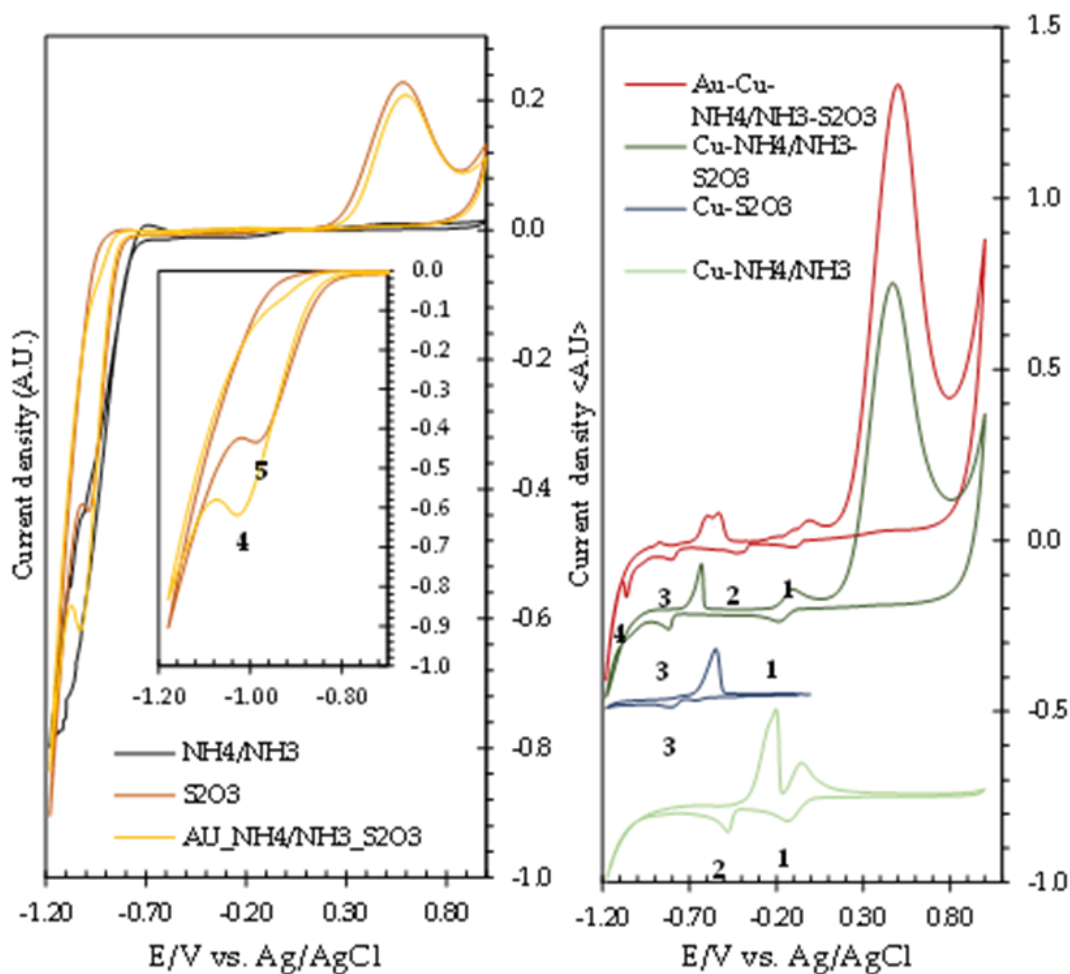
Figure 3.3. Voltammogram characterization of **a)** NH4/NH3, S2O3, and Au_ NH4/NH3_S2O3 **b)** Au_Cu_NH4/NH3_S2O3, Cu_NH4/NH3, Cu_NH4/NH3_S2O3 and Cu_ S2O3

Figure 3.3(b) shows the effects of cupric species on cyclic voltammogram. When CuSO4 was added to NH4/NH3 buffer solution, Cu(NH3)4^{2+} was formed. With Cu (NH3)4^{2+} , two cathodic peaks centered at approximately -0.2 V and -0.5 V, and two anodic peaks appeared. The presence of two cathodic peaks implies that Cu^{2+} in Cu(NH3)4^{2+} undergoes a two-step reduction process; the cathodic peak at -0.2 V may correspond to the reduction of Cu^{2+} to Cu$^+$, while the peak at -0.5 V corresponds to the reduction of Cu$^+$ to Cu^0.

Two anodic peaks in the cyclic voltammogram with $Cu(NH_3)_4^{2+}$ may be the back reactions of the two-step reduction process; the oxidation of Cu^0 to Cu^+ and Cu^+ to Cu^{2+} occurs at - 0.2 V and 0 V, respectively. When $CuSO_4$ and $S_2O_3^{2-}$ were added into the NH_4/NH_3 buffer solution together, two sets of reduction and anodic peaks were observed in the cyclic voltammogram; one was around - 0.2 V, and the other was around – 0.8 V (approximate values). The cathodic peak at - 0.2 V was also observed in the voltammogram without $S_2O_3^{2-}$, confirming that this peak is due to the reduction of $Cu(NH_3)_4^{2+}$ to $Cu(NH_3)_2^+$ species.

Table 3.1 Summary of reduction reactions and its corresponding potential peak observed in the cyclic voltammograms using Pt as a working electrode in **Figure 3.3.**

Assigned Reductions Reactions	Potential (V)
$Cu(NH_3)_4^{2+} + e^- \rightarrow Cu(NH_3)_2^+ + 2NH_3$	-0.2
$Cu(NH_3)_4^+ + e^- \rightarrow Cu^0 + 4NH_3$	-0.5
$Cu(S_2O_3)_2^{3-} + e^- \rightarrow Cu^0 + 2S_2O_3^{2-}$	-0.8
$2S_2O_3^{2-} + 6H_2O + 8e^- \rightarrow 4S^0 + 12OH^-$	-0.9
$Au(S_2O_3)_2^{3-} + 6H_2O + 9e^- \rightarrow Au^0 + 4S^0 + 12\ OH^-$	-1.0

The peak at - 0.8 V was not observed without $S_2O_3^{2-}$ and $CuSO_4$, implying that this cathodic peak reduces cuprous thiosulfate complexes such as $Cu(S_2O_3)^-$ to Cu^0. Cuprous thiosulfate complexes may be formed from the amine complex $Cu(NH_3)_2^+$, which was the reduction product of $Cu(NH_3)_4^{2+}$. **Table 3.1** summarizes the reduction reactions observed in the cyclic voltammograms in **Figure 3.3.**

$$Au(S_2O_3)_2{}^{3-} + e^- = Au^0 + 2(S_2O_3)_2{}^{2-}$$

(a)

(b)

(c)
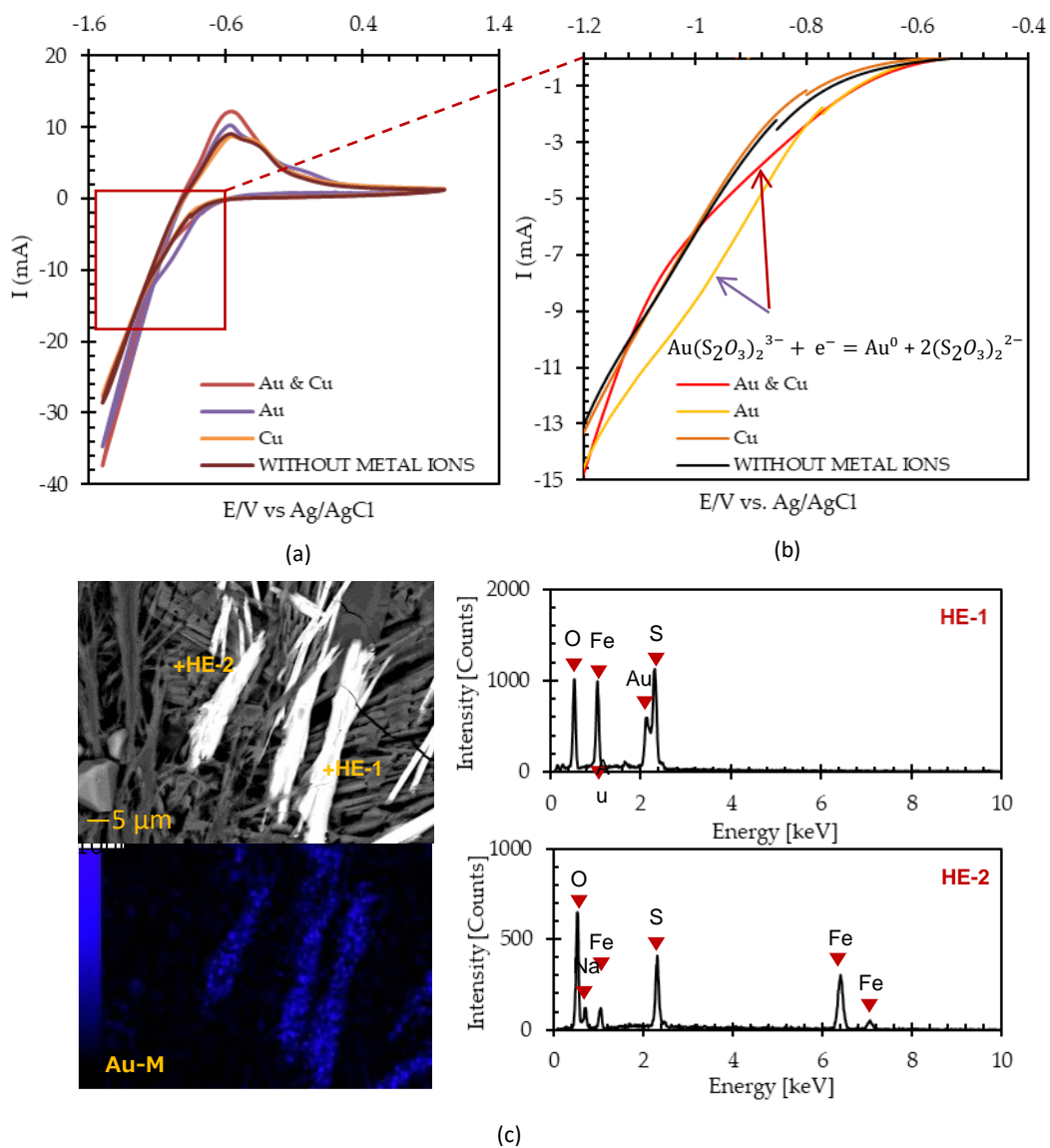
Figure 3.4 Cyclic Voltammogram of Fe_2O_3/Al electrode at different electrolytes a) Wide Scan b) Narrow Reduction Voltammogram c) Back scattered electron photomicrograph with elemental mapping and point eds analysis of Cu-Au electrolytes.
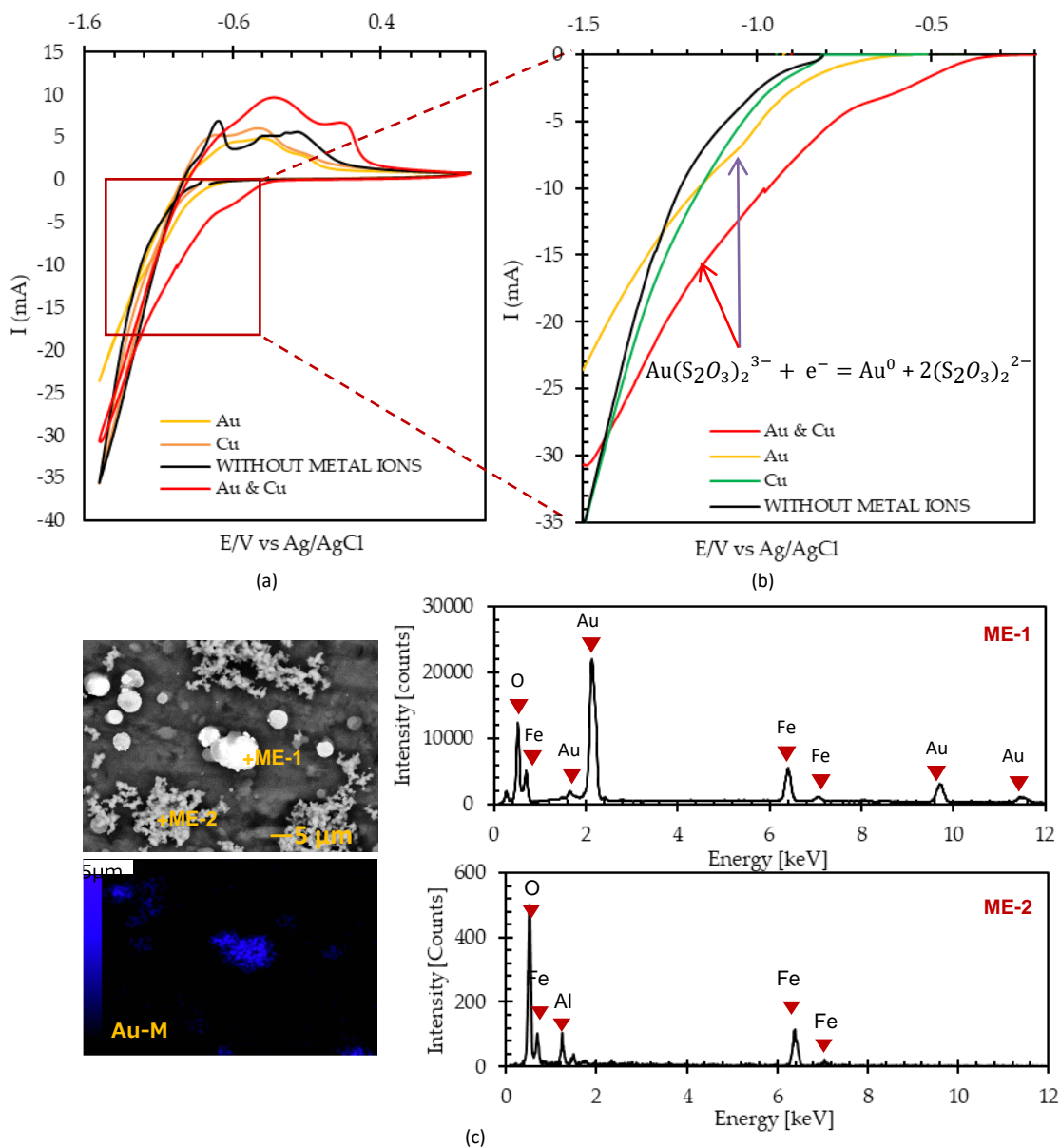
Figure 3.5 Cyclic Voltammogram of Fe_3O_4/Al electrode at different electrolytes a) Wide Scan b) Narrow Reduction Voltammogram c) Back-scatter electron photomicrograph with elemental mapping and point eds analysis of Cu-Au electrolytes.

Figures 3.4 and 3.5 illustrate the voltammogram of Fe_2O_3/Al and Fe_3O_4/Al working electrodes in different electrolyte systems (i.e., 10 mM Cu ions, 10 mM Au ions, 10mM Cu& Au ions, and without metal ions), respectively. The cathodic sweep parts were highlighted and projected at the right-side corner of the figures. When comparing the results without metal ions and with only Cu^{2+}, there was no significant difference in the current-potential curves, indicating that Cu^{2+} was not reduced on iron oxide/Al electrodes. On the other hand, the cathodic current with Au^+ was larger than without metal ions, indicating that gold ions can be reduced on iron oxide/Al electrodes. The cathodic current with Cu and Au ions was the same as that with the electrolyte containing only Au ions, confirming that only Au was reduced on the electrode.

In contrast, Cu^{2+} was not reduced, i.e., selective reduction of gold ions occurs on iron oxide/Al electrodes. Previous papers reported that when the Al electrode was used without an electron mediator, there was no significant reduction current due to metal ions like Cu and Au deposition [18-19]. Considering this, it can be concluded that the reduction of metal ions occurs only when iron oxides are attached to the surface of the Al electrode. This result suggests that iron-oxides function as electron mediators from Al to metal ions.

Furthermore, to elucidate the electrochemical behavior of the different improvised electrodes, **Figure 3.6** shows the narrow reduction curves of a) AC/Al, b) Fe_3O_4/Al c) Fe_2O_3/Al and d) the comparative reductive scan using Au and Cu electrolytes. It can be observed that using AC/Al, two shoulder-like peaks were observed around -0.5V and -1.0V, while for the iron oxides/Al electrode, only one shoulder-like peak was observed assigned to the reduction of gold ions.
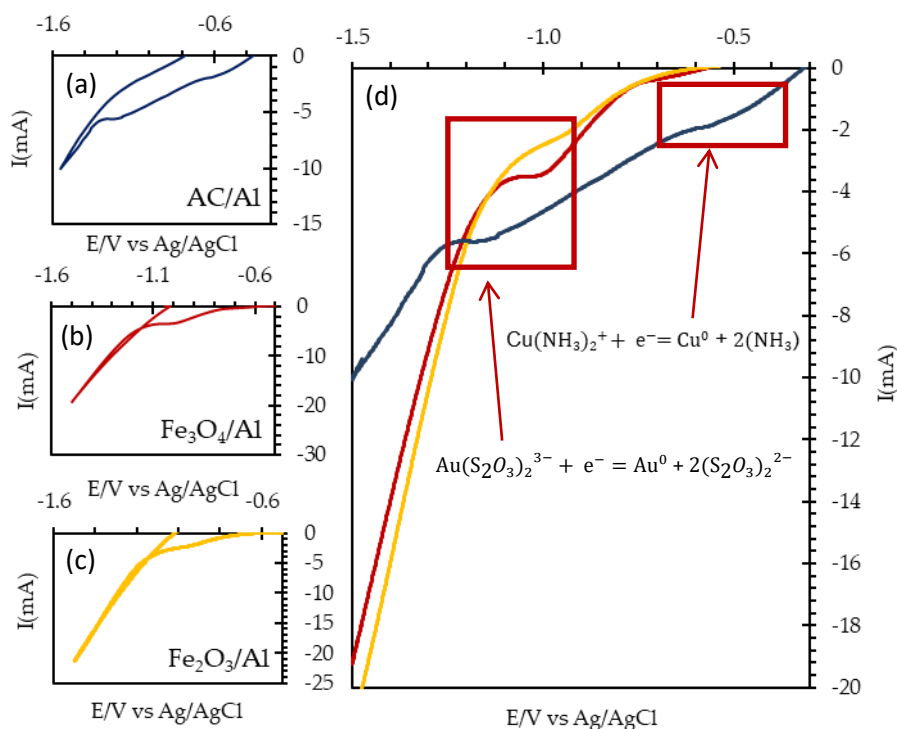
Figure 3.6 Cyclic voltammogram narrow reduction curve a) AC/Al b) Fe₃O₄/Al c) Fe₂O₃/Al and d) Narrow reductive scan of all improvised electrode at Cu and Au electrolytes.

The results suggest that the cyclic voltammogram agrees with the results of cementation experiments in chapter 2, where only gold ions can be cemented when using iron oxide as electron mediator with ZVAl as electron doner. Chronoamperometry was conducted by applying a fixed electrode potential of -1.0 V in the stirred solutions for 60 minutes to confirm the deposition of Au on the working electrodes. After 60 minutes, the electrodes were taken out and dried to be analyzed by SEM-EDX. Elemental mapping and point analysis results were illustrated at the bottom side of **Figures 3.4 and 3.5.** The point analysis results show that Au peaks were observed along with S peaks at the point **HE-1** in **Figure 3.4** and the point **ME-1 in Figure 3.5.** At the same point, Fe and O peaks were detected, implying that gold ions were reduced and deposited on the surface of iron oxide particles attaching to the Al electrode.

As shown in **Figure 3.7**, gold deposited on iron oxide shows similar morphology with the iron oxide particles (morphology here pertains to the shape of iron oxides); hematite and deposited gold are in longitudinal orientation **(Figure 12. A)** while magnetite and gold have an endless array of "nodular-like" particles **(Figure 12. B).** These morphological observation results from further support that iron oxides are an electron mediator between the electron donor (Al) and electron acceptor, $Au(S_2O_3)_2^{3-}$ ions, as already discussed with the following equations:

$$Au\,(S_2O_3)_2^{3-} = Au^+ + 2\,S_2O_3^{2-} \tag{4}$$

$$2S_2O_3^{2-} + 6\,H_2O + 8\,e^- = 4S^0 + 12OH^- \tag{5}$$

$$Au^+ + e^- = Au^0 \tag{6}$$

$$Au\,(S_2O_3)_2^{3-} + 6\,H_2O + 9\,e^- = Au^0 + 4S^0 + 12\,OH^- \tag{7}$$
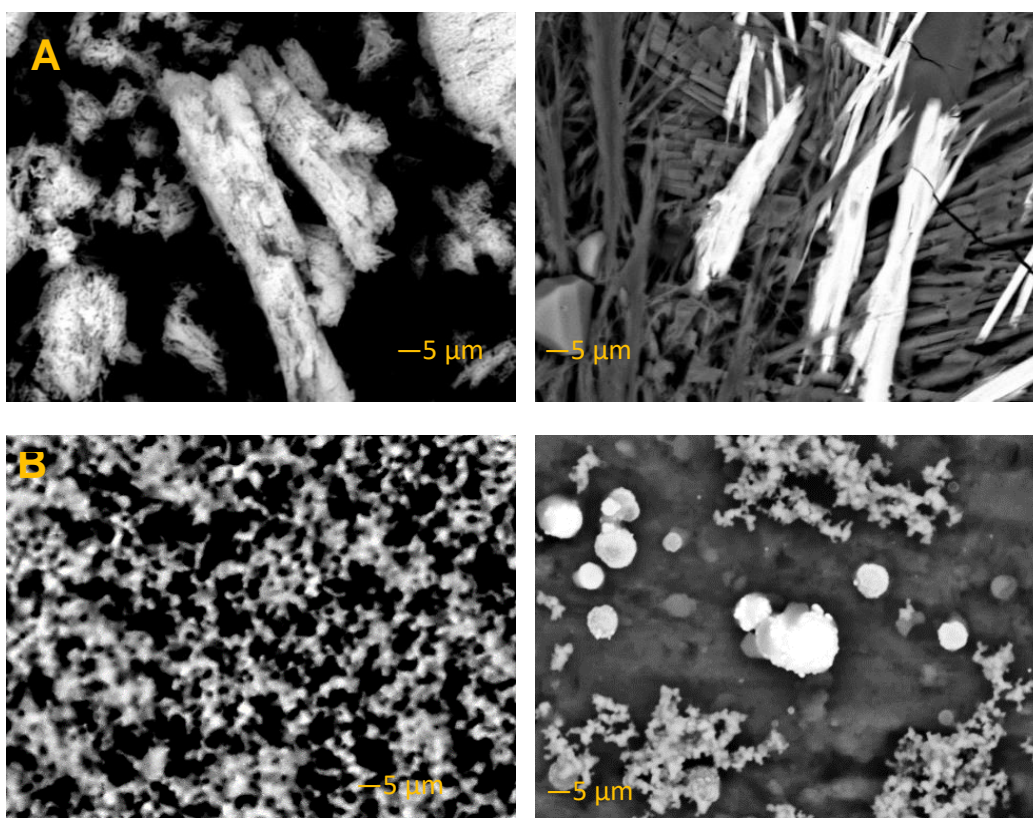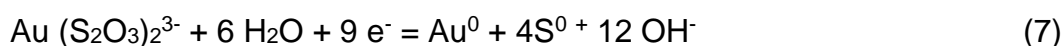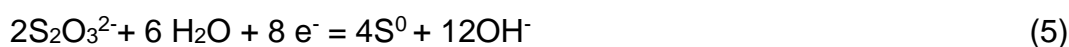
Figure 3.7 Back scattered electron photomicrograph of **a)** Hematite particles (left), Hematite with Au (right) **b)** Magnetite particles (left), Magnetite with Au (right).

Figure 3.8 High-Purity iron oxide specimens used as working electrode; hematite (left) and magnetite (right), respectively.

Figure 3.8 shows the high-purity hematite (left) and magnetite (right) specimens as working electrodes to further investigate the electrochemical behavior of iron oxide. The results of cyclic voltammetry and surface analysis after chronoamperometry experiments was presented in **Figure 3.9.** The results obtained that using high-purity iron oxides as the working electrode in-gold-copper ammoniacal thiosulfate medium, one reduction peak was observed at -1.1 V suggesting that the peak corresponds to the reduction of gold ions, also upon applying a bias potential of -1.1 V during chronoamperometry, the surface of the working electrode was investigated using SEM-EDX analysis. The results of surface analysis confirmed that the cemented metal (bright objects observed in the backscattered electron photomicrographs) and that it was gold as per the results generated using point analysis in the surface of the working iron oxide electrodes as shown in **Figure 3.9** (right side).

The results of electrochemical and surface analysis using high-purity iron oxides supports the selective cementation of gold and that the electron mediator itself facilitates the selective cementation.
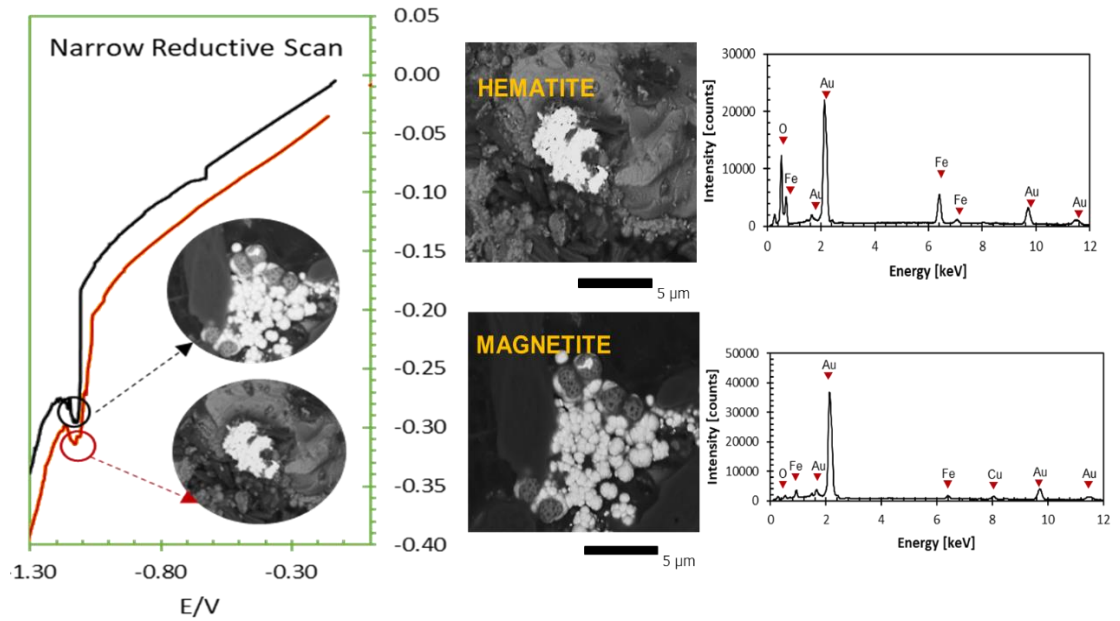
Figure 3.9 Electrochemical profile of high purity working electrodes in gold-copper ammonium thiosulfate solution.

3.5 PROPOSED CEMENTATION MODEL
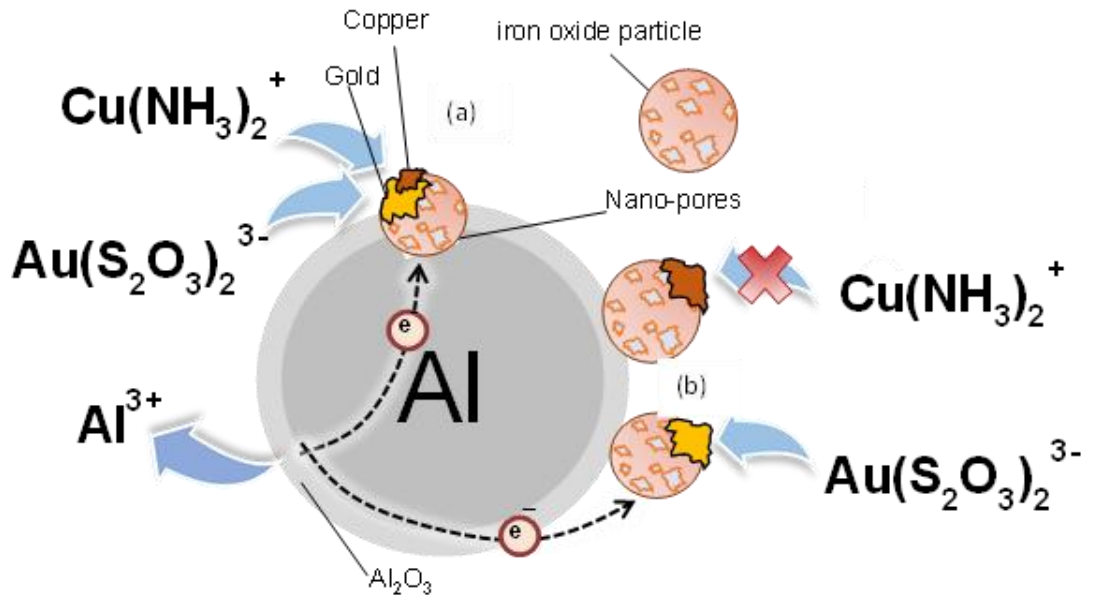
Figure 3.10: Schematic diagram of the proposed galvanic electron transfer mechanism of iron oxide and zero-valent aluminum. (a) Direct contact on the porosity within Al-oxyhydroxide layer and (b) Direct transfer through Al-oxyhydroxide layer.

Figure 3.10 shows the schematic diagram of the proposed cementation model of gold using iron oxides and ZVAl. In this model, ZVAl acts as an electron donor or anode where the anodic dissolution of ZVAl occurs (**equation 1**). An iron oxide particle attached to the ZVAl particle surface acts as an electron mediator or cathode: electrons from ZVAl pass through the iron oxide to gold thiosulfate complexes adsorbed on the surface. The cathodic reaction is the cementation (reductive deposition) of Au and S from $Au(S_2O_3)_2^{3-}$ (**equation 7**); this ion will be assigned as electron acceptors. This mechanism is supported by the electrochemical and surface analysis results presented in **Figures 3.4 and 3.5.**

Interesting matters that can be observed in the proposed model are the following:

First, is the electron transfer mechanism across the Al_2O_3 layer between ZVAl and iron oxide particle: ZVAl surface might be covered with a fragile layer of Al_2O_3 due to autogenous oxidation. Since Al_2O_3 is an electric insulating material, direct current cannot pass through this layer. Interpretation for the electron transfer through the insulating Al_2O_3 layer is via: **(1)** the quantum tunnelling effect [33] and **(2)** alternative current transfer through the Al_2O_3 layer acting as a capacitor [4].

The tunnelling effect can interpret the electron transfer when the Al_2O_3 layer is fragile, where a thin Al_2O_3 layer can be broken down upon continuous agitation where particles collide. On the other hand, the electron transfer through the Al_2O_3 capacitor may be possible when electrochemical reactions (anodic and cathodic reactions) or physical contact of ZVAl and iron oxides are dynamically changed with time.

Lastly, the most important issue associated with the proposed model is the selective deposition of gold. Gold was deposited on the iron oxide surface when iron oxides were used as an electron mediator, but copper deposition was limited. Furthermore, the reduction potential of $Au(S_2O_3)_2^{3-}$ is much lower than that of $Cu(NH_3)_4^{2+}$, indicating that from the thermodynamic viewpoint, reductive deposition of copper is more accessible than gold. This result was confirmed when using activated carbon as an electron mediator: both copper

and gold were deposited. These results further suggest that the selective gold deposition is due to the properties of iron oxide used as electron mediators, and simple thermodynamic considerations cannot interpret the mechanism.

Selective deposition of gold in an ammonia thiosulfate leaching system is significant and industrially attractive since this system requires cupric ions as a leaching catalyst, and extremely high concentrations of copper ions coexist with low concentrations of gold leached from ores. If selective deposition of gold is possible, separating gold and copper is not required after the deposition step, and the process becomes more straightforward compared to previous research conducted [1-5], where both Cu and Au were cemented using AC as the electron mediator. Thus, understanding the mechanism of selective gold deposition with iron oxide is essential and further studies are needed and might be presented in the following paper.

3.6 CONCLUSIONS

The potential of iron oxides (Fe_2O_3 and Fe_3O_4) as an electron mediator and its galvanic interaction with zero-valent aluminum for enhancing gold cementation from gold-copper ammoniacal thiosulfate solution was evaluated. Electrochemical analysis further validates the selective cementation; when using iron oxides as well as high-purity iron oxides as working electrodes, the cyclic voltammograms obtained one "shoulder-like" peak centered at - 1.0 V for hematite and magnetite, which can only be assigned to reducing gold ions. Compared to activated carbon, the voltammogram spectra obtained two "shoulder-like" peaks centered at - 1.0 V and - 0.5 V, which can be assigned to gold and copper reduction, respectively.

Lastly, the surface analysis revealed that the morphology of metal deposited on the surface of the iron oxide/Al electrode after chronoamperometry mimicked the morphology of iron oxide particles and was assigned to gold only. With these results, a promising effective technology can be used to treat the century-old problem dealing with pyritic-gold bearing ore, of which, after the roasting process, gold can be recovered via a thiosulfate leaching-cementation process without using activated carbon as an absorbent. Though this research is focused on the technical feasibility of iron oxides as an

electron mediator, this warrants an in-depth investigation using natural refractory gold ores and might be presented in the following paper.

REFERENCES

31. S. Jeon et. al, 2021. "The effects of Coexisting Copper, Iron, Cobalt, nickel and zinc ions on Gold recovery by enhanced cementation via Galvanic Interactions between zero-valent aluminum and activated carbon in ammonium thiosulfate system." Metals 2021, 11, 1352. https://doi.org/10.3390/met11091352

32. S. Jeon et. al., 2020. "Enhanced Cementation of gold via galvanic interaction using activated carbon and zero-valent aluminum: A novel Approach to recover gold ions from ammonium thiosulfate medium. http://dx.doi.org/10.1016/j.hydromet.2019.105165

33. S. Jeon et.al, 2021. "A simple and efficient recovery technique for gold ions from ammonium thiosulfate medium by galvanic interactions of zero-valent aluminum and activated carbon: A parametric and mechanistic study of cementation. https://doi.org/10.1016/j.hydromet.2021.105815

34. S. Jeon et. al, 2022. "A kinetic study on enhanced cementation of gold ions by galvanic interactions between aluminum as an electron donor and activated carbon as an electron mediator in ammonium thiosulfate system." https://doi.org/10.3390/min12010091

35. Arima, H., Fujita, T., Yen, W., 2002. Gold cementation from ammonium thiosulfate solution by zinc, copper, and aluminum powders. Mater. Trans. 43 (3), 485–493. http://dx.doi.org/10.2320/matertrans.43.485

36. D. Feng, J.S.J. van Deventer, Effect of hematite on thiosulphate leaching of gold, International Journal of Mineral Processing, Volume 82, Issue 3, 2007, Pages 138-147, ISSN 0301-7516, https://doi.org/10.1016/j.minpro.2006.09.003.

37. Karavasteva, M., 2010. Kinetics and deposit morphology of gold cemented on magnesium, aluminum, zinc, iron, and copper from ammonium

thiosulfate-ammonia solutions. Hydrometallurgy 104 (1), 119–122. https://doi.org/10.1016/j.hydromet.2010.04.007

38. Gallagher, N.P., Hendrix, J.L., Milosavljevic, E.G., Nelson, J.H., Solujic, L., 1990. Affinity of activated carbon towards some gold (I) complexes. Hydrometallurgy 25, 305–316. https://doi.org/10.1016/0304-386X(90)90046-5

Sanghyeon Choi et. al, 2021. "Addition of Fe3O4 as electron mediator for enhanced cementation of cd2+ and Zn2+ on aluminum powder from sulfate solutions and magnetic separation to concentrate cemented metals from cementation products". Journal of Environmental Chemical Engineering 9(2021) 106699. https://doi.org/10.1016/j.jece.2021.106699

39. Fu, P.; Li, Z.; Feng, J.; Bian, Z. Recovery of Gold and Iron from Cyanide Tailings with a Combined Direct Reduction Roasting and Leaching Process. *Metals* **2018**, *8*, 561. https://doi.org/10.3390/met8070561

40. C.B. Tabelin, Suchol Veerawattananun, Mayumi Ito, Naoki Hiroyoshi, Toshifumi Igarashi, Pyrite oxidation in the presence of hematite and alumina: II. Effects on the cathodic and anodic half-cell reactions, Science of The Total Environment, Volumes 581–582, 2017, Pages 126-135, ISSN 0048-9697, https://doi.org/10.1016/j.scitotenv.2016.12.050

41. Ke, B., Li, Y., Chen, J., Zhao, C., Chen, Y., 2016. DFT study on the galvanic interaction between pyrite (100) and galena (100) surfaces. Appl. Surf. Sci. 367, 270–276. https://doi.org/10.1016/j.apsusc.2016.01.063

CHAPTER IV

SELECTIVE CEMENTATION MECHANISM OF IRON OXIDES TO GOLD UPON GALVANIC INTERACTION WITH ZERO-VALENT ALUMINUM IN GOLD-COPPER AMMONIACAL THIOSULFATE MEDIUM

4.1 INTRODUCTION

Gold and the lucrative value it bears have caused and continue to cause an increase in demand that spiked its price up to 2000 USD per ounce as of December of 2023. This precious and novel metal has been used in several applications, such as the use of gold as official coins, in electronic devices, and other applications such as the used of gold in medical applications (H.M. King, 2023). These demands become a significant research interest for sustainability, knowing that the natural gold ore reserves are depleting and are finite resources; as such, finding alternative resources is an important issue to be addressed (Hong Qin et al., 2021).

One potential gold resource is the tailings deposits operated by mining companies dealing with refractory gold pyritic ores. This mining company has 60-70% overall recovery; thus, this refractory gold encapsulated in the sulfur matrix of pyrite is a potential resource for gold production (Hong Qin et al., 2020). Researchers have been dealing with this type of ore as to how this material can be re-exploited. This natural reserve is difficult to refine as pyrite has a complicated mineralogy. Conventionally, a two-step process has been employed to recover gold from this type of ore successfully. The pyrometallurgical process is conventionally employed to alter pyrite's surface property to expose the gold on its surface via sulfur oxidation in the oxidation roasting process. The roasted pyrite is now susceptible to chemical dissolution via cyanide leaching (X. et al., 2013; P. et al., 2018).

On the other hand, many countries have banned this toxic chemical, as this lixiviant has caused and continues to cause detrimental effects to humans and the environment. Much research has been driven to find alternatives, such as investigating halide groups and thiourea, but these chemicals have proven

highly corrosive (R. et al., 2018; H.X. (Wang et al., 2013; S.S. Konyratbekova et al., 2015). One of the potential candidates is the use of thiosulfate in the gold leaching process. However, it is not currently in use because of its low recovery in pregnant solution; its higher selectivity and leaching rate to gold warrants to be investigated concerning recovery techniques. To address this issue, Jeon et al., 2019 have proven the possibility of increasing gold recovery via galvanic interaction with zero-valent aluminum, which accounts for up to 99.99% of gold recovery via reductive deposition.

Previous research has been employed to investigate the feasibility of iron oxides (the main product of roasting pyrite) as electron mediators in galvanic interaction with zero-valent aluminum in gold-copper ammoniacal thiosulfate medium to resolve the issue of refractory gold pyritic ores. Also, the previous study reported that iron oxide can be used as an electron mediator and can cement gold up to 90% on its surface. Also, the difference between activated carbon and iron oxide has been highlighted and becomes the main interest of this study; activated carbon was able to recover both gold and copper at 99.99%, while the use of iron oxides was able to recover gold and copper around 86-90 % and 15-21%, respectively. Thus, using iron oxides as electron mediators has selectively cemented gold in a copper ammoniacal thiosulfate medium (Zoleta et al., 2023). The previous findings are advantageous because the copper in a barren solution with ammoniacal thiosulfate can be re-used for gold dissolution, as copper is the main component in catalyzing gold dissolution. Considering the semiconductive properties of hematite and magnetite, this research is governed by investigating the primary mechanism of selective cementation in iron oxide-electrolyte interface by conducting in-depth electrochemical impedance spectroscopic analyses of various semiconductive materials.

4.2 MATERIALS AND METHODS

4.2.1 Materials

ZVAl (99.99%, CAS No.: 012-19172, Wako Pure Chemical Industries, Ltd., Japan) and activated carbon (99.99%, CAS No.: 031-02135, Wako pure Chemical Industries, Ltd., Japan) having about 800–1500 m^2/g of specific surface area were used to recover Au ions from ammonium thiosulfate solutions. Also, 99.99% purity synthetic hematite (Fe_2O_3), magnetite (Fe_3O_4), TiO_2 (anatase) and TiO_2 (rutile) were purchased from Wako Pure Chemical Industries, Ltd., Japan having a CAS No: 096-02821, 093-01035, 1317-70-0, and 1317-80-2, respectively. **Table 4.1** summarizes the sample transmittal used in this study.

4.2.2. Recovery of gold ions from ammonium thiosulfate solution

Ammonium thiosulfate solution containing 100 mg/l of Au ions (i.e., Au-ammonium thiosulfate solution), 1 M $Na_2S_2O_3$.$5H_2O$ (CAS No.: 197-03585), 0.5 M NH_3 (CAS No.: 016-03146), 0.25 M $(NH_4)_2SO_4$ (CAS No.: 016-03445), and 10 mM $CuSO_4$ (CAS No.: 034-04445) from Wako Pure Chemical Industries, Ltd., Japan, with pH 9.5-10 were used in the Au recovery experiments. The Au-ammonium thiosulfate solution was prepared by leaching 0.01g of Au powder (99.999%, CAS No.: 937902 Wako Pure Chemical Industries, Ltd., Japan) in 100 ml of ammonium thiosulfate solution using 300 ml Erlenmeyer flask shaken in a thermostat water bath shaker at 30°C for 24 h with a constant shaking amplitude and frequency of 40mm and 600 min^{-1}, respectively.

Furthermore, to evaluate the recovery of dissolved Au, 0.15g of ZVAl and/or 0.15g of activated carbon, 0.15g ZVAl and/or 0.15g hematite (Fe_2O_3), 0.15g ZVAl and/or 0.15g magnetite (Fe_3O_4), 0.15g ZVAl and/or 0.15g Anatase (TiO_2) and 0.15g ZVAl and/or 0.15g Rutile (TiO_2) were mixed with 10 ml of gold-ammonium thiosulfate solution in 20-ml Erlenmeyer flasks at room temperature (25°C), note that the gold thiosulfate solution was purged with

ultra-pure nitrogen (N_2) gas to take out all dispersed dissolve oxygen in the system as per the previous research, where the absence of O_2 in the system leads to a more significant metal recovery. The shaking amplitude was maintained to 40mm at a frequency of 120 per minute. The residues were thoroughly washed with deionized water (18 MΩ·cm, Mill-Q® Integral Water Purification System, Merck Millipore, USA), followed by drying the residues in a conventional oven at 105°C for 1 hr and then further analyzed by SEM-EDX (SEM-EDS, JSM-IT200TM, JEOL Co., Ltd., Japan). SEM-EDX was operated at an accelerating voltage of 15 kV, 1000x to 1500x magnification and a working distance (WD) of 12 mm. The elemental maps were taken at 6,000 cps with 60 min time constant and high pixel resolutions of 256x256 (~10-minute scans). Also, the solid particles were subjected to X-ray photoelectron spectroscopic (XPS) analysis using a JEOL JPS-9200 spectrometer (JEOL Ltd., Japan) equipped with a monochromatized Al Kα X-ray source operating at 100W under ultrahigh vacuum (about 10^{-7} Pa). Wide scan and narrow scan spectrum of Au and Cu were obtained using the binding energy of adventitious carbon (285.0eV). All XPS data were deconvoluted using JEOL Specsurf Analysis using a true Shirley background and a 20%-80% Lorentzian-Gaussian peak model.

Simultaneously, the concentrations of gold ions suspected to be remained at the pregnant solution were analyzed using inductively coupled plasma atomic emission spectroscopy (ICP-AES) (ICPE-9820, Shimadzu Corporation, Japan, with a margin of error= ±2%) and Au recovery (Au_R) was calculated accordingly (Equation 1).

Single System		Binary System	
Sample Name	**Sample ID.**	**Sample Name**	**Sample ID.**
Zero-Valent Aluminum	Al		
Activated Carbon	AC	Activated Carbon-Zero-Valent Aluminum	AC/Al
Synthetic Magnetite	Mag	Synthetic Magnetite-Zero-Valent Aluminum	Mag/Al
Synthetic Hematite	Hem	Synthetic Hematite-Zero-Valent Aluminum	Hem/Al
Synthetic TiO_2 (Anatase)	Anatase	Synthetic TiO2 (Anatase)-Zero-Valent Aluminum	Anatase/Al
Synthetic TiO_2 (Rutile)	Rutile	Synthetic TiO2 (Rutile)Zero-Valent Aluminum	Rutile/Al

Table 4.1. Sample transmittal Summary.

4.2.3 Electrochemical measurements

4.2.3.1 Electrode preparation

Improvised metal oxide/Al electrode was described in detail in chapter three (3) where working electrodes was cut in a cuboid around (10 ×10 × 2mm) out of a large aluminum metal sheet using a diamond cutter, connecting it to copper wire attached with silver conducting paste, and fixing it inside a plastic mold (25mm diameter and 10mm height) with Technovit® non-conductive resin (Heraeus Kulzer GmbH, Germany). Al in the electrode was exposed by polishing it using silicon carbide papers of decreasing grain size (#200, #600, #1000, #1500), followed by polishing with 5 and 1 μm Al_2O_3 pastes on a smooth glass plate. Finally, the polished electrode was ultrasonically cleaned for 5 min to remove residually attached Al_2O_3 particles and washed several times with DI water (18 MΩ·cm, Milli-Q® Integral Water Purification System, Merck Millipore, USA). After which, the polished Al working electrode was oxidized under atmospheric conditions for 2 days to mimic the oxide layer on Al upon the cementation process. Mag/Al, Hem/Al, Anatase/Al and Rutile/Al working electrode was then prepared by mixing 0.05g of electron mediator with 5mL acetone, the resulting mixture was then carefully attached on the whole surface of Al electrode and used as the working electrode after acetone evaporation. This procedure was chosen to prevent "scratching" of the Al oxide layer formed on the electrode and has been successfully used in the previous electrochemical studies by Seng et al., 2019a; and Tabelin et al., 2017b.

Comparatively, to further understand the mechanism of selective cementation, high purity hematite ore, magnetite ore, rutile ore was used to make a working electrode. Ore specimens were shown in **Figure 4.1,** and it was prepared similarly as described in previous section above.

Figure 4.1 *Ore specimen used as improvised working electrode **a)** Rutile, TiO$_2$ **b)** Hematite, Fe$_2$O$_3$ and **c.)** Magnetite, Fe$_3$O$_4$.*

4.2.3.2 Cyclic Voltammetry (LSV) Measurements

Cyclic voltammetry is a surface sensitive technique capable of identifying the redox properties of surface-bound species by measuring the current generated by an applied potential (Kelsall et al., 1999; Mishra and Osseo-Asare, 1988).CV was conducted using a computerized driven potentiostat (SP-300, Biologic, France) with a conventional three-electrode system to elucidate the electrochemical properties of each working electrode. In this chapter, CV experiments was conducted using synthetic anatase and rutile (attached to ZVAL as working electrode) to compare its electrochemical property from the previous chapter using synthetic magnetite and hematite, Ag/AgCl$_2$ electrode filled with saturated KCl as the reference electrode, and platinum (Pt) electrode as the counter electrode. CV measurements were conducted in anoxic condition (without dissolved oxygen) by purging the prepared 150-ml electrolyte solution with ultrapure N$_2$ gas (99.99%) for 45 min prior to electrochemical measurements. The electrolyte solution was prepared with the same conditions presented during the cementation process. Three electrodes were immersed in a glass cell with a water jacket prior to N$_2$ purging and equilibrated at 25°C for 30 min. In all cases, measurements were always done after equilibration of the working electrode to its open circuit potential (OCP). Equilibrium here means that the measured current of the working electrode did not change by more than 2 mV for 60 s. The scan started from the OCP and moved towards more positive potentials at a rate of

10 mV/s up to +1.0 V, after which, the sweep direction was reversed and moved towards increasingly negative potentials. The scan direction was again reversed after reaching -1.5 V and then moved back to the starting position (i.e., OCP). This entire process constituted one cycle and each measurement lasted for 3 cycles under unstirred conditions. Finally, the polished electrode was ultrasonically cleaned for 5 min to remove residually attached Al_2O_3 particles and washed several times with DI water (18 MΩ·cm, Milli-Q® Integral Water Purification System, Merck Millipore, USA). Triplicate measurements were done using this technique.

After which, cyclic voltammetry was also used to investigate the electrochemical properties of pure ore specimens.

4.2.3.3 Chronoamperometry measurement

Chronoamperometry is an electrochemical technique whereby a fixed potential is applied to the working electrode and current density change is recorded with respect to time (Tabelin et. al, 2017). Chronoamperometry measurements were conducted using a computer driven potentiostat electrochemical measurement (SP-300, Biologic, France) with a conventional three-electrode system. After equilibration of each improvised working electrode to the OCP, it was polarized at fixed potential of -1.0 V for 60 min and at constant agitation speed at 120rpm using magnetic stirrer, and the entire system was maintained at 25°C. After the process, the whole working electrode was immersed in deionized water and cured at vacuum oven at 40°C for 24h. The surface of all improvised working electrode was then investigated using scanning electron microscopy with energy dispersive X-ray, SEM-EDX.

4.2.3.4 Potentiostatic Electrochemical Impedance Spectroscopy (PEIS)

Electrochemical Impedance spectroscopy analysis is a powerful tool to determine the mechanism involved in an electrochemical reaction and the values of the kinetic parameters of this mechanism, and it is used for the

electrical characterization of semiconducting material. Potentiostatic EIS performs impedance measurements into potentiostatic mode by applying a sinus around a potential that can be set to a fixed value or to the cell equilibrium potential. The PEIS experiments were conducted using a computer driven potentiostat electrochemical measurement ((SP-300, Biologic, France) with a conventional three-electrode system. After equilibration of each improvised working electrode to the OCP after 60 minutes, it was then polarized at biased potential from 1.0 V to -1.5 V with 0.1 V interval at 200-100 Hz frequency range, and the entire system was maintained at 25°C. The resulting impedance spectroscopy data was then analyzed with appropriate equivalent circuit using "Z Fit" analytical software embedded in SP-300, Biologic, France as analytical tool interface to calculate the resulting EIS data.

4.2.3.5 Staircase Potentio Electrochemical Impedance Spectroscopy (Mott-Schottky Plot)

SPEIS is a powerful techniques designed to perform successive impedance measurements (on a whole frequency range) during a potential scan. The main Application of these techniques is to study the electrochemical reaction kinetics along voltaperometric curves in analytical electrochemistry. This technique consists of a staircase potential sweep (in this case 1.0 V to -1.5 V). Impedance measurements with respect to different frequencies is performed in each potential step. For all these applications a Mott-Schottky plot ($1/C^2$ VS Ewe) can be displayed, and a special linear fit is applied to extract the semi-conductor parameters such as the flat-band potential.

In this experiment, the impedance of different electron mediators (high purity magnetite, hematite, and rutile) was measured at bias potentials ranging from +1.0 V to -1.5 V (versus Ag/AgCl) in 0.1 V increments, 60 minutes was used to allow equilibration at each new potential. The frequency range was performed at 20kHz t0 1khz. The Mott-Schottky plot was automatically plotted in analytical software embedded in SP-300, Biologic, France, and flat band potential can be determined using BioLogic EC-Lab V11.10 software.

4.2.4 UV-VIS Spectroscopy (Direct Bandgap Measurement)

The bandgap represents the minimum energy difference between the top of the valence band and the bottom of the conduction band. UV-VIS spectroscopy which measures light absorption as function of wavelength gives information on electronic transitions occurring in semiconductor materials as a function of incident light wavelength thus acts as a tool to estimate the optical band gap. Optical band gap is approximated to electronic band gap which is defined as energy difference between conduction band maximum and valence band minimum. Reference UV-VIS spectra (background measurement) was measured by putting the glass tube with ultra-pure water. The UV-VIS absorbance spectra of the solid samples were measured by ultrasonically dispersing the particles in the glass tube following the measurement using UV-VIS V-630 Spectrophotometer. This technique was operated in 1000 nm to 190 nm wavelength range (Deuterium lamp: 190-350 nm, Halogen Lamp: 330nm-1000nm) at 12000 nm/min measurement rate.

4.3. RESULTS AND DISCUSSIONS

4.3.1 Cementation of metals from gold-copper ammoniacal thiosulfate medium

As already reported in previous chapters, when iron oxides (hematite and magnetite) were used as electron mediator for cementation of metals from copper-gold ammonium thiosulfate solutions using aluminum as electron doner, selective deposition of gold occurred, and copper cementation was limited. To investigate the effect of semiconductor materials on the recovery of copper in ammoniacal thiosulfate medium, different semiconductive materials were used to further understand the relative effect on the difference of metal recovery. **Figure 4.2** shows the percent Au and Cu recovery of the different electron mediator after cementation process in **a)** single system (zero-valent aluminum, activated carbon, magnetite, hematite, anatase and rutile), **b) binary system** using Al as electron donor and different electron mediators. The results of cementation experiments in single system were presented in **Figure 4.2a,** noticeably, in single system, all constituents were able to recover

gold and copper; 38.2% Au-18.9% Cu for aluminum, 30.1% Au-6.1% Cu for activated carbon, 22.1% Au-0% Cu for magnetite, 24.2% Au- 0% Cu for hematite, 32.5% Au-16.4% Cu for anatase, 26.1% Au-12.4% Cu for rutile, respectively. Comparatively, TiO$_2$ (anatase) and TiO$_2$ (rutile) have been shown to have higher copper recovery compared to other electron mediators, having 16.4% Cu and 12.4% Cu, respectively as presented in **Figure 4.2.a.**

In binary system as shown in **Figure4.3b,** gold recovery was significantly increase using aluminum as electron donor, which were further validate using other semiconductive material using TiO$_2$ (anatase) and TiO$_2$ (rutile), having 92.6% and 93.5% gold recovery, respectively. The results also obtained significant difference with respect to copper recovery, around 62.2% and 66.9 % for anatase and rutile, respectively. This further suggests that the semiconductive property of electron mediators has influenced the increase of copper recovery. **Table 4.2** presents some semiconductive property of electron mediators being used in this research.
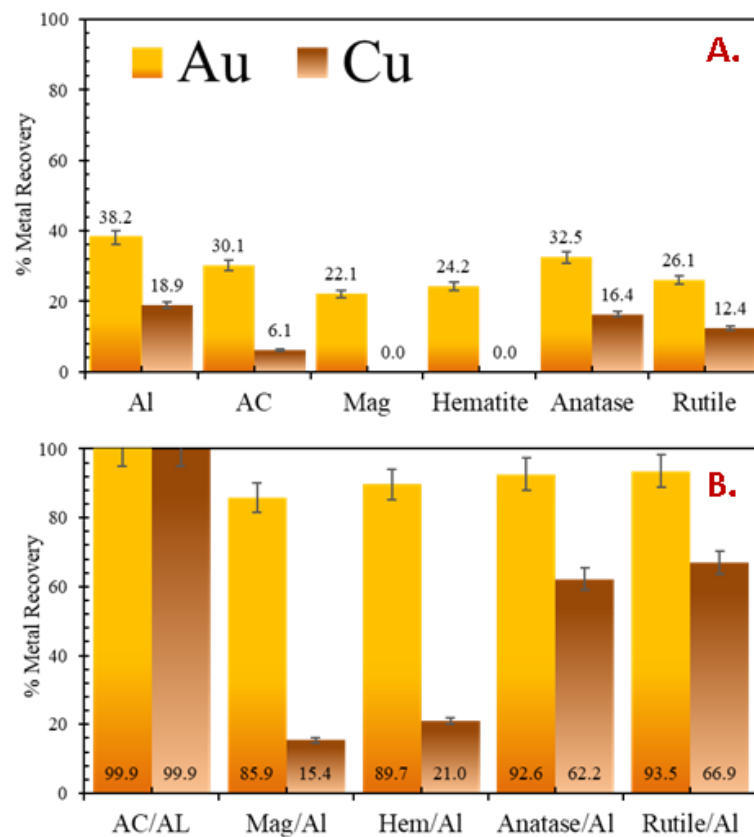

Figure 4.2. Percent metal recovery using different electron mediators after cementation process in **a)** single system and **b)** binary system.

Given the following information in **Table 4.2,** we can initially infer that the bandgap has something to do with increase of copper recovery in binary system. Wherein, the greater the bandgap, the higher is the copper recovery. Although many researchers have reported the semiconductive properties of some metal oxides, the values of these properties depend on many factors, such as the materials particle size, pH , crystal structure of the materials etc. (50-53). For these reason, further electrochemical experiments were conducted to evaluate the semiconductive properties of metal oxides being used in this research and presented in the following sections.

Table 4.2 Some semiconductive properties of electron mediators (D. Flaka et. al, 2020).

Semiconductors	Semiconductivity bandgap [eV]	Semiconductivity Type
Activated Carbon (AC)	3.5	n-type/p-type
Hematite, Fe_2O_3	1.9- 2.2	n-type
Magnetite, Fe_3O_4	0.9-1.9	n-type
Anatase,TiO_2	3.0	n-type
Rutile, TiO_2	3.3	n-type

To confirm the presence of metal deposition after cementation experiments, SEM-EDX spectroscopy was conducted. **Figure 4.3** presents the scanning electron microscopy profile (analyzed using elemental mapping and point eds) of the different electron mediators in single system, **a)** magnetite **b)** hematite **c)** anatase and **d)** rutile. It can be observed that fine particles of electron mediators (gray objects in back scattered electron (BSE) photomicrographs) were spontaneously covering the cemented metal (bright objects in BSE photomicrographs) which can further be detected using point analysis technique and elemental mapping. Comparatively, using iron oxides as electron mediator (**Figure 4.3a and b**), the bright particles detected were assigned to gold particle only, no copper was detected compared to titanium oxides **(Figure 4.3c and d)** as presented on its corresponding elemental mapping and point eds analysis.

Figure 4.3. SEM photomicrographs of gold cemented in different semiconductive material in single system A) magnetite B) hematite C) anatase and D) rutile.

Figure 4.4 presents the SEM-EDX profile of the different electron mediators in binary system using zero-valent aluminum as electron donor. It can be observed in all photomicrographs, the cemented bright particles were all detected along with spherical-shape particle which is the oxidized aluminum oxide layer which can be observed in **Figure 4.4a-d**. The backscattered electron (BSE) photomicrographs alongside its corresponding elemental mapping and point eds analysis, it was confirmed that all electron mediator used were able to cement gold. Noticeably, copper was also cemented but its intensities are much lower in iron oxides, averaging around 5000 cps,

compared to titanium oxides ranging from 5000 cps to 20,000 cps. The results of SEM-EDX analysis further suggest that when we used iron oxides as electron mediator along with zero-valent aluminum as electron donor, it presents better selectivity compared to titanium oxides.

Furthermore, X-ray photoelectron spectroscopic analysis (XPS) was conducted to further validate the presence of cemented metals using the different electron mediators in single and binary system. XPS was conducted using JEOL JPS-9200 spectrometer (JEOL Ltd., Japan) equipped with a monochromatized Al Kα X-ray source operating at 100 W under ultrahigh vacuum (about 10^{-7} Pa). A wide scan (**Figure 4.5-7**) and narrow scan (**Figure 4.7-8**) spectrum of oxygen (O1$_S$) and carbon (C1$_S$) were obtained and corrected using the binding energy of the adventitious carbon (9285.0 eV). All XPS spectra were deconvoluted with XPSPEAK version 4.1 using a true Shirley background and a 20-80% Lorentzian-Gaussian peak model (Zoleta et.al, 2019).

Figures 4.5 and 4.6 present the XPS wide spectra of selected electron mediators (rutile, magnetite, and hematite) and compare it to Zero-Valent Aluminum in single and binary systems. The results revealed that XPS spectra of single and binary system were able to detect the presence of Au peaks at different energy levels; Au 5p 3/2, Au 4f 7/2, and Au 4f 5/2 detected at binding energy range 68-85 eV. On the other hand, in single system, using magnetite and hematite presents no significant copper peaks compared to rutile (slightly forming amorphous-like peak) and aluminum detected at binding energy range of 926-925 eV for Cu 2p1/2 and Cu 2p3/2, which is with the agreement with the results of metal recovery upon cementation process where no copper was recovered when we used iron oxides as electron mediator.

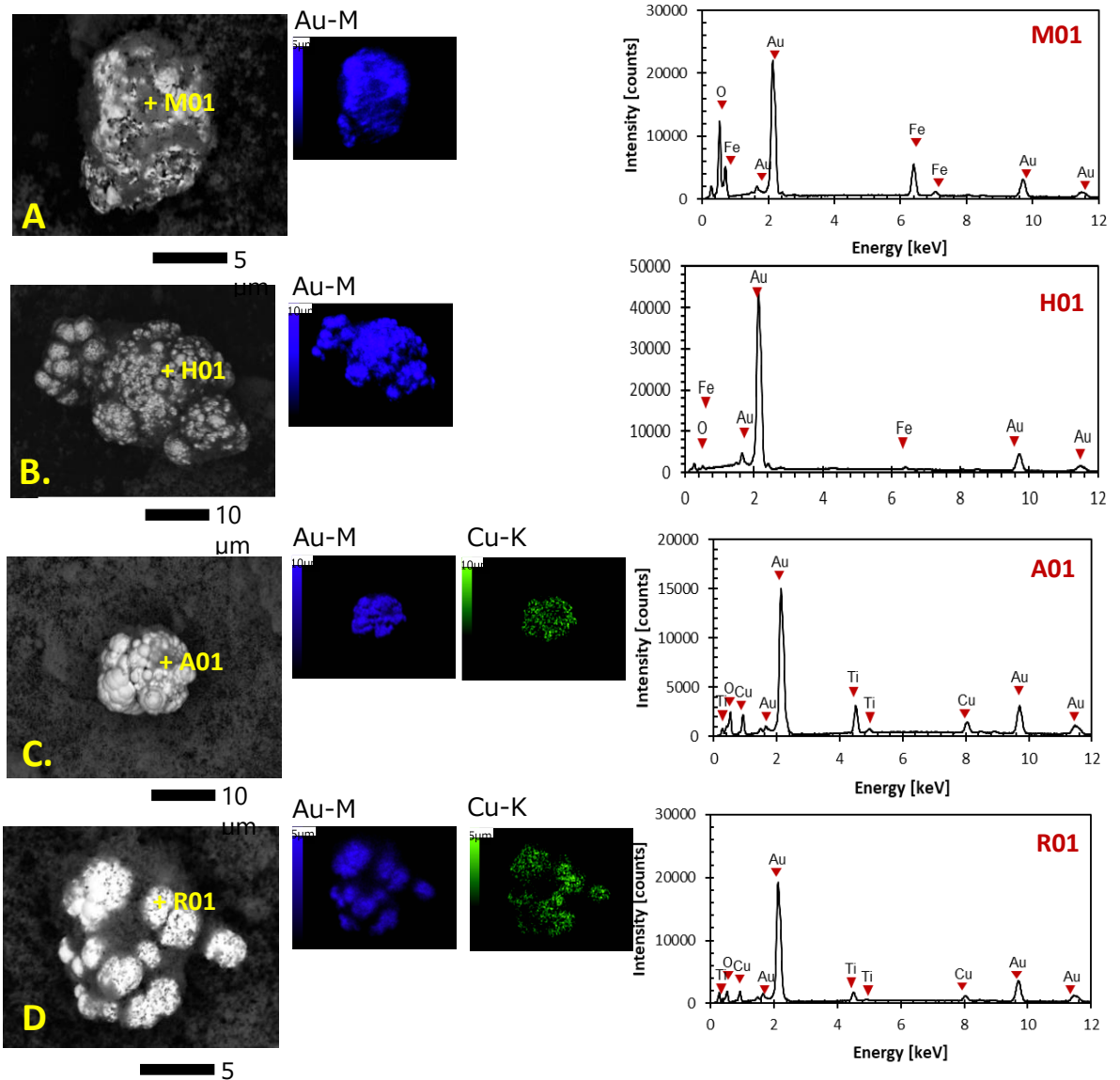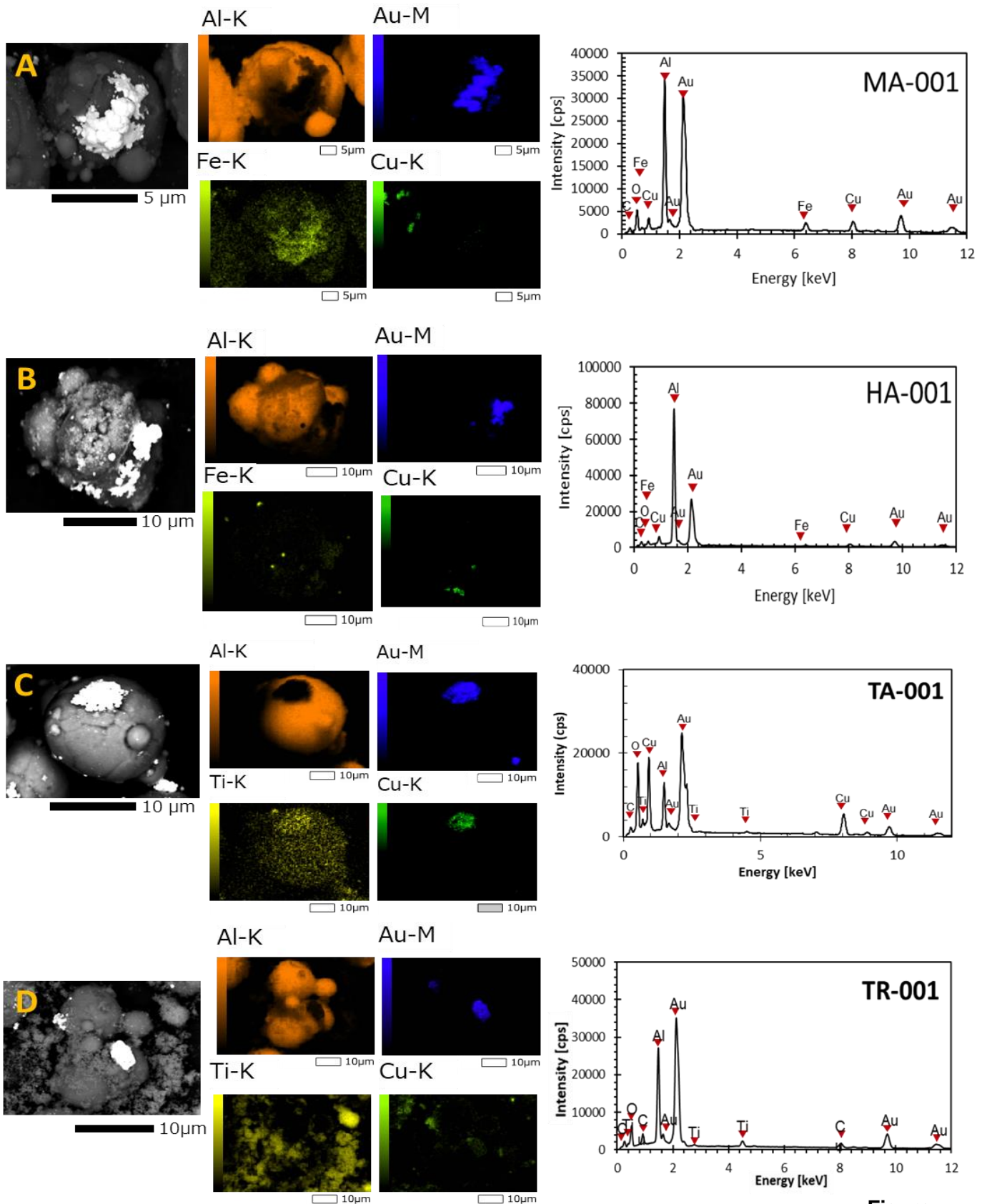**Figure**

4.4. SEM photomicrographs of gold cemented in different semiconductive material in binary system a) Mag/Al b) Hem/Al c) Anatase/Al and f) Rutile/Al.
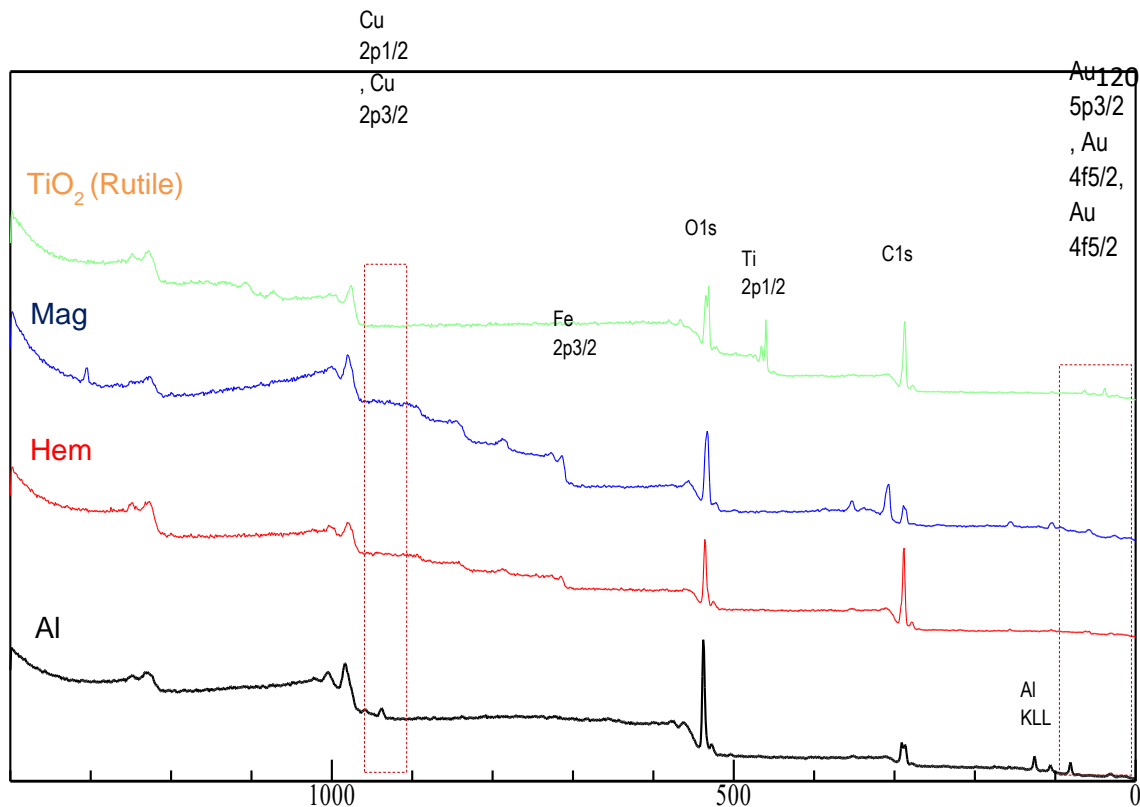
Figure 4.5 XPS wide scan spectra of selected electron mediators (Rutile, Magnetite, Hematite) and Zero-Valent Aluminum (Al) in single system.
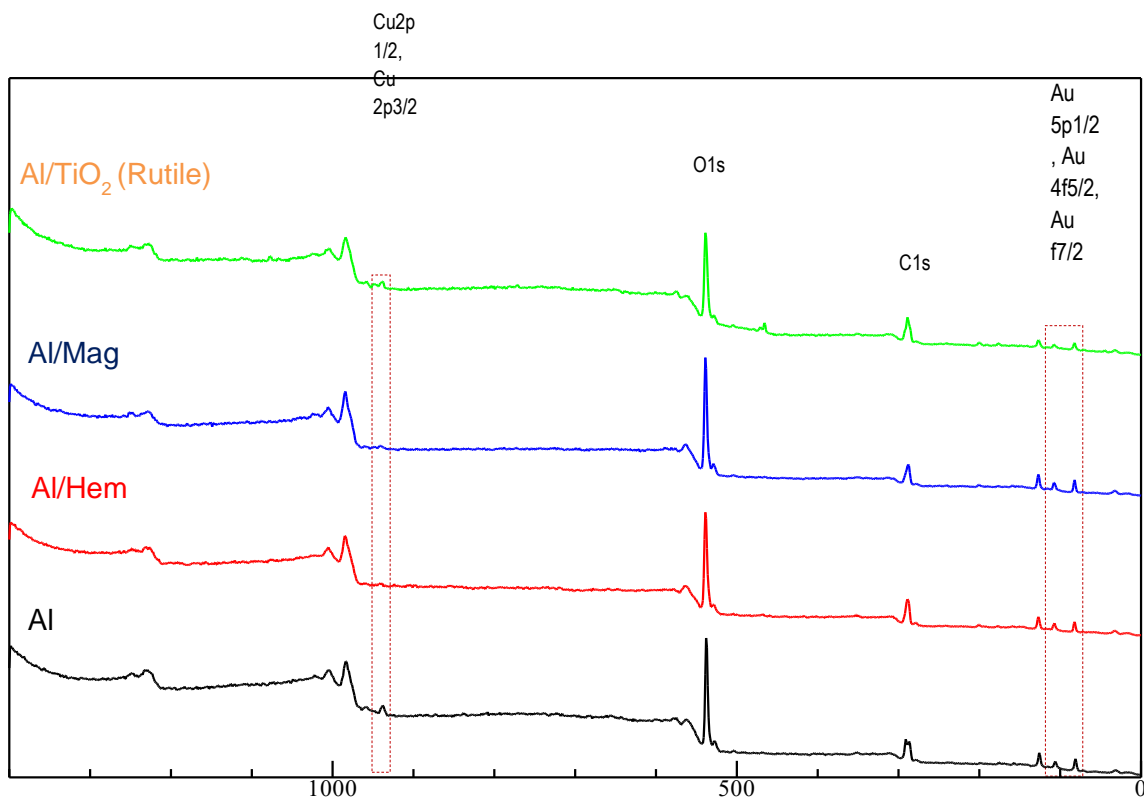
Figure 4.6 XPS wide scan spectra of selected electron mediators (Rutile, Magnetite, Hematite) and Zero-Valent Aluminum (Al) in binary system.

Also, in binary system, we can observe clearly that copper was detected in all systems, comparing the XPS spectra of aluminum to electron mediator-electron donor system, we can infer that the copper detected using iron oxides was made possible due to the presence of aluminum that act as an electron donor and as a reductant of copper simultaneously, which agrees with the results presented in **Figure 4.4 a-b** SEM-EDX elemental mapping, where the illuminated copper was detected separately at the surface of aluminum, while titanium oxides where able to cement Au and Cu in same position **Figure 4.4 c-d.** To determine the exact energy positions and detailed components of the wide spectra, a narrow scan was conducted at specified binding energy range of gold and copper and the XPS narrow scan spectra is presented in **Figure 4.7-8**, respectively.
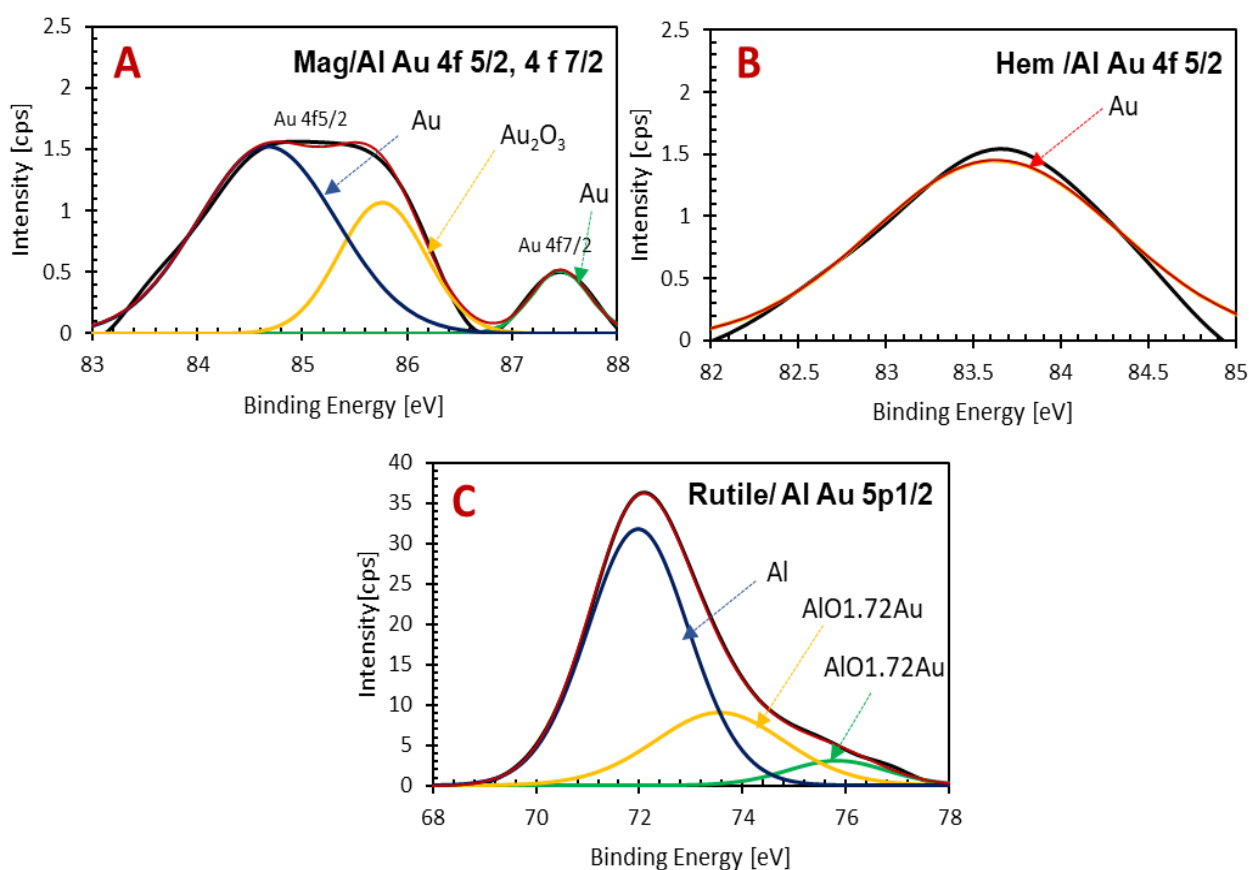
Figure 4.7 XPS Au narrow scan of selected electron mediator-electron donor system A) Mag/Al B) Hem/Al and C) Rutile/Al.
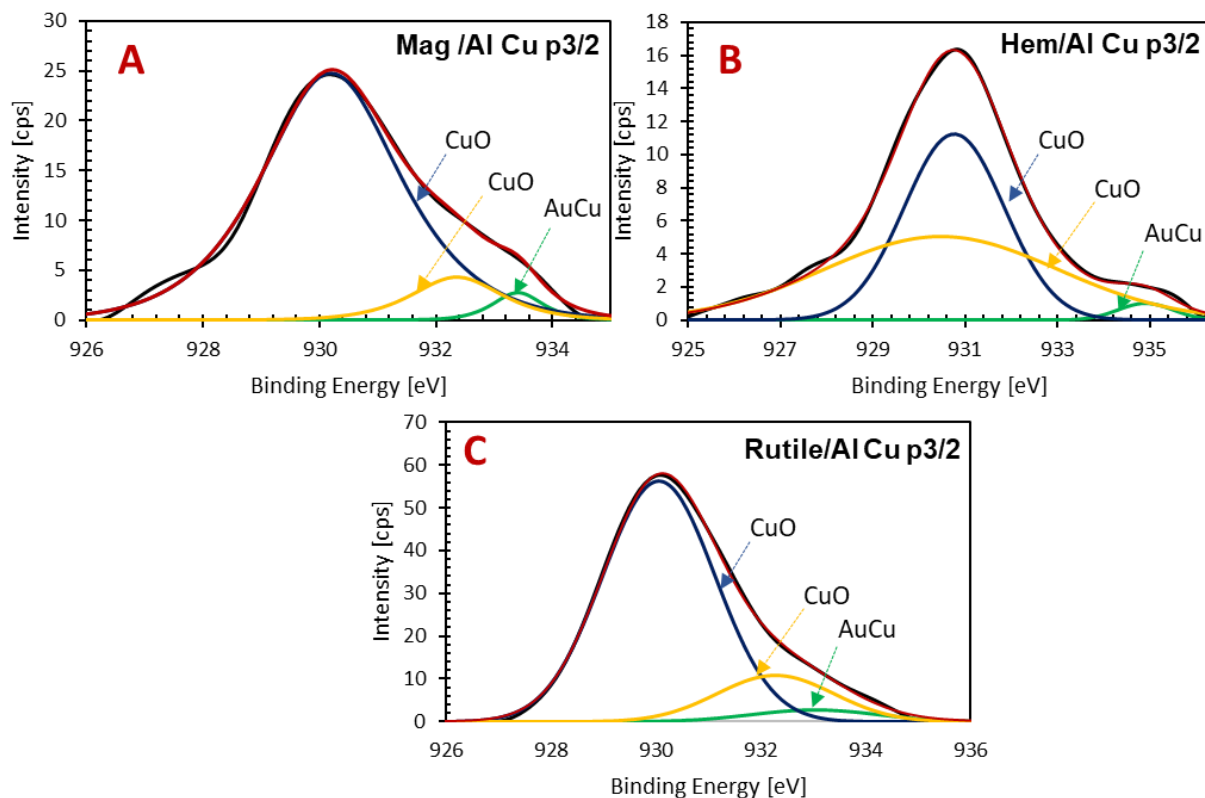
Figure 4.8 XPS Cu narrow scan of selected electron mediator-electron donor system a) Mag/Al b) Hem/Al and C) Rutile/Al.

Deconvoluted narrow XPS spectra of gold were presented in **Figure 4.7.** The scan range was based on the wide scan XPS spectra, where Rutile/Al binary system shown to have a gold peak at binding energy range around 68-78 eV which belongs to Au 5p1/2 electron orbital, while iron oxides, have gold peaks binding energy range of 82-88 eV which belongs to Au 4f5/2 and Au 4f 7/2 electron orbital. The results revealed that Mag/Al detected three major peaks centered at 84.6 eV, 85.7 eV and 87.5 eV which belongs to Au, Au_2O_3 and Au, respectively. Also, hematite/Al obtained only one gold peak centered at 83.6 eV which belongs to elemental Au, while rutile/Al obtained two major gold peaks which belongs to $AlO_{1.72}$ and Au centered at 73.7 and 75.8 eV.

On the other hand, the deconvoluted narrow XPS spectra of copper was the same in all binary system constituents where the narrow scan was focused on binding energy range of 926-936 eV. The results obtained three major peaks for all binary system constituents. For binding energy centered at 929-930 eV, 931-932 eV and 933-934 eV, it was assigned to Cu, CuO and AuCu,

respectively. The results concerning XPS copper intensities is with the agreement with the results obtained using SEM-EDS point analysis shown in **Figure 4.4**, where the used of titanium oxide as electron mediator, it obtained a stronger signal of copper compared to iron oxides. This research further suggests that the use of SEM-EDX and X-ray photoelectron spectroscopic analysis can confirm the selective cementation of iron oxide to gold upon cementation in copper ammoniacal thiosulfate medium.

4.3.2. Electrochemical experiments
4.3.2.1 Cyclic voltammetry (CV)

Figure 4.9 illustrate the voltammogram of titanium oxide (Anatase/Rutile)/Al working electrodes using gold and copper electrolyte. The previous chapter discusses the galvanic interaction between ZVAL and iron oxides and compare it to Al/AC working electrode, it was reported that the used of iron oxides as electron mediator facilitate the selective cementation of gold. Like the voltammogram generated using AC/Al working electrode, two reduction peaks were observed. When the potential sweep moves towards a more negative potential, a "shoulder-like" peak was observed around -0.7 V for anatase/Al and rutile/Al working electrode, and this peak is assigned to the reduction of copper ions. Furthermore, around -1.0 V "shoulder-like" peak was observed and assigned to the reduction of gold ions. This results further validate that both gold and copper can be reduced using titanium oxide/Al working electrode suggesting that it doesn't possess selective cementation property.
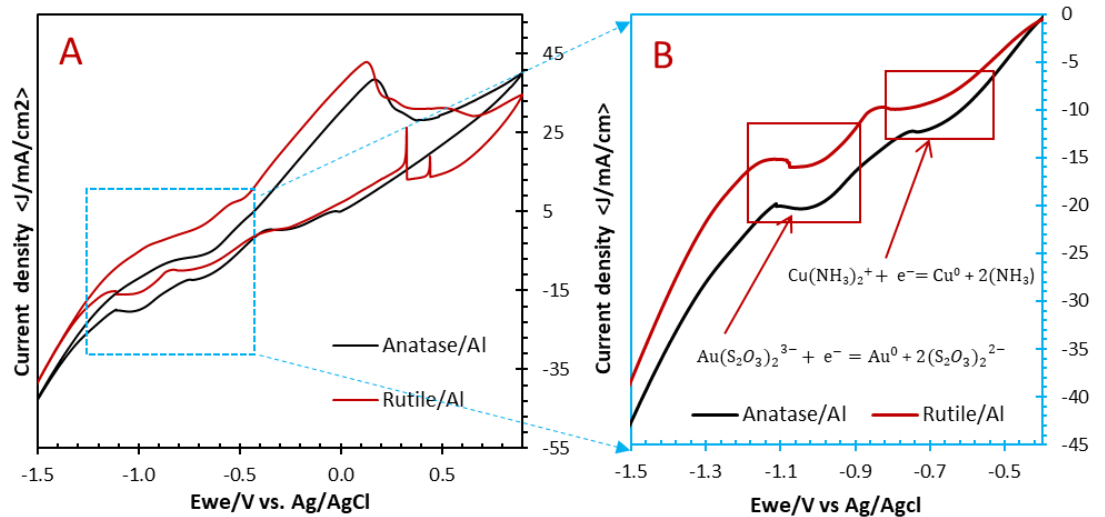
Figure 4.9 Cyclic voltammogram profile of titanium oxide (Anatase and Rutile)/Al working electrode.

To further understand if the titanium oxide facilitates the cementation of gold and copper, the same procedure was conducted in previous chapter using high purity ore specimen as a working electrode and its corresponding electrochemical profile was illustrated in **Figure 4.10.**
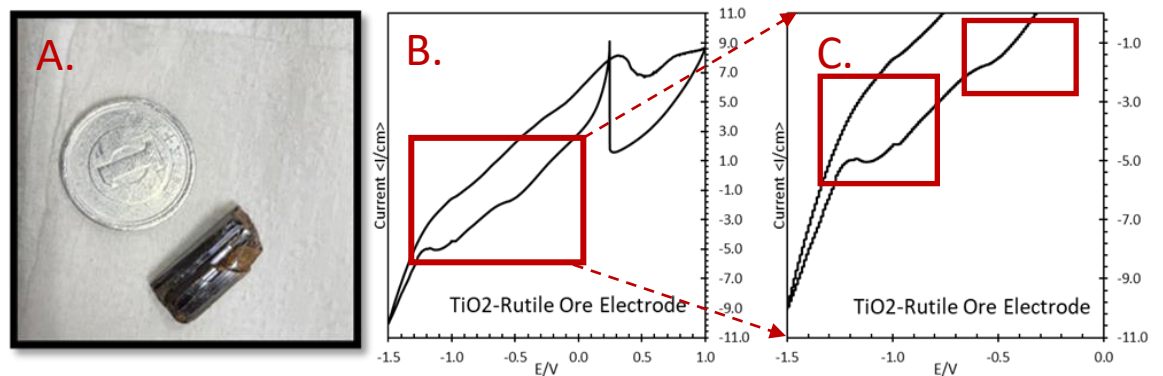
Figure 4.10 Electrochemical profile using rutile crystal **A)** rutile crystal specimen **B)** Cyclic voltammogram **C)** Narrow reductive scan.

Figure 10.b demonstrates the cyclic voltammogram of rutile crystal subjected to potential scan from 1.0 V to -1.5 V versus AgCl. Its narrow potential scan was illustrated in **Figure 10.c** and the results further validates, that the used of titanium oxide alone can reduce $Au(S_2O_3)^{3-}$ species into metallic gold as well as $Cu(NH_3)_2^+$ species into metallic copper, the reduction potential peak was observed around -1.1 V and -0.5 V for gold and copper, respectively. This results further suggest that the cementation using titanium oxide was facilitated by the electron mediator itself and that the cementation of gold and copper was enhanced by the used of electron donor which is in this case ZVAl.
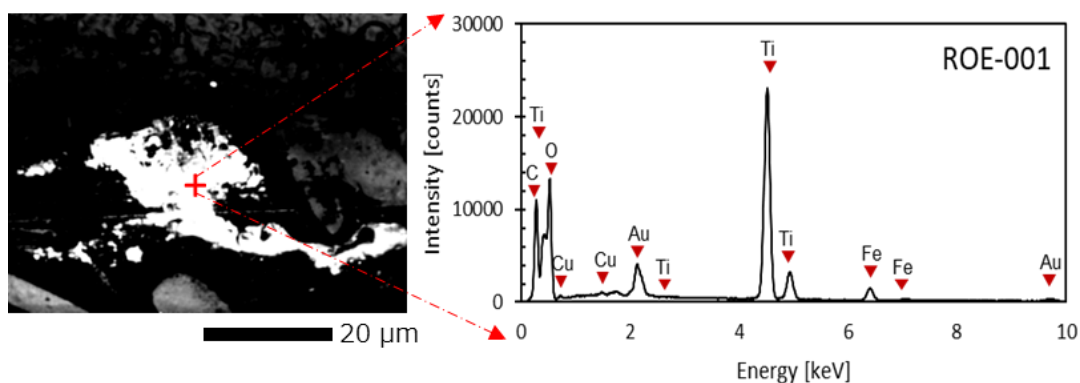
Figure 4.11 SEM-EDX profile of rutile crystal working electrode after cementation.

Figure 4.11 presents the SEM-EDX profile of a rutile working electrode after chronoamperometry subjected to a fixed potential of -1.1 V for 1 hour in gold-copper ammoniacal thiosulfate medium. The results further validate gold and copper were detected. This results further supplement the results on the claim that the electron mediator itself plays an important role on the selective cementation of electron mediators.

4.3.2.2 Potentiostatic Electrochemical Impedance Spectroscopy

PEIS permits us to identify and analyze, in each frequency and temperature domain, the contributions of different parameters such as the impedance and the bulk capacitance. For this purpose, the PEIS data simulated by an equivalent circuit was presented using the Nyquist plot. In the Nyquist plot, the modulus IZI and the phase angle define the position of each frequency dependent data point in a complex plane. In the Bode plot, IZI and phase angle were plotted against the modulation frequency. This maximum of "-Im(Z) [Ω]" (Imaginary impedance) corresponds to the inflexion point in the "Re(Z) [Ω]" (real impedance). Otherwise, the Nyquist representation is characterized by an existence of impedance spectra that intercepts the real impedance.
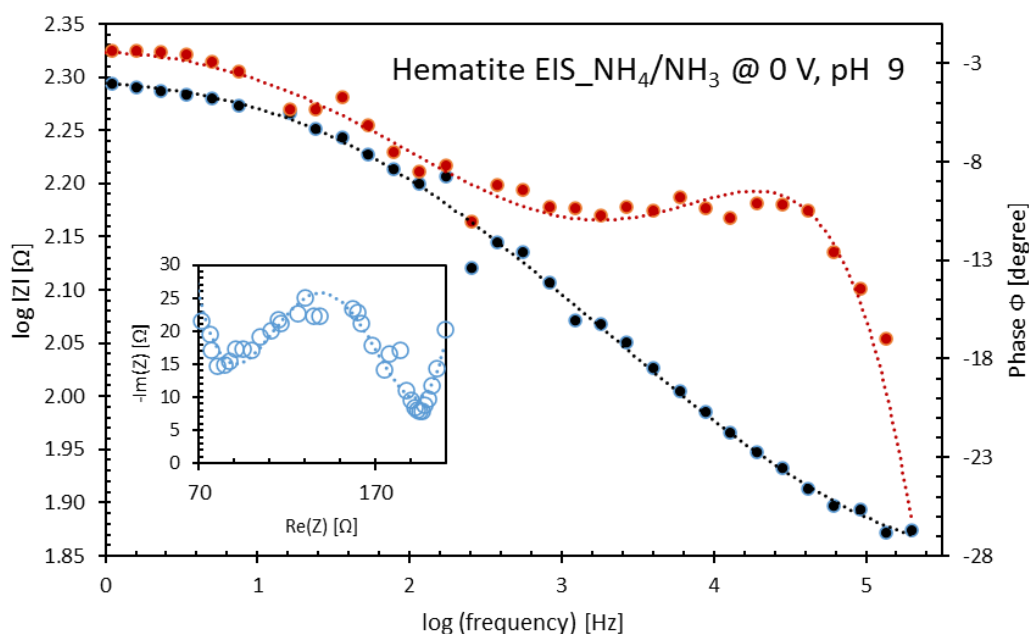
Figure 4.12 Representative electrochemical impedance spectroscopic analysis profile of a hematite working electrode at applied bias potential of 0 V and constant pH 9 at 25 °C.

The behaviors of Nyquist plot, as shown in **Figure 4.12** for our representative material and for a representative temperature of 25°C and a bias potential at 0 V maintained d at pH 9, indicates the contribution of only one process at maximum frequency. It can be noticed that the Nyquist plot (inset figure) is not really a full semi-circle. It is a depressed semi-circular arc where its center lies below the real impedance axis, suggesting the poly dispersive non-Debye relaxation type in our case. In this situation, constant phase elements (CPE) must be used in addition to resistors and capacitors to describe the equivalent circuit, which will be discussed later, to provide a complete picture of the system. Also, the no observation of peaks in the frequency domain (2–1 log frequency, KHz) suggests that the observed single peak in the plots of imaginary impedance represents the grain boundary component.

Impedance

$$Z(f) = R_1 + \frac{R_2}{1 + j2\pi f R_2 C_2} + \frac{\sqrt{2}\,\sigma_3}{\sqrt{j2\pi f}}$$

Nyquist Diagram (-Im(Z) vs. Re(Z))
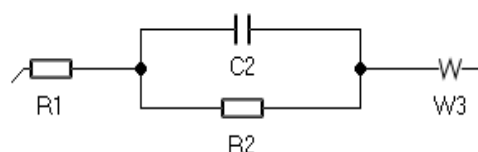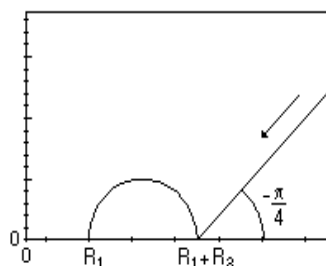
Figure 4.13 Equivalent circuit used to analyze the EIS profile of different working electrodes using EC-Lab V11.10 ZFit-Bio Logic software.

Also, Single semi- circular arcs are observed in **Figure 4.12** and are related to the dominance of the contribution of grain boundaries process in the considered temperature and frequency ranges. To understand and extract meaningful information from EIS data presented in **Figure 4.12**, it must be fit to an equivalent circuit model which combines fundamental elements such as resistors, capacitors, inductors, constant phase elements, and diffusion elements.

The process of fitting the data by considering different electrical circuits, depending on applied voltage domain, has been described by Bredar et. al, 2020. An important feature of this EIS diagram is the linear increase of impedance observed in the midfrequency range, this can be attributed to Warburg diffusion. As such, **Figure 4.13** shows the selected equivalent circuit for analyzing data generated from EIS experiments, this equivalent circuit was suggested by EC-Lab V.11.10 ZFit-Bio Logic Software. This model has been used to explain the resistance to charge transfer between metal oxides and conductive substrates, often called contact resistance. This circuit is a modification to the Randle's circuit where a Warburg diffusion (ZW) term has been included in series with the charge transfer resistance. This arrangement is meant to describe the physical reality of diffusion of electroactive species to the surface of the electrode where they undergo oxidation or reduction via charge transfer.

To identify the contribution of bias voltage, **Figure 4.14** shows the comparison of the Nyquist plot for the different working electrodes using NH_4/NH_3 buffer solution (pH 9) at two representative bias voltage at 1.0 V and 0 V versus Ag/AgCl reference electrode. In these curves, a maximum of imaginary impedance was observed at different bias voltage applied, specifically when 1.0 V was applied, indicating the displacement of the peak towards higher frequencies with increasing voltage.
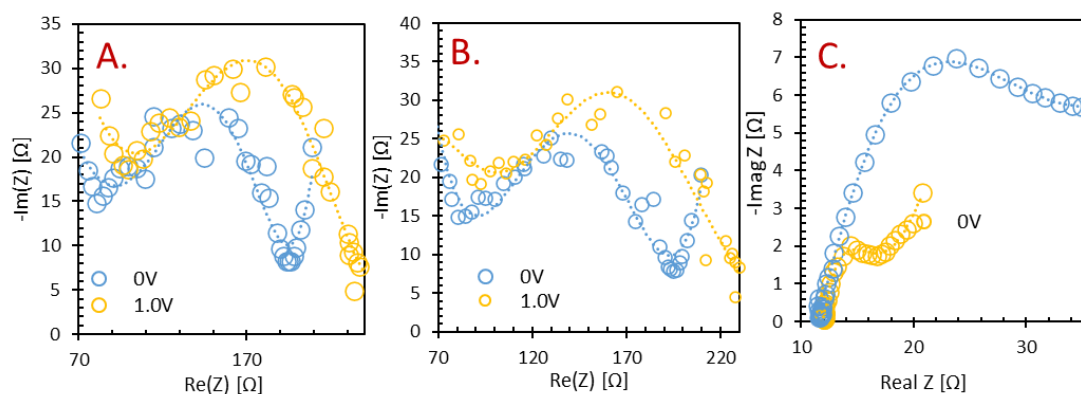
Figure 4.14 EIS profile of different working electrode represented using the Nyquist plot subjected at 1.0 V and 0 V using NH_4/NH_3 buffer solution (pH 9) at 25°C a) Magnetite b) Hematite c) Rutile.

To further understand the behavior of metal oxides as electron mediators, EIS was conducted using gold ions only and copper ions only, in ammoniacal thiosulfate medium as electrolytes. The EIS profile of each electrode was illustrated in **Figure 4.14** represented in Nyquist plot.
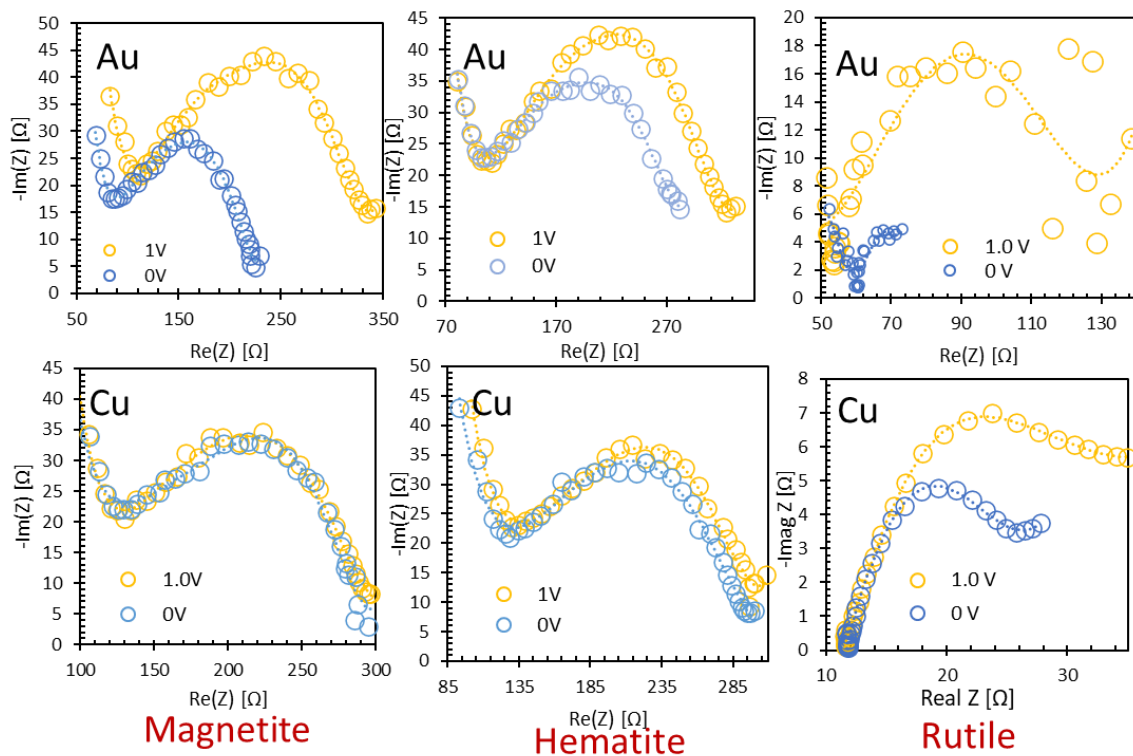
Figure 4.15 EIS profile of the different working electrodes using metallic electrolytes (pH 9) subjected at different bias voltage from 1.0 V to 0 V represented in Nyquist plot.

The results of Potentiostatic impedance spectroscopy were calibrated by applying a bias potential from 1.0 V to 0 V, we can observe that the charge transfer resistance (semi-circle) of all working electrodes were decreasing as shown in **Figure 4.15** when using gold ions only as the electrolyte. These results further suggest that electrodes might be able to develop a solid-liquid interface that affects the electron transfer more favorably and become a conducting surface when approaching a more negative potential.

On the other hand, PEIS Nyquist plot of hematite and magnetite working electrodes also suggests that when using copper electrolytes, the contact

resistance of both electrodes did not develop any significant change when bias potential was applied from 1.0 V to 0 V, which is contrary to the Nyquist plot generated using rutile as the working electrode.

Also, as the potential approaches 0 V, the semi-circle became more well-defined, this indicates that the ionic resistance for Au^+ decreases in all metal oxide electrodes, while Cu^+ migration through the solid-electrolyte interface decreases only when using rutile electrode.

Overall, Potentiostatic electrochemical impedance spectroscopic analysis represented by Nyquist plot demonstrated the ability of impedance in the form of charge transfer resistance to differentiate the semiconductive behavior of metal oxide (magnetite, hematite, and rutile), while considering the unique contributions of the different metallic electrolytes in different applied bias potentials.

4.3.2.3 Staircase Potentio Electrochemical Impedance Spectroscopy (Mott-Schottky Plot)

SPEIS was conducted by applying a staircase potential sweep from a positive to negative potential (1.0 V to -1.5 V) versus Ag/AgCl reference electrode. The Mott-Schottky plot was automatically plotted in analytical software embedded in SP-300, Biologic, France, and flat band potential can be determined using BioLogic EC-Lab V11.10 software as illustrated in **Figures 4.16.**

Figure 4.16 illustrates the Mott-Schottky plots for a) Magnetite b)Hematite and c) rutile in NH_4/NH_3 buffer solution. The plots were acquired in potential sweep from 1.0 V to -1.5 V in frequency ranging from 200 kHz to 1 kHz, but only lower frequencies (1 kHz, 1.5 kHz and 2.3lHz) where represented to refine the presentations.
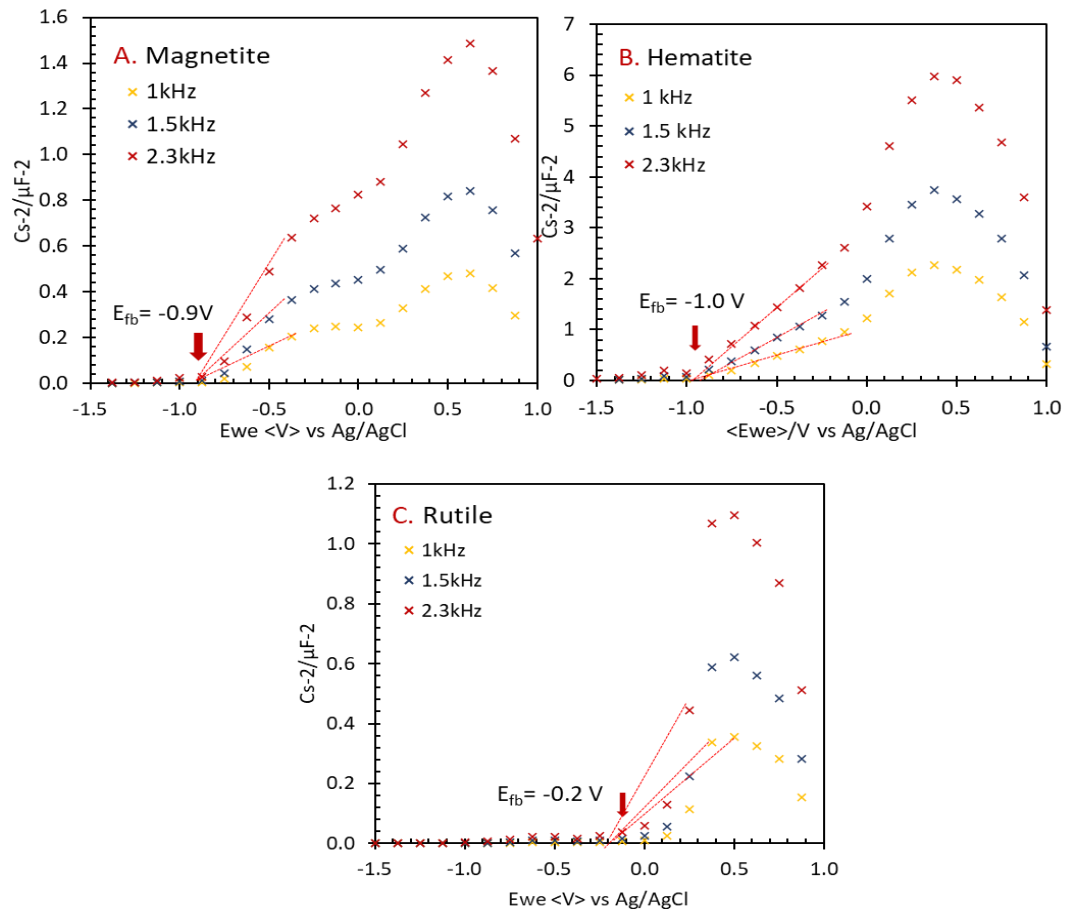
Figure 4.16 Mott-Schottky plots of different metal oxide ore specimen performed in NH_4/NH_3 buffer solution a) Magnetite b) Hematite and c) Rutile.

When the applied potentials approach more negative, around 0.5 V to -0.9 V, 0.5 V to -1.0 V, and 0.5 V to -0.2 V, the plots have a positive slope for magnetite, hematite, and rutile, respectively. More than that of 0.5 V, the Mott-Schottky plots starts to decrease, suggesting that in this region, no direct correlation between the semiconducting properties can be established. On the other hand, the positive slope of the Mott-Schottky plot at lower potentials, in the passive region, leads to confirmation that magnetite, hematite and rutile behave like n-type semiconductors (J. Wielant et. al, 2007). To recognize whether a linear dependence exists over a certain potential range, and thus, to obtain a reliable estimation, a limited linear region at potentials was used to estimate the flat band potential using the BioLogic EC-Lab V11.10 software. The results obtained different flat band potentials, -0.9 V, -1.0 V and -0.2 V for magnetite, hematite, and rutile, respectively.

4.3.3 Ultraviolet-Visible Spectroscopy (UV-VIS)

This technique allows us to understand the optical and electronic properties of the semiconductors being investigated, which in this case magnetite, hematite, and rutile. In this research, band gap (E_g) energy of the semiconductor being used is focused to be quantitatively determined. The band gap energy of a semiconductor describes the energy needed to excite an electron from the valence band to the conduction band. An accurate determination of the band gap energy is crucial in predicting the photophysical and photochemical properties of semiconductors.

The band gap energy can be determined by using the UV-VIS spectra between the absorbance and its corresponding UV light wavelength and convert it to Tauc's plot (P. Makula et. al, 2018.). The Tauc method assumes that the energy-dependent absorption coefficient α can be expressed in the following equation :

$$\alpha h v^{1/\gamma} = B(hv - E_g) \qquad (4.1)$$

Where h is the Planck constant, v is the photon's frequency, Eg is the band gap energy, and B is a constant. The γ factor depends on the nature of the electron transition and is equal to ½ or 2 for the direct and indirect transition band gaps, respectively.

Figure 4.17 shows the absorbance spectrum of the different semiconductors transformed according to equation 1 plotted against the photon energy. The region showing a steep, linear increase of light absorption with increasing energy is a characteristics of n-type semiconductor. The X-axis intersection points of the linear fit of the Tauc plot gives an estimate of the band gap energy.
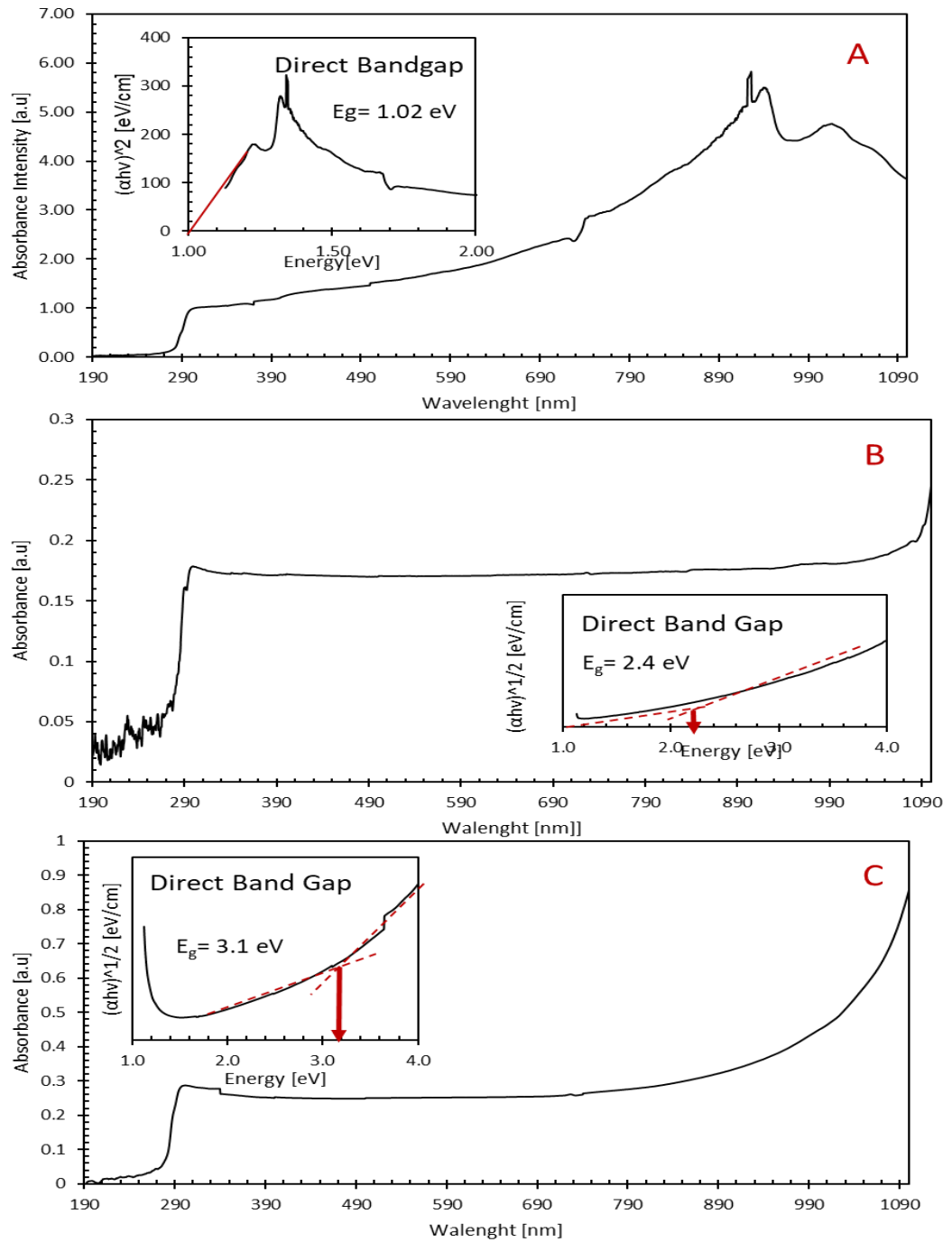
Figure 4.17 UV-Vis spectroscopy spectra of the different semiconductors and its corresponding Tauc's plot (inset of the UV spectra) of a) magnetite b) hematite and c) Rutile.

The Tauc's plot was plotted on the inset figure of the UV-Vis spectra of the different semiconductors as illustrated in **Figure 4.18**. Configuring interpolation of the linear portion of the Tauc's plot, the band gap energy was estimated to be: 1.1 eV, 2.4 eV and 3.2 eV for magnetite, hematite, and rutile, respectively. To evaluate the relationship of electrochemical impedance spectroscopy and spectrophotometric analysis, the electronic band structure of the semiconductors can now be understood as shown in **Figure 4.19**.
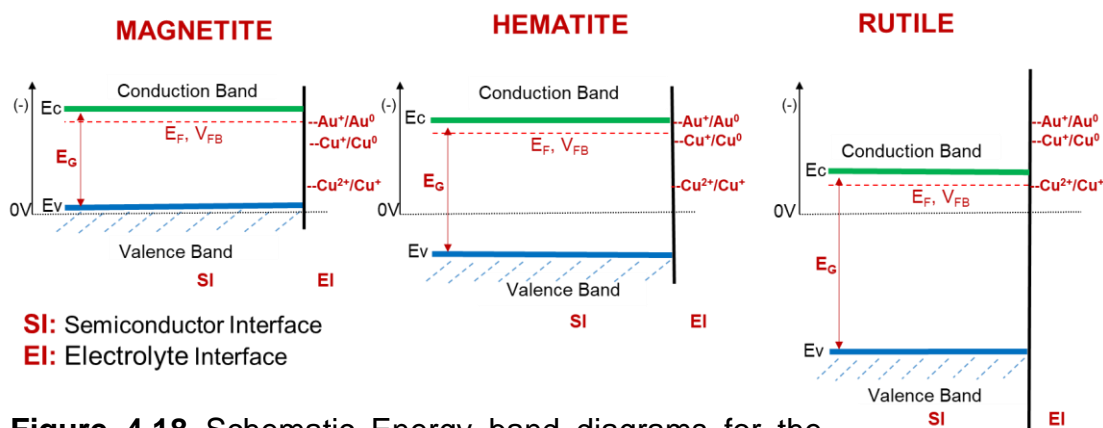
Figure 4.18 Schematic Energy band diagrams for the semiconductor-electrolyte interface (SEI) for a) Magnetite b) Hematite and c)Rutile.

In the schematic diagram illustrated in **Figure 4.18**, two interfaces were shown in each figure. First is the semiconductor interface (left side of the vertical line), where the bottom edge of the conduction band (Ec) and top edge of the valence band (Ev), flat band potential (Vfb) or equilibrium Fermi level (Ef); red line below the conducting band edge, and the energy band gap (Eg) are shown. Also, in the electrolyte interface (right side of the vertical line), the reduction potential of Au^+ species at -1.0 V, Cu^+ species at -0.8 V and Cu^{2+} species at -0.2 V are shown with short horizontal lines pinned at the interface.

Figure 4.18 describes the energy band diagram when a flat band structure is realized. When a flat band structure is realized, the bottom edge of the conduction band (Ec) and the top edge of the valance band (Ev) do not depend on the position (distance from the solid surface). They are horizontally distributed in the bulk solid phase. The flat band potential corresponds to the

Fermi level of this state (E_F) (R. van de Krol et al., 2011). Generally, the Fermi level in the diagram corresponds to electrode potential. As already discussed, the linear positive slope at the higher potential region in the M-S plot (**Figure 4.16**) indicates that the material is an n-type semiconductor, which is, in this case, and the Fermi level of the semiconductor, $E_F(s)$, sits just below the conduction band edge (Ec). This is considered to make **Figure 4.18**, i.e. the position of Ec is assumed to be almost the same as that of observed flat band potentials of magnetite (-1.0 V), hematite (-0.9 V), and rutile (-0.2 V). The position of Ev was decided from the observed energy band gap of the materials (1.1 V for magnetite, 2.4 V for hematite, and 3.1 V for rutile).

Note that in the case of iron oxides like magnetite and hematite, the reduction potential of Au^+ (-1.0 V) is close to that of the bottom edges of the conduction band (Ec), while the reduction potentials of Cu^+ and Cu^{2+} are far from Ec. The reduction potentials of Cu^+ and Cu^{2+} are positioned in the energy levels of the band gap of magnetite and hematite, where the electrons cannot be present in the solid phase. On the other hand, in the case of rutile, the redox potential of Cu^+ and $Cu^{2+,}$ as well as Au^+, are relatively higher than Ec. This means that the reduction potential of these metal ions is positioned at the conduction band level of rutile, where electrons can be present in the solid phase. These differences in the energy band diagrams among the three metal oxides may cause a difference in the selective deposition of metals. Details will be discussed in the next section.

4.4. PROPOSED SELECTIVE CEMENTATION MECHANISM

In the previous chapter, in the galvanic cementation method using ZVAI as an electron donor and iron oxides as an electron mediator, it was found that selective deposition of Au from Cu^{2+}-Au^+ ammoniacal thiosulfate solutions occur, and by various experimental methods, including cementation experiments, surface analysis, and electrochemical experiments carefully confirmed this. Gold was deposited on the iron oxide surface, but copper deposition is limited. The reduction potentials of copper ions are more positive than gold ions in the solutions, implying that the reduction (or cementation) of copper ions is thermodynamically easier than gold ions. However, this suggests that simple thermodynamic considerations cannot interpret the mechanism of the selective deposition of gold. In this section, based on the energy band diagram established in the last section, the mechanism of selective deposition of gold from Cu^{2+}- Au^+ ammoniacal thiosulfate solution using iron oxide (magnetite and hematite) as electron mediator with ZVAI as electron donor is discussed.
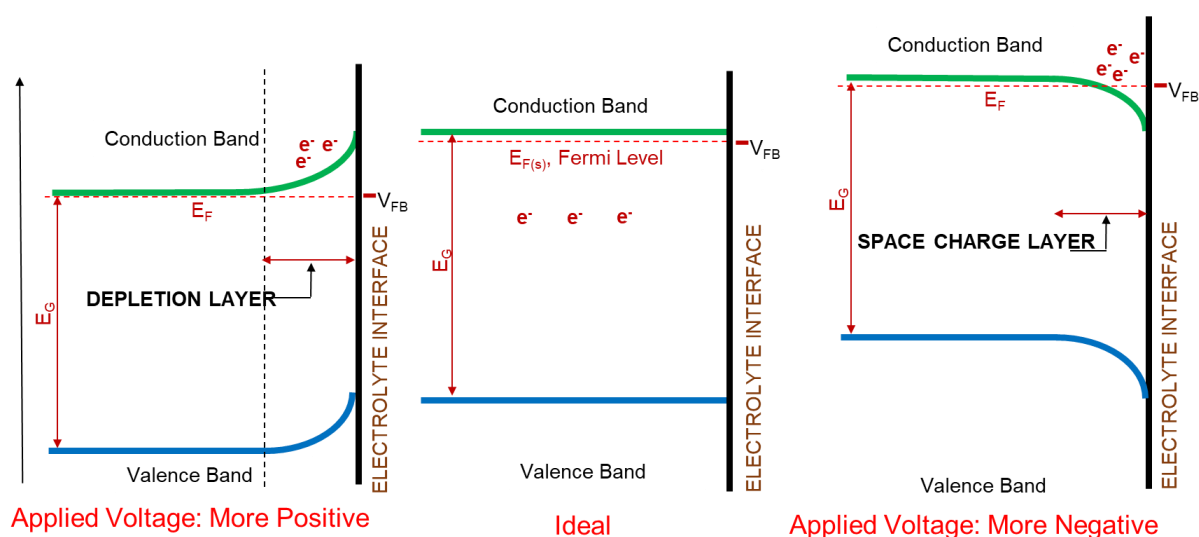

Figure 4.19 Schematic diagram of energy band of n-type semiconductors upon A) Applying more positive potential B) Ideal C) Applying more negative potentials.

Figure 4.19. a shows the energy band diagram when a positive potential is applied to an n-type semiconductor electrode. When the applied electrode potential is more positive than the flat band potential, the Fermi level in the

energy diagram is shifted down from the flat band potential. As a result, Ev and Ec bend like **in Figure 4.19a**, i.e., the energy level is lower at the solid bulk phase and higher at the surface. Because of the bending, electrons in the conducting band move from the solid surface (higher energy level) to the solid bulk phase (lower energy level). This causes a rack of electrons near the surface of the solid electrode, and the surface layer formed by this process is termed the "depletion layer". When the depletion layer is formed, electron transfer from the solid electrode to the electrolyte in the solution phase becomes difficult due to the lack of electrons near the solid electrode surface.

Figure 4.19c shows the energy band diagram when a negative potential is applied to the semiconductor electrode. When the applied potential is more negative than flat band potential, fermi level shifts up, and Ev and Ec bend like the figure, i.e. energy level is higher at solid bulk phase and lower at the surface. In this case, electrons in the conduction band move to the surface (lower energy level) from bulk phase (higher energy level), and a "electron rich" surface layer termed as "space charge layer" is formed near the surface. Because of the presence of electrons near the surface, electron transfer from the solid electrode to electrolyte in solution phase become more accessible, thus a reduction of electrolyte can occur. In most cases, the electron transfer rate or reduction rate of the electrolyte is proportional to the number density of the surface electrons at the energy level, the same as the reduction potential of the electrolyte (oxidized chemical species). If the reduction potential is positioned in the range between Ec at the surface and Ef, the number density of electrons is high, and a rapid reduction proceeds. If the reduction potential is out of the range, however, there is no electron at the same energy level as the reduction potential of electrolyte, and reduction of the electrolyte do not occur (or the reduction rate is very slow).
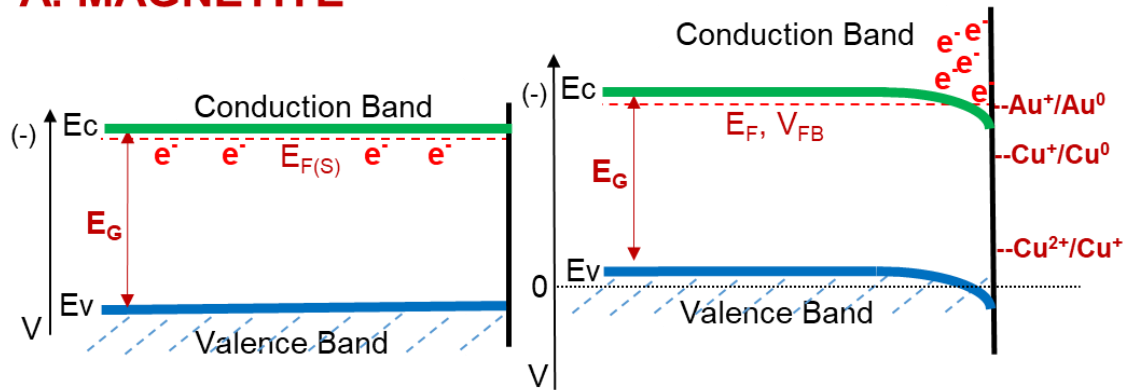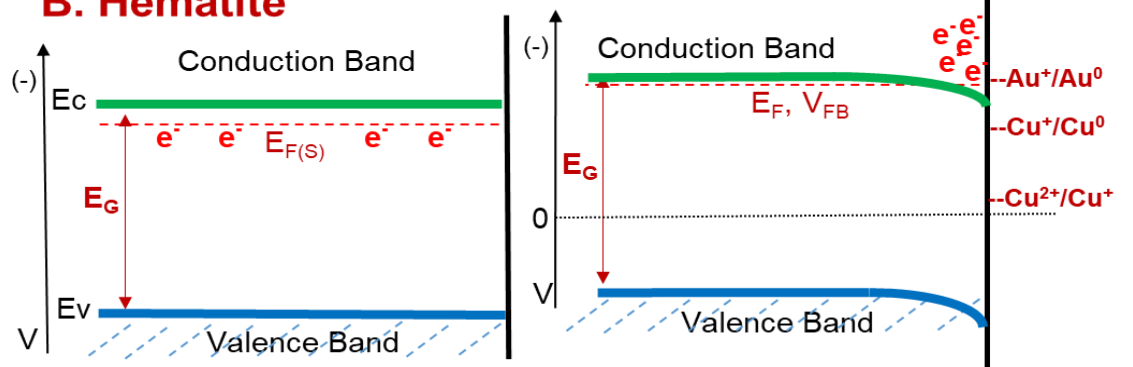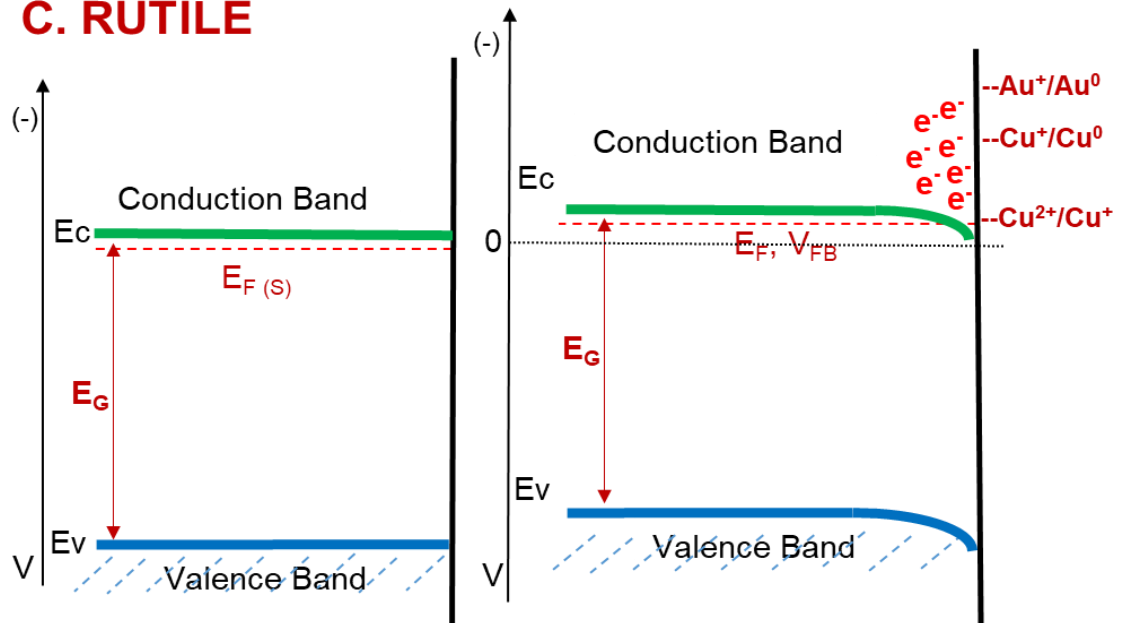
Figure 4.20 Energy band diagrams before (left) and after negative electrode potential is applied for **A.)** Magnetite **B.)** Hematite) and **C.)** Rutile.

Figure 4.20 compares the energy band diagrams for two iron oxides (magnetite and hematite) and rutile when applying negative electrode potential. In the case of rutile (**Figure 4.20 c**), the positions of reduction potential for the electrolytes, such as Au^+, Cu^+, and Cu^{2+}, are higher than that of Ec at the surface. Because of this relative position, a rapid electron transfer from rutile to these species may be possible when the applied electrode potential is low enough and the corresponding Fermi level is higher than the reduction potential. On the other hand, in the case of iron oxides (**Figure 4.20 a and b**), the position of reduction potential for Au^+ is higher than Ec for magnetite or near Ec for hematite, while the Cu^+ and Cu^{2+} positions are inside the band gap and below Ec. This means reducing Au^+ is possible but reducing Cu^{2+} and Cu^+ is difficult. This may be the reason why iron oxides selectively cement gold.

CATHODE:
$$Au(S_2O_3)_2^{3-} + 6H_2O + 9e^- \rightarrow Au^0 + 4S^0 + 12\ OH^-$$

Small iron oxide particle

ANODE:
$$3Al^0 = 3Al^{3+} + 9e^-$$

$Au(S_2O_3)_2^{3-}$

Al

Al^{3+}

e⁻

IRON OXIDE-ELECTROLYTE INTERFACE
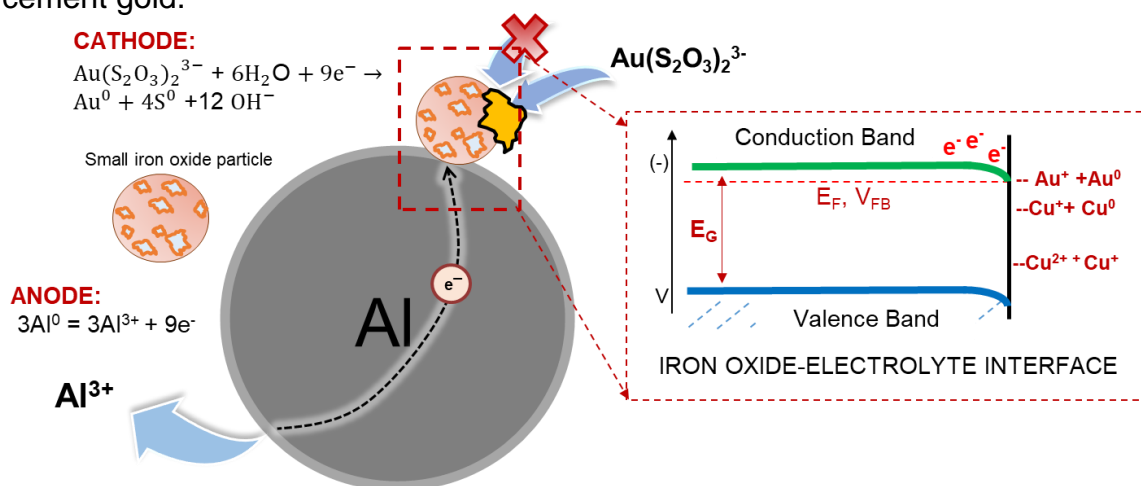
OVER-ALL CEMENTATION REACTION: (ΔG = - 3502.61 kJ/mole)

$$2Au(S_2O_3)_2^{3-}{}_{(aq)} + 6Al^0{}_{(s)} + 6H^+ \rightarrow 2Au^0{}_{(s)} + 8S^0{}_{(s)} + 3Al_2O_3{}_{(s)} + 3H_2O{}_{(l)}$$

Figure 4.21 Schematic diagram of iron oxide's selective cementation mechanism to gold as an electron mediator upon galvanic interaction with zero-valent aluminum.

The proposed selective mechanism of iron oxide to gold is presented in **Figure 4.21**. The proposed mechanism was supported by various electrochemical, spectrophotochemical and surface analysis results in **Figures 3-17. The** electron transfer mechanism across the Al_2O_3 layer between ZVAl and iron oxide particles was discussed in **Chapter 3,** where the ZVAl surface might be covered with a fragile layer of Al_2O_3 due to autogenous oxidation. Since Al_2O_3 is an electric insulating material, direct current cannot

pass through this layer. Interpretation for the electron transfer through the insulating Al_2O_3 layer is via **(1)** the quantum tunnelling effect [33] and **(2)** alternative current transfer through the Al_2O_3 layer acting as a capacitor [17]. From then on, electrons that pass through the solid-electrolyte interface can be interpreted using the energy band diagram. By staircase, potential electrochemical impedance spectroscopy, iron oxides confirm that the flat band potential of magnetite and hematite is around -0.9 V and -1.0 V, respectively. This confirms that by linear interpolation on the positive slope in the M-S plot, both iron oxides used in these experiments are n-type semiconductors, as presented in **Figure 4.16.**

The Fermi level and flat-band potential of the n-type semiconductor sit just below the conduction band edge. Initially, this edge has no depletion layer (empty) at the junction between the electrolyte and the semiconductor. Then, electrons will flow from the semiconductor to the electrolyte interface, filling the depletion layer with electrons. This transfer of electrons bends and creates a layer near the semiconductor surface called the space charge layer. The extent of bending using iron oxides will only create a space charge layer across the $Au(S_2O_3)_2^{3-}$ reduction band edge around -1.0 V since the flat band potential of magnetite and hematite is around -0.9 V and -1.0 V, respectively. Relatively, copper ions will not be able to accept electrons from the semiconductor interface since the electrolytes' reduction potentials are around -0.8 V for Cu^+/C^0 and -0.2 V for Cu^{2+}/Cu^+ , respectively. This phenomenon is being proposed, that the semiconductive properties of hematite and magnetite and by configuring their relative energy band diagram, the travel of electrons from iron oxide-electrolyte interface facilitates the selective cementation towards $Au(S_2O_3)_2^{3-}$ ions in gold-copper ammoniacal thiosulfate solutions.

4.5. CONCLUSION

Cementation experiments were conducted using titanium oxides (anatase and rutile) to investigate the direct influence of semiconductive properties. The results presented in **Figure 4.2** show that titanium oxides can recover gold and copper in a single system with 32.5% Au-16.4% Cu for anatase and 26.1% Au-12.4% Cu for rutile, respectively. Furthermore, when zero-valent aluminum was introduced into the system as an electron donor, a significant increase in metal recovery was observed, having 92.6% Au-62.2% Cu for anatase and 93.5% Au-66.9 % Cu for rutile, respectively. Comparatively, this research further suggests that the use of iron oxides has been shown to have better selectivity to gold upon the cementation process than titanium oxides and that the electrochemical experiments and surface analysis supported the results, as shown in **Figure 4.3-4.**

The latter investigated the potential properties of metal oxides that would explain its selective cementation to gold, such as the energy band gap and the flat band potential, to estimate the energy band diagram of the metal oxides. Staircase potentio-electrochemical impedance spectroscopy was conducted to determine the corresponding flat-band potentials of metal oxides in NH4/NH3 buffer solution maintained at pH 9 at 25°C. The mott-Schottky plot was generated by computerized driven software to estimate reliable values, and the results obtained a flat-band potential of around -0.9 V, -1.0 V and -0.2 V for magnetite, hematite, and rutile, respectively, as shown in **Figure 4.16**.

Furthermore, the M-S plot confirms that the metal oxides used in this experiment are n-type semiconductors. Furthermore, the band gap energy was estimated by configuring the positive slope of Tauc's plot by linear interpolation from results generated by UV-VIS spectrophotometric analysis, and the results obtained a band gap energy of 1.02 eV, 2.4 eV, and 3.1 eV for magnetite, hematite, and rutile, respectively as shown in **Figure 4.17.**

By configuring the energy band diagrams of magnetite and hematite, it was found that the bending occurs from the conducting band edge to the flat band potential edge; in both cases, magnetite and hematite have a flat band potential near the conduction band edge where electrons can transfer from the semiconductive electrode interface across the electrolyte interface (reduction band edge) of gold around -1.0 V only as shown in **Figure 4.21.** This research concludes that the representation of energy band diagrams was able to explain why iron oxides are selective only to gold upon the cementation process in gold-copper ammoniacal thiosulfate medium and that the semiconductive property governs the said selective cementation.

4.6 REFERENCES:

1. Hong Qin et. al, 2020. "Pyrite enhanced chlorination roasting and its efficacy in gold and silver recovery from gold tailing." https://doi.org/10.1016/j.seppur.2020.117168

2. Hong Qin et. al, 2021. "Recovery of Gold from sulfide refractory gold ore: Oxidation roasting pretreatment and gold extraction." Minerals Engineering 164 (2021) 106822. https://doi.org/10.1016/j.mineng.2021.106822

3. K.T. Konadu et. al, 2019. "Sequential pretreatment of double refractory gold ore (DRGO) with a thermophilic iron oxidizing archaeon and fungal crude enzymes." https://doi.org/10.1016/j.mineng.2019.04.043

4. Sanghyeon Choi et. al, 2021. "Addition of Fe3O4 as electron mediator for enhanced cementation of cd2+ and Zn2+ on aluminum powder from sulfate solutions and magnetic separation to concentrate cemented metals from cementation products". Journal of Environmental Chemical Engineering 9(2021) 106699. https://doi.org/10.1016/j.jece.2021.106699

5. Sanghee jeon et. al, 2021. "The effects of Coexisting Copper, Iron, Cobalt, nickel and zinc ions on Gold recovery by enhanced cementation via Galvanic Interactions between zero-valent aluminum and activated carbon

in ammonium thiosulfate system." Metals 2021, 11, 1352. https://doi.org/10.3390/met11091352

6. Sanghee Jeon et. al., 2020. "Enhanced Cementation of gold via galvanic interaction using activated carbon and zero-valent aluminum: A novel Approach to recover gold ions from ammonium thiosulfate medium. http://dx.doi.org/10.1016/j.hydromet.2019.105165

7. Sanghee Jeon et.al, 2021. "A simple and efficient recovery technique for gold ions from ammonium thiosulfate medium by galvanic interactions of zero-valent aluminum and activated carbon: A parametric and mechanistic study of cementation. https://doi.org/10.1016/j.hydromet.2021.105815

8. Sanghee Jeon et. al, 2022. "A kinetic study on enhanced cementation of gold ions by galvanic interactions between aluminum as an electron donor and activated carbon as an electron mediator in ammonium thiosulfate system. https://www.mdpi.com/2075-163X/12/1/91/pdf

9. Gallagher, N.P., Hendrix, J.L., Milosavljevic, E.G., Nelson, J.H., Solujic, L., 1990. Affinity of activated carbon towards some gold (I) complexes. Hydrometallurgy 25, 305–316. https://doi.org/10.1016/0304-386X(90)90046-5

10. Ke, B., Li, Y., Chen, J., Zhao, C., Chen, Y., 2016. DFT study on the galvanic interaction between pyrite (100) and galena (100) surfaces. Appl. Surf. Sci. 367, 270–276. https://doi.org/10.1016/j.apsusc.2016.01.063

11. Diggle, J.W., Downie, T.C., Goulding, C.W., 1969. Anodic oxide films on aluminum. Chem. Rev. 69 (3), 365–405. https://doi.org/10.1021/cr60259a005

12. Dong, Z., Jiang, T., Xu, B., Yang, Y., Li, Q., 2017. Recovery of gold from pregnant thiosulfate solution by the resin adsorption technique. Metals 7 (12), 555. http://dx.doi.org/10.3390/met7120555

13. Arima, H., Fujita, T., Yen, W., 2002. Gold cementation from ammonium thiosulfate solution by zinc, copper, and aluminum powders. Mater. Trans. 43 (3), 485–493. http://dx.doi.org/10.2320/matertrans.43.485

14. Karavasteva, M., 2010. Kinetics and deposit morphology of gold cemented on magnesium, aluminum, zinc, iron, and copper from ammonium thiosulfate-ammonia solutions. Hydrometallurgy 104 (1), 119–122. https://doi.org/10.1016/j.hydromet.2010.04.007

15. Guilin Hu et. al, 2006. "Decomposition and Oxidation of Pyrite." doi: 10.1016/j.pecs.2005.11.004

16. Mark Alymore et. al, 2000. Mechanochemical milling-induced reactions between gases and sulfide minerals: I. Reactions of SO_2 with arsenopyrite, pyrrhotite and pyrite. https://doi.org/10.1016/S0925-8388(00)00916-6

17. K.T. Konadu, R.J. Huddy, S.T.L. Harrison, K. Osseo-Asare, and K. Sasaki, Sequential pretreatment of double refractory gold ore (DRGO) with a thermophilic iron oxidizing archeaon and fungal crude enzymes, *Miner. Eng.*, 138(2019), p. 86.
https://doi.org/10.1016/j.mineng.2019.04.043

18. C. Ince, Reusing gold-mine tailings in cement mortars: Mechanical properties and socio-economic developments for the Lefke-Xeros area of Cyprus, *J. Cleaner Prod.*, 238(2019), art. No. 117871. https://doi.org/10.1016/j.jclepro.2019.117871

19. I. Alp, O. Celep, D. Paktunç, and Y. Thibault, Influence of potassium hydroxide pretreatment on the extraction of gold and silver from a refractory ore, *Hydrometallurgy*, 146(2014), p. 64.

https://doi.org/10.1016/j.hydromet.2014.03.007

20. R. Ahtiainen and M. Lundström, Cyanide-free gold leaching in exceptionally mild chloride solutions, *J. Cleaner Prod.*, 234(2019), p. 9. https://doi.org/10.1016/j.jclepro.2019.06.197

21. Sun, Cb., Zhang, Xl., Kou, J. *et al.* A review of gold extraction using noncyanide lixiviants: Fundamentals, advancements, and challenges toward alkaline sulfur-containing leaching agents. *Int J Miner Metal Mater* **27,** 417–431 (2020). https://doi.org/10.1007/s12613-019-1955-x

22. L. Tremblay, G. Deschênes, E. Ghali, J. McMullen, and M. Lanouette, Gold recovery from a sulphide bearing gold ore by percolation leaching with thiourea, *Int. J. Miner. Process.* 48(1996), No. 3–4, p. 225. https://doi.org/10.1016/S0301-7516(96)00029-4

23. C.J. Ma, J.Y. Li, and R.J. Liu, A review of thiocyanate hydrometallurgy for the recovery of gold, *Appl. Mech. Mater.*, 768(2015), p. 53. https://doi.org/10.4028/www.scientific.net/AMM.768.53

24. M.G. Alymore and D.M. Muir, Thiosulfate leaching of gold—A review, *Miner. Eng.*, 14(2001), No. 2, p. 135. https://doi.org/10.1016/S0892-6875(00)00172-2

25. R. Ahtiainen, M. Lundström, and J. Liipo, Preg-robbing verification and prevention in gold chloride-bromide leaching, *Miner. Eng.*, 128(2018), p. 153. https://doi.org/10.1016/j.mineng.2018.08.037

26. Wang, Hx., Sun, Cb., Li, Sy. *et al.* Study on gold concentrate leaching by iodine-iodide. *Int J Miner Metal Mater* **20,** 323–328 (2013). https://doi.org/10.1007/s12613-013-0730-7

27. S.S. Konyratbekova, A. Baikonurova, G.A. Ussoltseva, C. Erust, and A. Akcil, Thermodynamic and kinetic of iodine-iodide leaching in gold hydrometallurgy, *Trans. Nonferrous Met. Soc. China*, 25(2015), No. 11, p. 3774. https://doi.org/10.1016/S1003-6326(15)63980-2

28. Qin, H., Guo, Xy., Tian, Qh. *et al.* Recovery of gold from refractory gold ores: Effect of pyrite on the stability of the thiourea leaching system. *Int J Miner Metal Mater* 28, 956–964 (2021). https://doi.org/10.1007/s12613-020-2142-9

29. D. Feng, J.S.J. van Deventer, AMMONIACAL Thiosulfate leaching of gold in the presence of pyrite, Hydrometallurgy 82 (2006) 126-132. https://doi.org/10.1016/j.hydromet.2006.03.006

30. Vladimir Morkun et. al. "Increasing the efficiency of iron ore magnetic separation by using ultrasonic technologies." S Web of Conferences 280, 08004 (2021), https://doi.org/10.1051/e3sconf/202128008004

31. Bjerge, L.-M. and P. Brevik (2014), "CO2 capture in the cement industry, Norcem CO2 capture Project (Norway)", Energy Procedia, Vol. 63, pp. 6455-6463. https://doi.org/10.1016/j.egypro.2014.11.680

32. Michael Alln McCrae, 2018. "Hitching Gold to the electric Vehicle Vanwagon). Mining 101. https://www.mining.com/hitching-gold-electric-vehicle-bandwagon/.

33. Julio Cézar Balarini, Ludmila de Oliveira Polli, Tânia Lúcia Santos Miranda, Roberto Machado Zica de Castro, Adriane Salum, Importance of roasted sulphide concentrates characterization in the hydrometallurgical extraction of zinc, Minerals Engineering, Volume 21, Issue 1, 2008, Pages 100-110, ISSN 0892-6875, https://doi.org/10.1016/j.mineng.2007.10.002.

34. T.T. Chen, J.E. Dutrizac Mineralogical changes occurring during the fluid-bed roasting of zinc sulfide concentrates JOM Journal of the Minerals Metals and Materials Society, 56 (12) (2004), pp. 46-51 https://doi.org/10.1007/s11837-004-0235-y

35. D.K. Xia, C.A. Pickles Kinetics of zinc ferrite leaching in caustic media in the deceleratory period Minerals Engineering, 12 (6) (1999), pp. 693-700 https://doi.org/10.1016/S0892-6875(99)00052-7

36. S.L. Harmer, L.V. Goncharova, R. Kolarova, W.N. Lennard, M.A. Muñoz-Márquez, I.V. Mitchell, H.N. Nesbitt Surface structure of sphalerite studied by medium energy ion scattering and XPS Surface Science, 601 (2007), pp. 352-361 https://doi.org/10.1016/j.susc.2006.10.001

37. D. Feng, J.S.J. van Deventer, Effect of hematite on thiosulphate leaching of gold, International Journal of Mineral Processing, Volume 82, Issue 3, 2007, Pages 138-147, ISSN 0301-7516, https://doi.org/10.1016/j.minpro.2006.09.003.

38. M.G. Alymore, Chapter 28 - Thiosulfate as an Alternative Lixiviant to Cyanide for Gold Ores, Editor(s): Mike D. Adams, Gold Ore Processing (Second Edition), Elsevier, 2016, Pages 485-523, ISBN 9780444636584, https://doi.org/10.1016/B978-0-444-63658-4.00028-1.

39. Feng XIE, Jun-nan CHEN, Jian WANG, Wei WANG, Review of gold leaching in thiosulfate-based solutions, Transactions of Nonferrous Metals Society of China, Volume 31, Issue 11, 2021, Pages 3506-3529, ISSN 1003-6326, https://doi.org/10.1016/S1003-6326(21)65745-X.

40. Bin Xu et. al, 2017. A review of thiosulfate leaching of gold: Focus on thiosulfate consumption and gold recovery from pregnant solution. Metal-open access metallurgy journal 7(6):222. DOI:10.3390/met7060222

41. Xin-yuan Nan, Xin Cai, Jun Kong, Pretreatment Process on Refractory Gold Ores with As, ISIJ International, 2014, Volume 54, Issue 3, Pages 543-547, Released on J-STAGE April 08, 2014, Online ISSN 1347-5460, Print ISSN 0915-1559. DOI: https://doi.org/10.2355/isijinternational.54.543

42. Fu, P.; Li, Z.; Feng, J.; Bian, Z. Recovery of Gold and Iron from Cyanide Tailings with a Combined Direct Reduction Roasting and Leaching Process. *Metals* **2018**, *8*, 561. https://doi.org/10.3390/met8070561

43. https://grist.org/accountability/electric-vehicles-drive-up-demand-for-green-metals/ [internet] Electric vehicles drive up demand for "green metals." Jonathan Thompson, January 28, 2022

44. M.G Aylmore, D.M Muir, Thiosulfate leaching of gold—A review, Minerals Engineering, Volume 14, Issue 2, 2001, Pages 135-174, ISSN 0892-6875. https://doi.org/10.1016/S0892-6875(00)00172-2.

45. HEMMATI M. A Study of The Thiosulfate Leaching of Gold from Carbonaceous Ore and The Quantitative Determination of Thiosulfate in The Leached Solution. [Order No. 1331035]. University of Nevada, Reno; 1987. http://hdl.handle.net/11714/1361

46. Carlito Baltazar Tabelin, Suchol Veerawattananun, Mayumi Ito, Naoki Hiroyoshi, Toshifumi Igarashi, Pyrite oxidation in the presence of hematite and alumina: II. Effects on the cathodic and anodic half-cell reactions,

Science of The Total Environment, Volumes 581–582, 2017, Pages 126-135, ISSN 0048-9697, https://doi.org/10.1016/j.scitotenv.2016.12.050.

47. Tao, Jiang et al. "Electrochemistry and Mechanism of Leaching Gold with Ammoniacal Thiosulphate." (2010). Corpus ID: 121151448

48. Aikawa, K.; Ito, M.; Orii, N.; Jeon, S.; Park, I.; Haga, K.; Kamiya, T.; Takahashi, T.; Sunada, K.; Sakakibara, T.; Ono, T.; Magwaneng, R.S.; Hiroyoshi, N. Flotation of Copper Ores with High Cu/Zn Ratio: Effects of Pyrite on Cu/Zn Separation and an Efficient Method to Enhance Sphalerite Depression. *Minerals* **2022**, *12*, 1103. https://doi.org/10.3390/min12091103

49. Yan Zhang, Qian Li, Xiaoliang Liu, Tao Jiang, A thermodynamic analysis on thiosulfate leaching of gold under the catalysis of Fe3+/Fe2+ complexes, Minerals Engineering, Volume 180, 2022, 107511, ISSN 0892-6875, https://doi.org/10.1016/j.mineng.2022.107511.

50. K. Gelderman, L. Lee, and S. W. Donne. Flat-band potential of a semiconductor: Using the mott–schottky equation. Journal of Chemical Education, 84(4):685, 2007.

51. W. John Albery, Gerald J. O'Shea, and Alec L. Smith. Interpretation and use of mott–schottky plots at the semiconductor/electrolyte interface. J. Chem. Soc., Faraday Trans., 92:4083–4085, 1996.

52. Anna Hankin, Franky E. Bedoya-Lora, John C. Alexander, Anna Regoutz, and Geoff H. Kelsall. Flat band potential determination: avoiding the pitfalls. J. Mater. Chem. A, 7:26162–26176, 2019.

53. M. Radecka, M. Rekas, A. Trenczek-Zajac, and K. Zakrzewska.Importance of the band gap energy and flat band potential for application of modified tio2 photoanodes in water photolysis. Journal of Power Sources, 181(1):46 – 55, 2008. SPECIAL SECTION Selected papers from the 1st POLISH FORUM ON FUEL CELLS AND HYDROGEN.

54. R. van de Krol. Principles of photoelectrochemical cells. In Photoelectrochemical Hydrogen Production, Electronic Materials: Science & Technology, chapter 2. Springer, 2011.

55. Patrycja Makuła, Michał Pacia, and Wojciech Macyk " How To Correctly Determine the Band Gap Energy of Modified Semiconductor Photocatalysts Based on UV–Vis Spectra" *The Journal of Physical Chemistry Letters* 2018 *9* (23), 6814-6817 DOI: 10.1021/acs.jpclett.8b02892

56. Şerban Ionel, Enesca Alexandru "Metal Oxides-Based Semiconductors for Biosensors Applications ", Frontiers in Chemistry Journal Volume 8 2020 ISSN=2296-2646. DOI=10.3389/fchem.2020.00354

CHATER 5

GENERAL CONCLUSIONS

1.Parametric cementation experiments were investigated concerning aerobic or anaerobic solution condition, electron mediator dosage, cementation time in single and binary systems, and electron donor dosage in binary systems. All experiments obtained consistency concerning the selective cementation of gold using iron oxides with zero-valent aluminum, and the optimum parameters were determined to be 10 mg of electron donor and 10 mg electron mediator for 60 mins cementation time in anaerobic (N_2 purged) solution condition maintained in pH 9-10 at 25°C. These optimum conditions obtained gold and copper recoveries of 89.7 % and 21 % for hematite and 85.9 % and 15.4% for magnetite, respectively as shown in **Figure 5.1.**
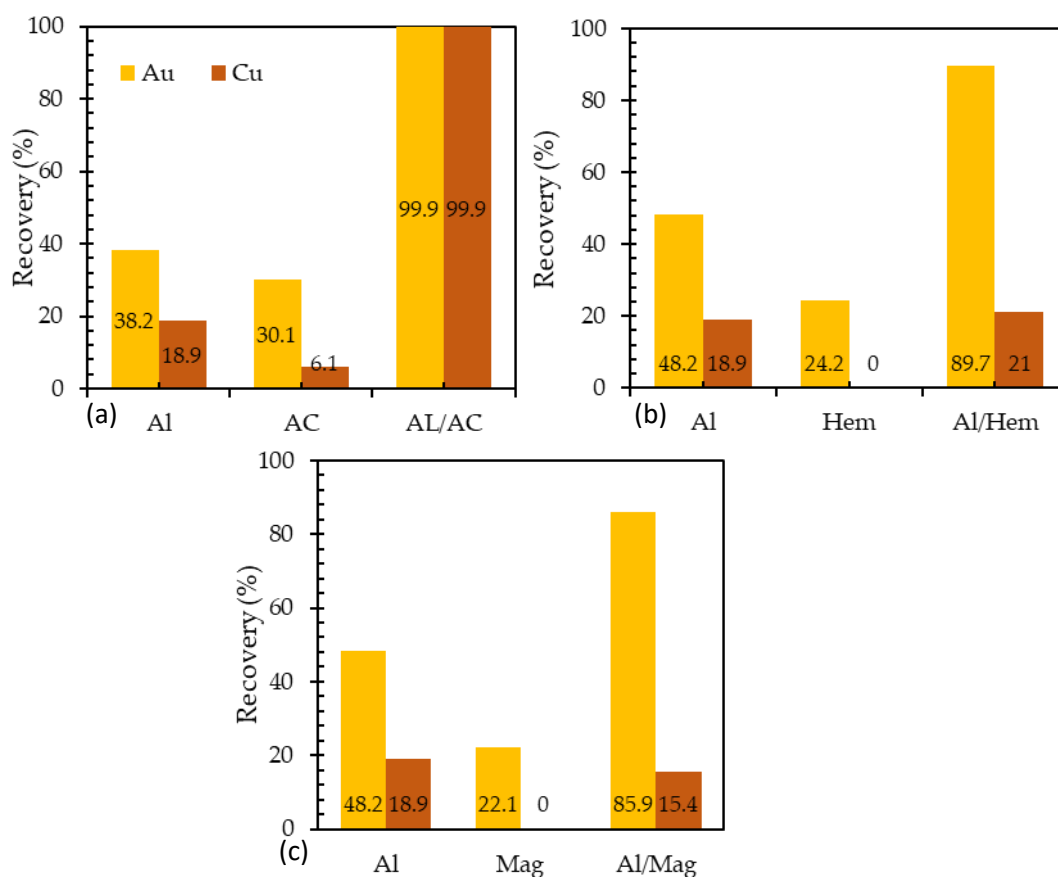

Figure 5.1 Percent (%) recovery of gold, Au and copper, Cu ions from different galvanic constituents in nitrogen atmosphere (anerobic) **a)** activated

carbon (AC) and or /ZVAl **b)** hematite (Hem) and or/ ZVAl and **c.)** magnetite (Mag) and or /ZVAl.

2.The electrochemical experiment was conducted to evaluate the galvanic interaction between the electron donor and electron mediator in a conventional electrochemical set-up (Fe_2O_3/ Fe_3O_4 -Al as the working electrode, Pt as the counter electrode, Ag/AgCl as the reference electrode) in gold thiosulfate medium. Cyclic voltammetry showed a gold reduction "shoulder-like" peak at -1.0 V using Fe_2O_3/Al and Fe_3O_4/Al electrodes. The results of SEM-EDX analysis on the surface of the working electrodes and electrochemical experiments confirmed that gold was selectively deposited on iron oxide's surface as an electron mediator as shown in **Figure 5.2 and 5.3.**

Figure 5.2 Cyclic Voltammogram of Fe_2O_3/Al electrode at different electrolytes a) Wide Scan b) Narrow Reduction Voltammogram c) Back scattered electron photomicrograph with elemental mapping and point eds analysis of Cu-Au electrolytes.

153

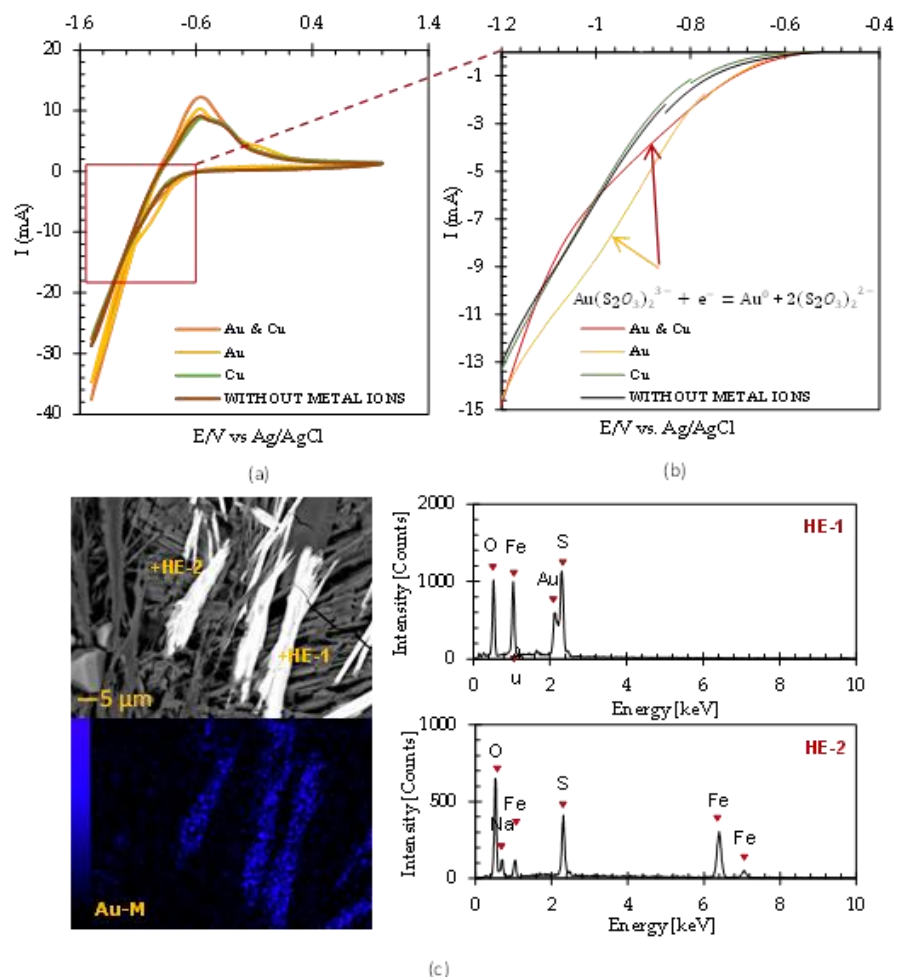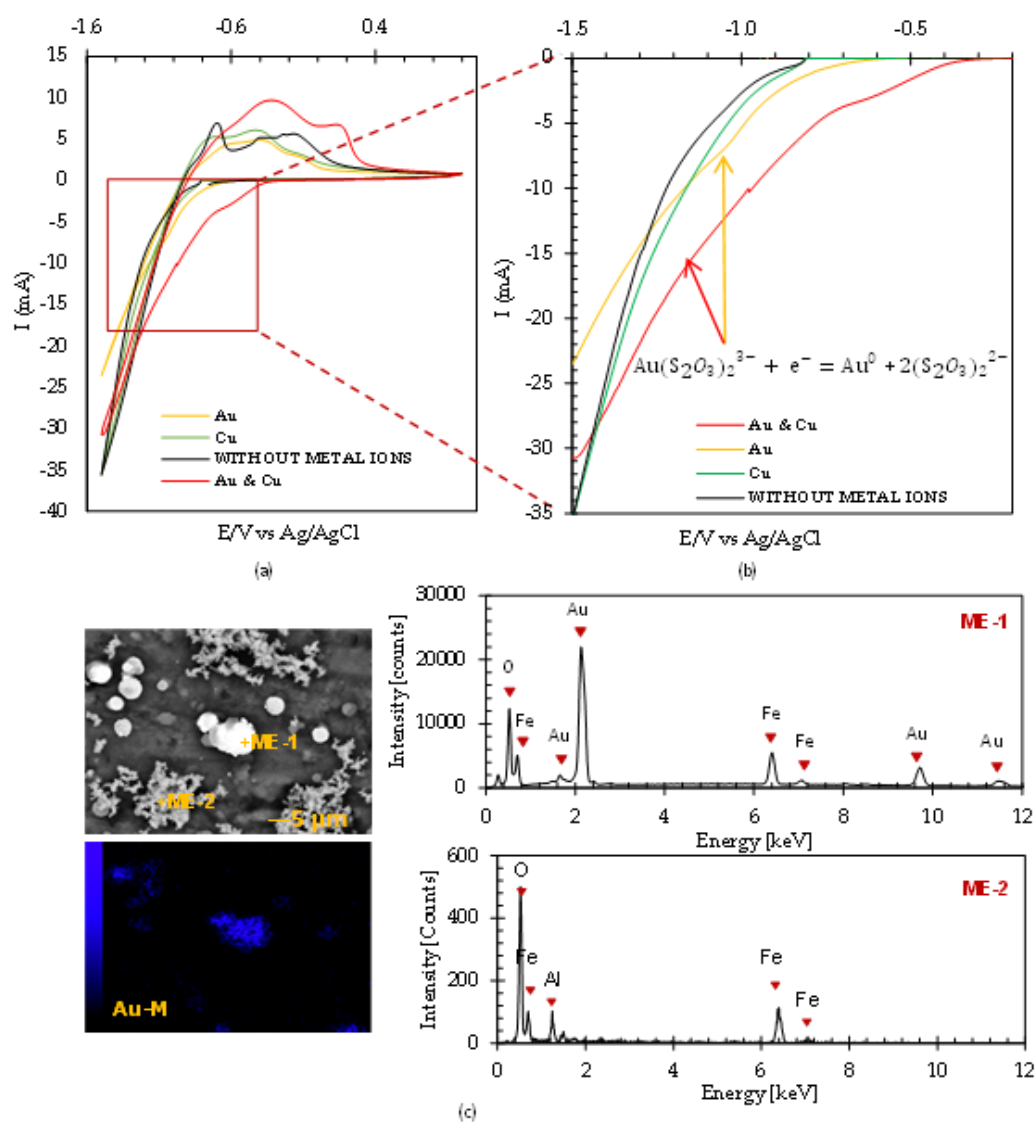**Figure 5.3** Cyclic Voltammogram of Fe_3O_4/Al electrode at different electrolytes a) Wide Scan b) Narrow Reduction Voltammogram c) Back-scatter electron photomicrograph with elemental mapping and point eds analysis of Cu-Au electrolytes.

3. The investigation of metal oxides' band gap and flat band potential to estimate critical potential band edges to configure the energy band diagram was evaluated. The Mott-Schottky (M-S) plot was generated by computerized driven software to estimate reliable values, and the results obtained a flat-band potential of around -0.9 V, -1.0 V and -0.2 V for magnetite, hematite, and rutile, respectively. the band gap energy was estimated by configuring the positive slope of Tauc's plot by linear interpolation from the results generated by UV-VIS spectrophotometric analysis, and the results obtained a band gap energy of 1.02 eV, 2.4 eV, and 3.1 eV for magnetite, hematite, and rutile, respectively as shown in **Figures 5.4.**
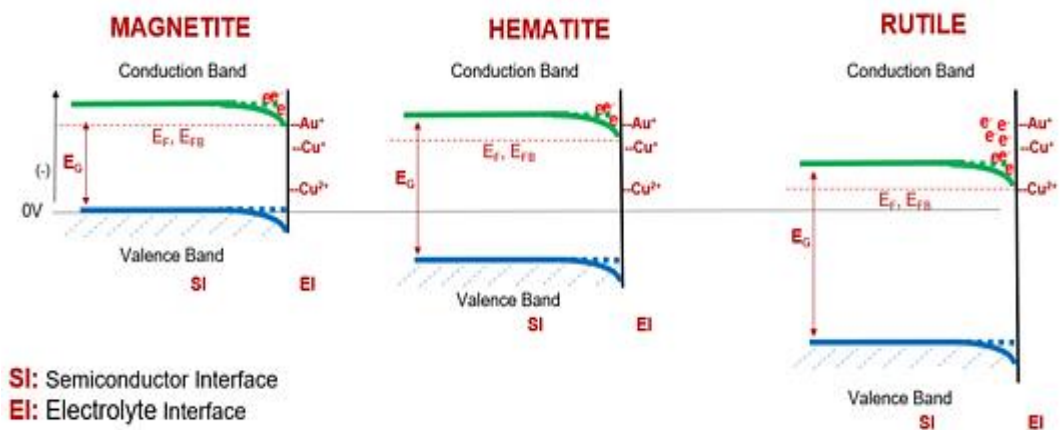
Figure 5.4 Schematic Energy band diagrams for the semiconductor-electrolyte interface (SEI) for a) Rutile b) Hematite and c) Magnetite.

4. This research concludes that iron oxides can be used as an electron mediator undergoing selective cementation to gold along with zero-valent aluminum as an electron donor during the cementation process and that the intrinsic semiconductive property of iron oxides govern the selective cementation mechanism and can be represented using the energy band diagrams, describing the selective electron transfer mechanism in the semiconductor-electrolyte interface in gold-copper ammoniacal thiosulfate medium as shown in **Figure 5.5.**

Figure 5.5 Schematic diagram of the proposed selective mechanism of iron oxides and their galvanic interaction with zero valent aluminum in gold-copper ammoniacal thiosulfate medium.

ACKNOWLEDGEMENTS

First, I must thank the people who loved me before I saw the light: my parents, **Rafael P. Zoleta** and **Rebecca B. Zoleta**. Thank you for your love and undying support throughout my life. Thank you both for giving me the strength to reach the stars. I LOVE YOU both. My sisters, brothers, and the entire family also deserve my wholehearted thanks.
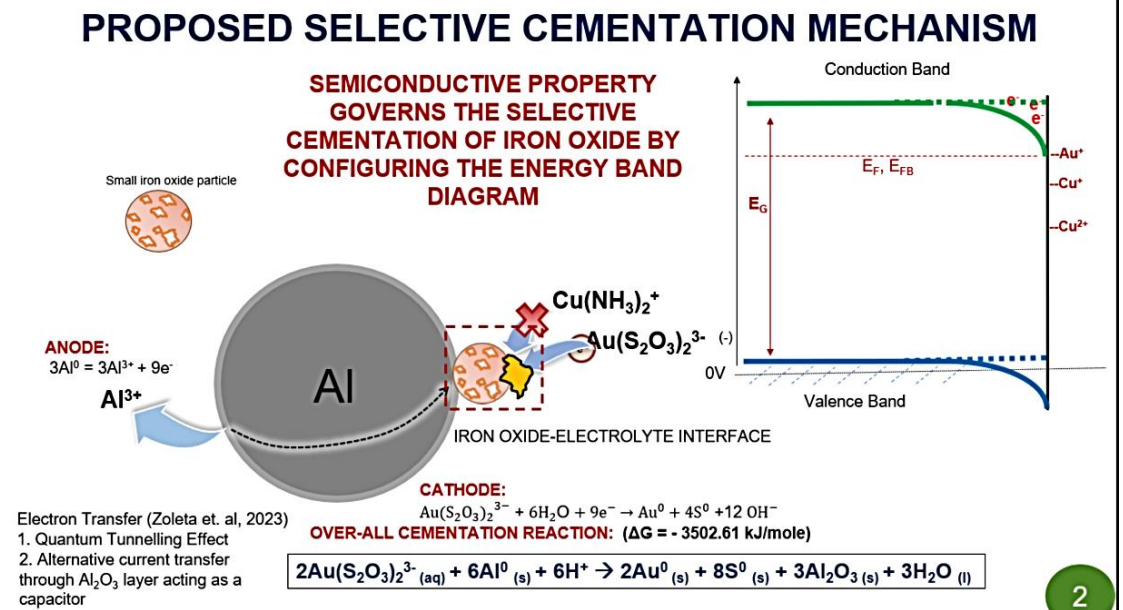
I sincerely thank my supervisor, **Prof. Naoki Hiroyoshi**, for his guidance and support throughout this study, especially his confidence in me.

I would also like to thank my Mindanao State University-Iligan Institute of Technology colleagues, especially **Prof. Gevelyn B. Itao**, for their never-ending support.

A lot of thanks to the **Department of Science and Technology-Engineering Research for Development and Technology- Faculty Development Program** (DOST-ERDT-FDP)- Scholarship for supporting and funding my PhD Degree to make this study possible.

To all my friends and the **Lavenia Family**, thank you for your understanding and encouragement in several crises. Your friendship makes my life a wonderful experience, especially for **Ben Barrientos**. I cannot list all the names here, but you are always in my mind.

Thank you, **Almighty God**, for always being there for me. Thank you for giving me enough understanding, knowledge and wisdom to accomplish this manuscript. Above all, thank you for the gift of life.

Finally, I want to keep the remaining space for **Prof. Mayumi Ito, Prof. Yogarajah Elakneswaran and Prof. Ilhwan Park** and all my laboratory mates at Hokkaido University, Laboratory of Mineral Resources and Recycling Engineering and Chemical Resources Engineering, Sapporo, Japan. Thank you for the great experience and hospitality.

CERTIFICATE OF AUTHENTIC AUTHORSHIP

I hereby declare that the submission is my own work, and, to the best of my knowledge, it contains no materials previously neither published nor written by other person. This work does not also contain material, which, to a substantial extent, has been accepted for an award of any other degree or diploma, except where due acknowledgement is made in the manuscript. Any contribution made to the research by others, with whom I have worked at MSU-IIT or elsewhere, is explicitly acknowledged in the manuscript.

I also declare that the intellectual content of this manuscript is the product of my own work, except the assistance that I received in the project's design, conception and style, presentation and linguistic expression which I also acknowledgement.

JOSHUA BRAVO ZOLETA
Signature over printed name

JOSHUA BRAVO ZOLETA
joshua.zoleta@g.msuiit.edu.ph
09171580601

WORK SPECIALIZATION:

National Research Council of the Philippines, Metallurgist License No: 0001221

Specialize in extracting refractory gold from low-grade pyritic ores of the Philippines. Also, specialize in developing intumescent coating and its pyrolysis mechanism in steel substrates using inorganic fillers as fire-retardant additives.

BACKGROUND INFORMATION:

Permanent Address: House No.9, Zoleta Residence, Zone 1, Engineer's Village, Awang, Datu Odin Sinsuat (Dinaig), Maguindanao, 9601, Philippines
Place of Birth: Cotabato Regional Hospital, Cotabato City, Philippines
Date of Birth: April 03, 1992   **Weight:** 80 kg   **Height:** 5'8''
Citizenship: Filipino   **Status:** Single   **Religion:** Protestant

ACADEMIC ACHIEVEMENT:

2024   Doctor of Engineering, Laboratory of Chemical Resources Engineering, Division of Sustainable Resources Engineering, Graduate School of Engineering, Hokkaido University, Sapporo Japan

2018   Master of Science in Material Science Engineering
MSU-Iligan Institute of Technology, Iligan City, 9200 Philippines

2018   Sandwich program, MS in Material Science Engineering
Hokkaido University, Hokkaido, Sapporo Japan

2014   Bachelor of Science in Metallurgical Engineering
MSU-Iligan Institute of Technology, Iligan City, 9200 Philippines

2008   Notre Dame HS-Special Education in Science Curriculum
Notre Dame Village, Cotabato City, 9601Philippines

2004   Camp Siongco Elementary School
Black 1, Ems Village, Awang, D.O.S, Maguindanao, 9601 Philippines

WORK EXPERIENCE:

Jan. 2018 - PRESENT	*Assistant Professor* **(Employment Status: PERMANENT)** College of Engineering and Technology MSU-Iligan Institute of Technology, Iligan City Philippines
Aug. 2014 – Dec. 2017	*Assistant Lecturer* College of Engineering and Technology MSU-Iligan Institute of Technology, Iligan City Philippines
Jan. 2016 - Aug. 2016	*Senior Research Associate* **Project:** Establishment of Common Service Facility for Artisanal Small-scale Gold Mining in Northern Mindanao College of Engineering and Technology MSU-Iligan Institute of Technology, Iligan City Philippines
July 2015- Dec. 2015	*Research Associate* **Project:** Development of Alternative Technologies for the extraction of Gold from CARAGA and South Cotabato Region College of Engineering and Technology MSU-Iligan Institute of Technology, Iligan City Philippines
Apr. 2014- June 2015	*Project Research Assistant* Project: Development of Alternative Technologies for the extraction of Gold from CARAGA and South Cotabato Region College of Engineering and Technology MSU-Iligan Institute of Technology, Iligan City Philippines
Apr. 2014- Mar. 2015	*Process Metallurgist* Rapu-Rapu Polymetallic Project Rapu-Rapu, Albay, Philippines

RESEARCH BACKGROUND:

PERIOD	PROGRAM	RESEARCH/INSTITUTION
2021-2024	Doctoral Program	Iron Oxide as Electron Mediator and Its Galvanic Interaction with Zero-valent Aluminum in Gold-Copper Ammoniacal Thiosulfate Medium
2016-2018	Masteral Program	CeO_2-Dolomite as Fire-Retardant Additives in Conventional APP-MEL-EG Intumescent Coating System
2008-2014	Bachelor's Program	Assessment on the Recovery of Gold from Low-Grade Pyritic Ore of Siocon Zamboanga Del Norte using Iodine-Iodide as Lixiviant

SCHOLARSHIP GRANTS

PERIOD	PROGRAM	RESEARCH/INSTITUTION
2021-2024	Doctoral Program	Department of Science and Technology- Engineering Research for Development and Technology- Faculty Development Program **(DOST-ERDT-FDP),** Philippines
2016-2018	Masteral Program	Department of Science and Technology- Engineering Research for the Development of Technology **(DOST-ERDT),** Philippines
2008-2014	Bachelor Program	Philippines-Australia Resources Excellence Education Program **(PAREEP)**, Australia-Philippines
2004-2008	High School	Department of Science and Technology

RESEARCH ACCOMPLISHMENTS/ AWARDS (RELATED TO DISSERTATION)

Best Presentation   CINEST 2022, International Symposium on Earth Science and Technology 2022, Kyushu University, Kyushu, Japan

RESEARCH ACCOMPLISHMENTS/ AWARDS (OTHERS)

Best Poster Presenter	15th ERDT Congress, Red Planet Hotel, Manila City Philippine, June 2018
Best Paper	11th AUNSEED-NET Conference for Energy Manila Hotel, Philippines, August 2018
Best Paper Presenter	International Conference on Advance Functional Materials and Nanotechnology Inland Hotel, Butuan City, Philippines October 2018
Best Paper Presenter	1ST International Conference on Materials Science Engineering in the Philippines, The Lake Hotel, Tagaytay City, Philippines
Best Paper Presenter	5th ASEAN Regional Symposium of Chemical Engineers, Diamond Residences, Makati City, Philippines November 2018

RESEARCH PUBLICATIONS (RELATED TO DISSERTATION):

[1] Zoleta, J.; Jeon, S.; Kuze, A.; Okada, N.; Park, I.; Ito, M.; Elakneswaran, Y.; Hiroyoshi, N. Selective Cementation of Gold Using an Iron Oxide and Zero-Valent Aluminum Galvanic System from Gold–Copper Ammoniacal Thiosulfate Solutions. *Metals* **2023**, *13*, 1289. https://doi.org/10.3390/met13071289

RESEARCH PUBLICATIONS (OTHERS):

[1] Zoleta et. al, " Improved pyrolysis behavior of ammonium polyphosphate-melamine-expandable graphite (APP-MEL-EG) intumescent fire-retardant coating system using ceria and dolomite as additives for I-beam steel application" 2020 Published Elsevier Cellpress, Heliyon 6(2020) e03119.

[2] Zoleta et. al., "Char formation mechanism of conventional intumescent coating system using CeO_2 and Dolomite as additives for material application", 2020, Materials International ISNN:2668-5728

[3] Zoleta et. al "CeO_2-Dolomite as fire retardant additives on the conventional intumescent coating in steel substrate for improved performance" 2019, Matec Web of Conferences 268, 04009 (2019)

[4] Einstine M. Opiso, Carlito Baltazar Tabelin, Leonard Marc Ramos, Leonar Jun R. Gabiana, Marybeth Hope T. Banda, Jet Ryan Y. Delfinado, Aileen H. Orbecido, Joshua B. Zoleta, Ilhwan Park, Takahiko Arima, Mylah Villacorte-Tabelin, Development of a three-step approach to repurpose nickel-laterite mining waste into magnetite adsorbents for As (III) and As(V) removal: Synthesis, characterization, and adsorption studies,
Journal of Environmental Chemical Engineering, Volume 11, Issue 1, 2023,108992, ISSN 2213-3437, https://doi.org/10.1016/j.jece.2022.108992.

[5] Junnile L. Romero , Carlito Baltazar Tabelin, Ilhwan Park , Richard D. Alorro , Joshua B. Zoleta, Leaniel C. Silva, Takahiko Arima , Toshifumi Igarashi , Takunda Mhandu , Mayumi Ito , Steffen Happel, Naoki Hiroyoshi Vannie Joy T. Resabal "Modified Diglycolamide Resin: Characterization and Potential Application for Rare Earth Element Recovery" . Minerals, Volume 13 Issue 1330.

[6] Joshua Pascual Pocaan, Casey Oliver A Turingan, Carlito Baltazar Tabelin, Joshua B Zoleta, Takahiko Arima, Ilhwan Park, Mayumi Ito, Aileen H Orbecido " A Mixed Media Approach Using Locally Available Neutralizing Materials for the Passive Treatment of Acid Mine Drainage

[7] Shem Quiawan Saldia, Joshua B Zoleta , Hernando P Bacosa, Maria Cristina Vegafria, , Naoki Hiroyoshi, Christian Dagunsa Calleno, Wilyneth Sindico Cantong, Ephraim Ibarra, Maricar Aguilos, Ruben F Amparado "Combined Potential of Quarry Waste Fines and Eggshells for the Hydrothermal Synthesis of Tobermorite at Varying Cement Content"

RESEARCH PROJECTS INVOLVEMENT FUNDED BY DOST-PCIEERD:

PROJECT LEADER (ON-GOING)
[1] Establishment of Common Service Facilities for Artisanal Small Scale Gold Mining in the Philippines.

RESEARCH ASSOCIATE (ON-GOING)
[2] Development of Alternative Technologies for the Extraction of Gold from Small-Scale Gold Mining of the Philippines.